

https://dspace.org/

Geotechnical review of stope design for the sf3 orebody at Rosh Pinah Zinc Mine

Shali, George Peingondjambi

2022

https://hdl.handle.net/10539/34165

Downloaded from a DSpace repository. https://dspace.org/



UNIVERSITY OF THE
WITWATERSRAND,
JOHANNESBURG

FACULTY OF ENGINEERING AND BUILT ENVIRONMENT

GEOTECHNICAL REVIEW OF STOPE DESIGN FOR THE SF3 OREBODY AT ROSH PINAH ZINC MINE

George Peingondjambi Shali

A thesis submitted to the Faculty of Engineering and Built Environment, University of the Witwatersrand, Johannesburg, in fulfilment of the requirements for a Master of Science in Engineering.

Johannesburg, 2021

DECLARATION

I declare that this dissertation is my own, unaided work. It is being submitted for the Degree of Master of Science in the University of the Witwatersrand, Johanesburg. It has not been submitted before for any degree or examination in any other University.



……

(Signature of candidate)

……04……day of ……November…….(year)……2021……..

At……Karibib……..

ABSTRACT

Rosh Pinah Zinc underground mine is located in the south of Namibia, 18 km from the Orange River and 100 km from the town of Oranjemund. The zinc-lead deposit is extracted via the open stoping mining method. The stability of open stopes was analysed with empirical and numerical modelling.

The application of the stability graph method proposed by Potvin was used to analyse the stability of stope surfaces. Care was taken concerning the limitations of the stability graph method, which does not take into account the stress orientation relative to the stoping method. Furthermore, the stability graph does not consider the blasting effects occurring during stope blasting as well as in the vicinity around the stoping area.

This project explores the impact of using a non-linear Improved Unified Constitutive Model (IUCM) using FLAC3D, which can provide estimates of the amount of over break to be expected as well as using traditional empirical stability methods to predict dilution. Over break in numerical modelling was interpreted using both the principal stresses and volumetric strain to forecast the expected level of dilution during the mining process using the numerical method. Furthermore, dilution using empirical methods was estimated using the equivalent linear overbreak slough.

The results from numerical modelling indicated that the upper mined out stopes were stable and no major dilution was envisaged, and this was proved by use of the Cavity Monitoring System for mined out levels of 230 and 200. Furthermore, it was found that both empirical models and numerical modelling indicated a large amount of dilution to be expected as mining progresses downwards from Level 050 to Level -040 – owing to an increase in size of the stopes.

ACKNOWLEDGEMENT

I acknowledge the guidance and assistance I got from my supervisor, Professor Rudrajit Mitra. His wide knowledge and experience on the subject, coupled with his patience and drive for excellence is much appreciated and I have gained invaluable skills.

Abouzar Vakili and Tom Styles from Carvroc Pty (Ltd), Australia for allowing me to use the StopeX model and in providing me assistance and resources used in this research.

I would like to thank the Management and staff at Rosh Pinah Zinc Mine for their cooperation, and for affording me the opportunity to use the operations as a case study.

TABLE OF CONTENTS

DECLARATION i
ABSTRACT ii
ACKNOWLEDGEMENT iii
List of Figures vi
List of Tables viii
1 Introduction 1
1.1 Background 1
1.2 Objective and scope of the thesis 1
1.3 Research methodology 2
1.4 Content of the dissertation 3
2 Literature Review 4
2.1 Background 4
2.1.1 Sublevel open stoping mining method 4
2.1.2 Dilution and its effects 5
2.2 Rock mass classification systems 6
2.2.1 Rock Quality Designation (RQD) 7
2.2.2 Geological Strength Index (GSI) 8
2.2.3 Rock Mass Rating System (RMR) 10
2.2.4 Rock Mass Index (RMi) 12
2.2.5 Rock Tunnelling Quality Index (Q-system) 15
2.3 Using empirical methods to estimate dilution 18
2.3.1 O'Hara's Dilution Method 19
2.3.2 Dilution graph ELOS method 20
2.3.3 Stability graph method 22
2.4 Cable bolt support 28
2.5 Numerical Modelling 30
2.5.1 Mohr–Coulomb failure criteria 31
2.5.2 Hoek–Brown Failure Criterion 33
2.5.3 Improved Unified Constitutive Model 36
2.5.3.1 Unconfined compressive strength and elastic modulus 38
2.5.3.2 Elastic properties 40
2.5.3.3 Rock strength anisotropy 42
2.5.3.4 Hoek-Brown material constant m_i 43
2.5.3.5 Disturbance factor (D) 44
2.5.4 Peak failure criteria 46

2.5.5 Post peak failure criteria 47
2.6 Summary 48
3 Review of Rosh Pinah Zinc Mine 49
3.1 Rosh Pinah Zinc mining history 49
3.2 Regional geology of Rosh Pinah Mine 50
3.3 Mining geology 51
3.4 Mining Method 55
3.4.1 In situ stress regime and measurement 55
3.4.2 Design of open stopes 61
3.4.3 Rock Mass Model 62
3.4.4 Rock Quality Designation 63
3.4.5 Geological Strength Index (GSI) 64
3.5 Rock Mass Classification 65
3.6 Empirical stope design methods 65
3.7 Stope excavation support 70
3.8 Support requirements for SF3 stopes 71
3.9 Summary 73
4 Numerical modelling of the SF3 orebody 74
4.1 Conceptual rock mass for SF3 orebody 74
4.2 Modelling construction and approach 75
4.3 Numerical modelling results and interpretation 77
4.3.1 Volumetric strain 78
4.3.2 Stress factor 80
4.4 Summary 81
5 Conclusions and recommendations 82
6 References 84
7 Appendix A 92
7.1 Mechanical properties of rock masses 92

List of Figures

Figure 1. Basic geometry of an underground open stope (Urli, 2015). 5
Figure 2. Conventional method of evaluating RQD from drill core (Hutchinson & Diederichs, 1996). 7
Figure 3. Geological Strength Index (GSI) for jointed rock masses (Hoek, 2003). 9
Figure 4. The joint parameter (JP) found from the joint condition factor (jC) and various measurements of jointing intensity (Vb, Jv, RQD). (Palmstrom, 1995) 13
Figure 5. Waste rock dilution estimate (O'Hara, 1980). 19
Figure 6. Equivalent Linear Overbreak Slough (ELOS) (Pakalnis & Clarke, 1994). 20
Figure 7. Stability graph (Clark, 1998). 21
Figure 8. Stability Graph Factor A (Potvin, 1988). 24
Figure 9. Stability Graph Factor B (Potvin, 1988) 25
Figure 10. Stability Graph Factor C (Potvin, 1988) 26
Figure 11. Hydraulic Radius, HR (Hutchinson & Diederichs, 1996). 27
Figure 12. Database of unsupported stope (Potvin, 1988; Nickson, 1992). 27
Figure 13. Cable bolt density chart (Potvin, 1988). 28
Figure 14. Guidelines for cable spacing and density - overall stope face stability (Nickson, 1992) 29
Figure 15. Schematic diagram suggesting the range of application of continuum and discontinuum modelling in relation to the Q-value (modified from Barton, 1998) 30
Figure 16. Mohr–Coulomb failure criterion in terms of: a) principal stresses; b) normal and shear stresses (Edelbro, 2004). 32
Figure 17. Quantification of GSI chart (Cai et al., 2003). 38
Figure 18. Scale effect relations for intact rock UCS (Yoshinaka et al., 2008) 39
Figure 19. Theoretical variation of uniaxial compressive strength depending on orientation with respect to anisotropy plane (Ramamurthy et al, 1993, as referenced by Palmstrom, 1994). 42
Figure 20. Location of Rosh Pinah Zinc Mine (Google Maps, 2019) 49
Figure 21. Tectonic subdivision of the Gariep Belt (modified from Frimmel, 2000a) 51
Figure 22. Simplified geological map of the SF3 orebody. 52
Figure 23. An example of arkose drill core. 53
Figure 24. An example of a microquartzite drill core. 53
Figure 25. An example of a carbonate drill core. 53

Figure 26. An example of a breccia drill core. 54
Figure 27. A section showing faults in the Rosh Pinah Mine area (Flavianu, 2015). .55
Figure 28. Orientation of horizontal *in situ* stresses (Stacey & Swart, 2001). 56
Figure 29. A plan showing the location of measurements in relation to the orebody mined out stopes (Handley & Piper, 2014).....57
Figure 30. Sections of over core showing strain cells (Handley & Piper, 2014).....58
Figure 31. A plot of stress vs depth for both measurement one and two.....60
Figure 32. A plot of the K ratio for both measurement one and two. 61
Figure 33. Rock mass model depicting RQD for SF3 orebody. 63
Figure 34. A histogram showing the log average RQD.....64
Figure 35. Stability graph for unmined stopes (Hutchinson & Diederichs, 1996). 68
Figure 36. A graph showing the Equivalent Linear Overbreak Slough (ELOS) (Brady et al., 2005). 69
Figure 37. Design chart for cable bolt density (cable bolt/m^2)(Potvin,1988).....72
Figure 38. A graph showing estimates of cable bolt lengths (Hutchinson & Diederichs, 1996). 73
Figure 39. Geometry of a model indicating the topography as well as the orebody geometry. 76
Figure 40. Front view, showing the model sequence (Shali & Vakili, 2019).....77
Figure 41. Visual representation of the degree of rock disintegration at various levels of volumetric strains (Vakili et al., 2012). 78
Figure 42. Isosurface of 0.5, 1 and 3% volumetric strain. 80
Figure 43. Visual representation of the minor and major principal stress. 81

List of Tables

Table 1. RMR classification of rock masses (Bieniawski, 1989). 11
Table 2. Input parameters to RMi (Palmstrom, 2014). 14
Table 3. RQD- Rock Quality Designation (NGI, 2014). 16
Table 4. In-Joint set number (NGI, 2014)..... 16
Table 5. Jr-Joint set-roughness number (NGI, 2014). 16
Table 6. Ja-Joint alteration number (NGI, 2014). 17
Table 7. Jw-Joint water reduction factor (NGI, 2014). 17
Table 8. SRF-Stress reduction factor (NGI, 2014). 17
Table 9. ELOS categories (Pakalnis et al., 1996) 22
Table 10. Input parameters used in the IUCM (Vakili, 2016) 37
Table 11. Classification of anisotropy intensity in various rocks (modified from Tsidzi, 1990; Singh et al, 1989; Ramamurthy et al, 1993; Palmstrom, 1994). 43
Table 12. Values of the constant mi for intact rock by group (Hoek & Brown, 1997). 44
Table 13. Guidelines for estimating the disturbance factor D (Hoek et al., 2002) 45
Table 14. Stress measurement readings at WF3 – 030. 59
Table 15. Joint properties from core logging 62
Table 16. Lithological domains and geotechnical rock mass parameters. 65
Table 17. Stability graph parameter estimates 66
Table 18. Relative block size factor for hanging walls 71
Table 19. Input parameters used for forward analysis for the SF3 orebody. 74

1 Introduction

1.1 Background

The increase in demand for raw material has placed a significant pressure on mining companies as this has led to a depletion of high grade ore bodies with good spatial conditions and less complex mineralogy for which operational costs were generally lower. Hence, the increase demand has led to the exploitation of deeper orebodies with lower ore grade and more complex mineralogy that in turn has led to an increase in operational costs as well as increased dilution. According to Le Roux (2015), dilution above 10% can affect the profitability of the mine.

In underground mines, an early attempt to minimise costs of mining is to ensure that minimum dilution takes place during the extraction of the orebody. According to Ponierwierski (2005), "stope sizes should be as large as possible to obtain high productivity and low unit costs – yet also small enough to achieve sustained production rates." Hence, as a result of less dilution, a mining project can become more economical, resulting in cost saving that can yield high returns for the company. Cepuritis (2010) noted that "in order to develop an appropriate mine design, a thorough understanding of the rock mass conditions and its potential response to mining is required." The use of both empirical methods and numerical modelling is required to assess the potential of dilution. When both empirical and numerical modelling are used together with site-based experience, a good understanding of the behaviour rock mass can be attained. Cepuritus (2010) highlighted that "a major stumbling block in the stope design process is the way in which geotechnical data are collected, analysed, interpreted and used to construct a geotechnical model".

1.2 Objective and scope of the thesis

The objective of this research is to enhance the understanding of the design of open stopes to be mined for the SF3 orebody – using both empirical methods and numerical modelling. The proposed mining sequence and mining method for the SF3 orebody is a total extraction top/down sublevel open stoping, which will be assessed. By using both empirical and numerical techniques, an estimate of the future dilution and stability of the stopes can be anticipated.

The research has the following objectives:

- Carry out geotechnical mapping and logging to characterise the rock mass
- Discuss different measures to reduce dilution
- Discuss and apply empirical methods to estimate stope stability
- Discuss and apply numerical modelling techniques to help with stope stability investigation
- Estimate the amount of dilution for the envisaged stopes
- Evaluate the outcomes of the study and provide recommendations.

1.3 Research methodology

Internal literature based on the geotechnical environment from the mine's data archive will form part of data collection. Mapping will focus on sidewalls forming the hanging walls and footwalls, in order to gather adequate information to estimate the mechanical properties of the rock mass that will be used for empirical and numerical methods.

In this research two design methods will be used to investigate the stability of stopes:

a) Empirical methods
b) Numerical modelling methods.

An investigation of the relevant parameters required to understand the geotechnical environment will be obtained from mapping as well as intact laboratory strength tests. According to Le Roux (2015), "empirical design methods involve making use of design criteria and design lines, which are estimated from the analysis of field data for case studies, coupled with engineering judgement." Furthermore, the use of numerical modelling will be carried out using the Improved Unified Constitutive Model proposed by Vakili (2017).

The methodology adopted can be summarised as follows:

- Determine the N' stability number as well as Q' from rock mass classification
- Calculate the hydraulic radius from open stopes
- Obtain the equivalent linear overbreak slough for all stopes
- Carry out numerical modelling using the Improved Unified Constitutive Model
- Evaluate the obtained volumetric strain from numerical modelling
- Compare the dilution obtained from empirical methods vs numerical modelling.

1.4 Content of the dissertation

Chapter 1 provides an overview of the research project and its objectives. Chapter 2 details the literature review of both empirical methods and the IUCM constitutive model used in FLAC3D. The strengths and limitations of both empirical and numerical modelling are explored. Chapter 3 covers the application of empirical methods by using the mechanical properties of the rock mass that were obtained from mapping to estimate the dilution of open stopes. The use of the Improved Unified Constitutive Model will be discussed in Chapter 4, which discusses the numerical modelling used to determine the stability of open stopes. The IUCM will be built into FLAC3D and results will be analysed.

The last chapter provides a summary and conclusions of the findings of the research. Future work and recommendations will also be included.

2 Literature Review

This chapter describes concepts used in the evaluation of stope stability, which will include empirical and numerical methods. The SF3 stopes will be analysed individually by use of empirical methods such as Matthews N' stability number, as well as the concept of equivalent linear overbreak slough.

2.1 Background

2.1.1 Sublevel open stoping mining method

According to Pakalnis et al. (1996), open stoping mining method has grown in popularity since 1970 and at the end of the 20th century more than 50% of all Canadian underground metal mines in production were using the underground open stoping mining method. The sublevel open stoping method is often used to extract massive or tabular ore bodies characterised as the high productivity method. Brady and Brown (1985) suggested that open stoping usually requires freestanding stope boundaries and hence the orebody as well as the country rock should have sufficient strength to provide stable wall faces and crown for excavation. Usually, open stoping methods are non-entry and are known as one of the low cost and safest of mining methods.

The configuration of stopes follows two basic concepts: longitudinal and transverse configurations. According to Villaescusa (2014), "for thick orebodies, the stopes are oriented perpendicular (transverse) to the strike of the deposit, with pillars left between the primary stopes." With narrow orebodies, a longitudinal configuration is favoured. Firstly, footwall haulage drifts are developed parallel to the orebody at the top and bottom of the orebody – from where blasted ore will be transported, as shown in Figure 1. Cross cuts perpendicular to the orebody are developed. For both methods, blast holes are drilled in fans from sill access drives and are charged with explosives. Once the ore is blasted, it is mucked from the draw points and is transported via the haulage drift to an ore pass or may be transported via a conveyor belt to the primary crusher.

Hustrulid and Bullock (2001) emphasised that “developing the set of drifts and drawpoints underneath the stope is an extensive and costly procedure.” Furthermore, sublevel open stoping can lead to high dilution, resulting from design parameters from a planning and geotechnical perspective.

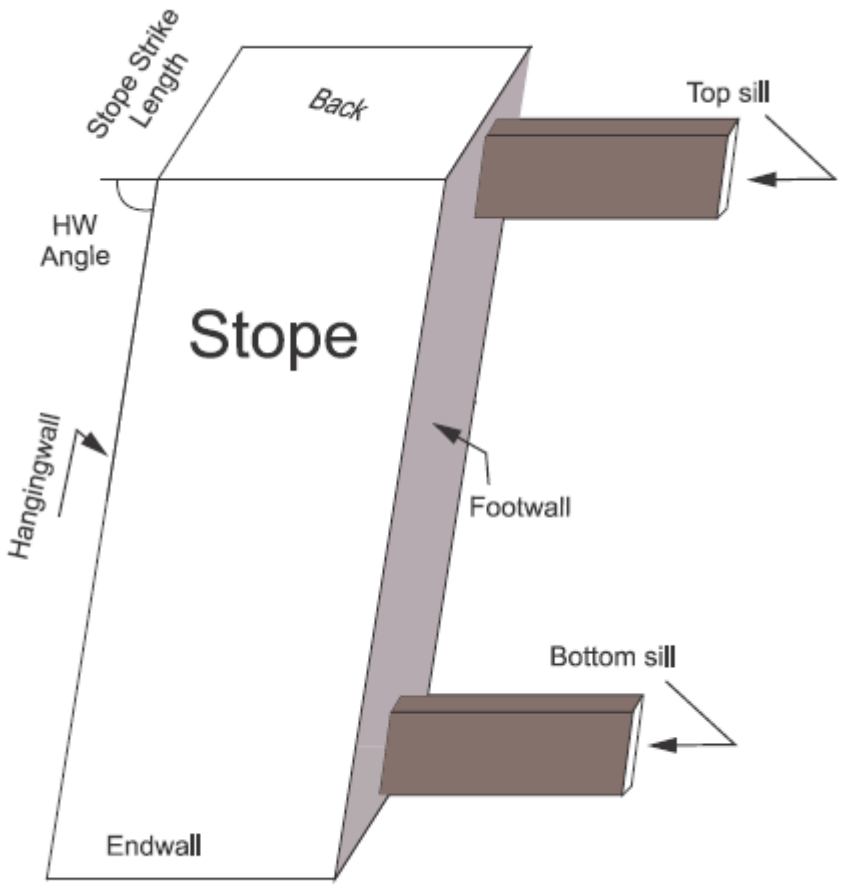


Figure 1. Basic geometry of an underground open stope (Urli, 2015).

2.1.2 Dilution and its effects

According to Urli (2015), the definition of dilution in the context of open stoping method is the amount of waste material that is drawn from the stope and which enters the ore-processing stream, lowering the average grade of the ore known as head grade. There are quite a number of definitions outlined by Pakalnis et al (1995); however, a more common definition of dilution is given in equation 2.1 as:

$$Dilution = \frac{Tons\ waste\ mined}{Tons\ ore\ mined} \quad 2.1$$

According to Elbrond (1994) “Life of mine, net present value, cost of producing metal, and loss of metal are all affected by dilution.” Usually, dilution is introduced into the stope from caved material in the hanging wall as well as the footwall of the stope. Several factors that contribute to dilution are mostly related to factors that contribute to stope wall instability such as poor drilling and blasting practices, weak ground conditions, irregular stope shapes and sizes. One of the common systems used to estimate dilution is by using rock mass classification systems in order to understand the inherent strength of the rock mass which will be explored in the next section.

2.2 Rock mass classification systems

According to Crockford (2012), “classification systems are empirical correlations between various quantifiable rock mass properties and the observed mechanical properties during underground excavations.” Various rock mass classification systems have been used by practitioners around the world and some of the widely used classification systems are Rock Tunnelling Quality Index (Barton et al., 1974); Rock Mass Rating (Bieniawski, 1989); Geological Strength Index (Hoek et al., 1992); and the Rock Quality Designation (Deere et al., 1967)

Bieniawski (1993) noted that rock mass classification methods had been designed to behave as an engineering design tool; however, they were not intended to substitute field observation, analytical consideration, measurements and engineering judgement. One of the advantages of rock mass classification is that it is easy to apply and acts as a means of understanding the geotechnical environment at the feasibility stage of the project. Hoek (2007), noted that a classification entity loses its significance and reliability when utilized in an area for which it will not be designed, or when it's utilized on a site with circumstances that had been not analysed within the empirical growth of the system.

2.2.1 Rock Quality Designation (RQD)

The concept of RQD was developed by Deere et al. (1967) to provide a quantitative means of measuring the quality of drilled core to assess support requirements. RQD can be defined as the percentage of intact core pieces of natural fractures that are greater than 10 cm long over the total core run (Figure 2) (Hutchinson & Diederichs, 1996). One of the advantages of using the RQD is that it is a quick and inexpensive method to determine the quality of the rock mass. According to ASTM (1997), RQD is widely used as an indicator of low-quality rock zones that may need greater attention or require additional boring or other investigational work. Figure 2 illustrates how the RQD can be calculated from the total length of the core run:

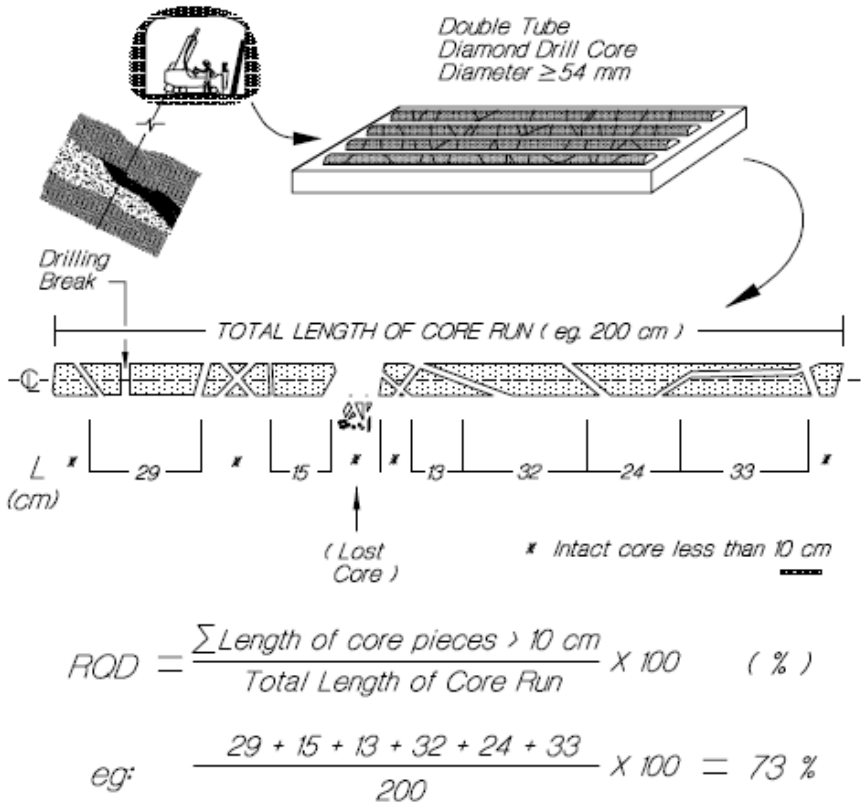


Figure 2. Conventional method of evaluating RQD from drill core (Hutchinson & Diederichs, 1996).

On the other hand, it is also noted that RQD can be affected by orientation of the borehole with respect to joint sets. Villaescusa (2014) further stated that some of the disadvantages of using the concept of RQD are highly dependent on factors such as

data collection from different core sizes, core loss experience in heavily fractured rock masses, as well as mechanical disturbances during the process of drilling.

A The RQD varies between 0 and 100%. A poor rock mass is represented by an RQD in the range of 0-25% whilst a good rock mass is represented by an RQD greater than 75%.

2.2.2 Geological Strength Index (GSI)

In search of a solution for a problem of estimating the strength of jointed rock masses and to provide a basis for design of underground excavations, Hoek and Brown (1980a,b) (Figure 3) developed the GSI to estimate the strength of the rock mass from the lithology, structure and surface conditions of the rock mass. Hence the GSI was developed out of a need for a quantifiable characterisation of the rock mass for use in the Hoek-Brown failure criterion and hence to overcome some of the deficiencies identified in the RMR (Hoek & Brown, 1997). On the other hand, the GSI does not exclusively include the Uniaxial Compressive Strength of the intact rock, as well as water and stress levels within a given rock mass.

The GSI of a rock mass can be defined by several charts, with the general chart shown in Figure 3. According to Crockford (2012), a high GSI value implies that the structure degrades the rock mass to a lesser extent from measured intact properties; whereas a smaller GSI value implies that the structural features influence the rock mass strength and intact values are not representative.

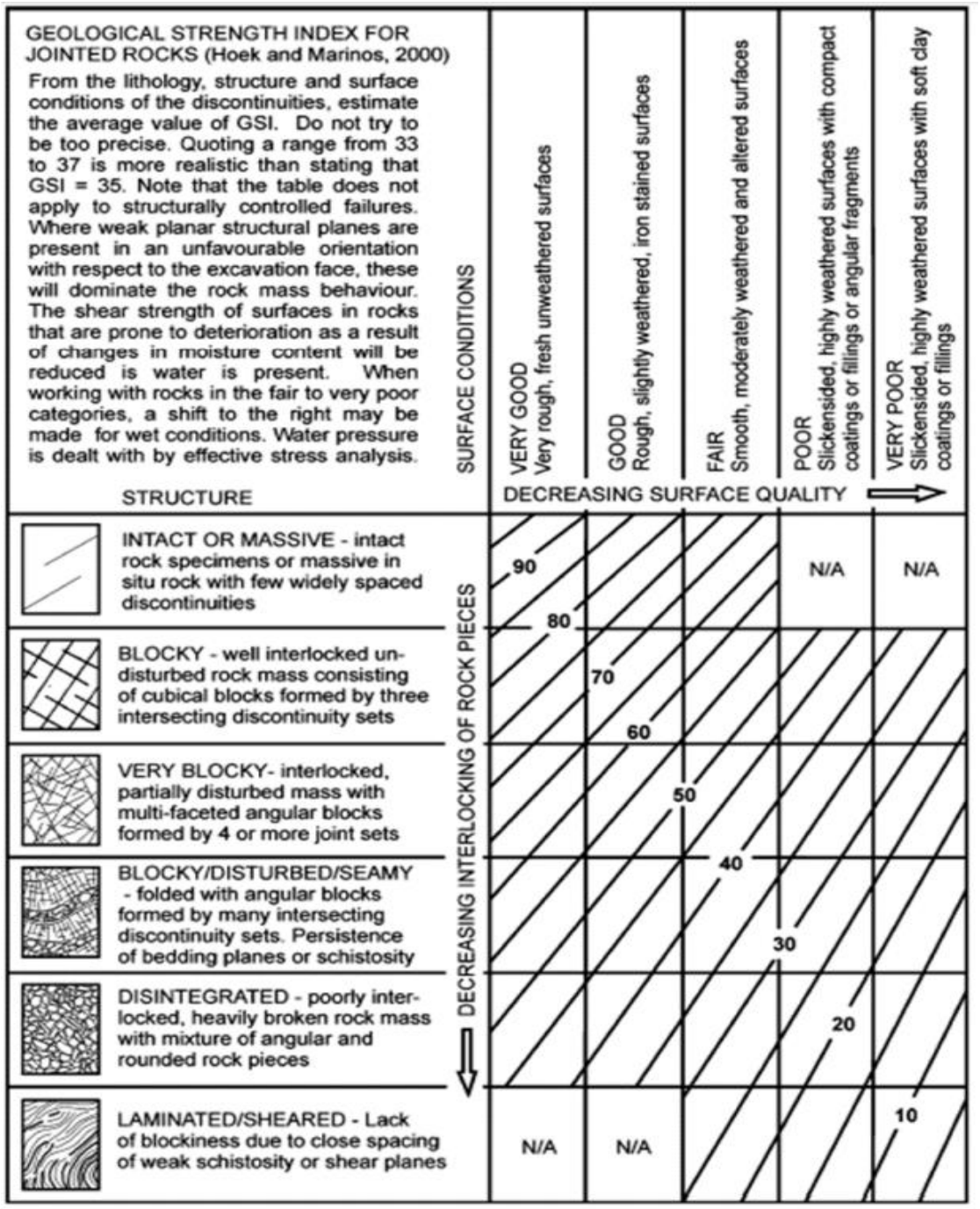


Figure 3. Geological Strength Index (GSI) for jointed rock masses (Hoek, 2003).

2.2.3 Rock Mass Rating System (RMR)

The Rock Mass Rating System developed by Bieniawski between 1973 and 1976 was developed in South Africa in shallow civil engineering excavations of sedimentary rocks. Since then, the method has successfully been refined and improved by Bieniawski and other authors to apply the RMR system in other geotechnical fields, such as mining, slopes, and dam foundation (Crockford, 2012). The method utilises six parameters in order to classify the rock mass and these parameters are obtained during site investigation and characterisation. The six parameters are:

- Uniaxial strength of intact rock material
- Rock Quality Designation
- Joint spacing
- Joint condition
- Ground water condition
- Joint orientation.

The parameters for the RMR are assigned values using Table 1. The overall RMR is obtained by adding the values of the ratings determined in sections A and B, and assigning a rock mass class in section C. The rock mass class determined in section C varies from 0 for poor rock masses to 100 for very good rock mass qualities. The rock mass class determined in section C can then be used to determine the cohesion, frictional angle and stand up time of the rock mass.

Table 1. RMR classification of rock masses (Bieniawski, 1989).

A. CLASSIFICATION PARAMETERS AND THEIR RATINGS

PARAMETER			Range of values // ratings						
1	Strength of intact rock material	Point-load strength index	> 10 MPa	4 - 10 MPa	2 - 4 MPa	1 - 2 MPa	For this low range uniaxial compr. strength is preferred		
		Uniaxial com-pressive strength	> 250 MPa	100 - 250 MPa	50 - 100 MPa	25 - 50 MPa	5 - 25 MPa	1 - 5 MPa	< 1 MPa
		RATING	**15**	**12**	**7**	**4**	**2**	**1**	**0**
2	Drill core quality RQD		90 - 100%	75 - 90%	50 - 75%	25 - 50%	< 25%		
		RATING	**20**	**17**	**13**	**8**	**5**		
3	Spacing of discontinuities		> 2 m	0.6 - 2 m	200 - 600 mm	60 - 200 mm	< 60 mm		
		RATING	**20**	**15**	**10**	**8**	**5**		
4	Condition of discon-tinuities	Length, persistence	< 1 m	1 - 3 m	3 - 10 m	10 - 20 m	> 20 m		
		Rating	**6**	**4**	**2**	**1**	**0**		
		Separation	none	< 0.1 mm	0.1 - 1 mm	1 - 5 mm	> 5 mm		
		Rating	**6**	**5**	**4**	**1**	**0**		
		Roughness	very rough	rough	slightly rough	smooth	slickensided		
		Rating	**6**	**5**	**3**	**1**	**0**		
		Infilling (gouge)	none	Hard filling		Soft filling			
			-	< 5 mm	> 5 mm	< 5 mm	> 5 mm		
		Rating	**6**	**4**	**2**	**2**	**0**		
		Weathering	unweathered	slightly w.	moderately w.	highly w.	decomposed		
		Rating	**6**	**5**	**3**	**1**	**0**		
5	Ground water	Inflow per 10 m tunnel length	none	< 10 litres/min	10 - 25 litres/min	25 - 125 litres/min	> 125 litres /min		
		p_w / $\sigma 1$	0	0 - 0.1	0.1 - 0.2	0.2 - 0.5	> 0.5		
		General conditions	completely dry	damp	wet	dripping	flowing		
		RATING	**15**	**10**	**7**	**4**	**0**		

p_w = joint water pressure; $\sigma 1$ = major principal stress

B. RATING ADJUSTMENT FOR DISCONTINUITY ORIENTATIONS

		Very favourable	Favourable	Fair	Unfavourable	Very unfavourable
RATINGS	Tunnels	**0**	**-2**	**-5**	**-10**	**-12**
	Foundations	**0**	**-2**	**-7**	**-15**	**-25**
	Slopes	**0**	**-5**	**-25**	**-50**	**-60**

C. ROCK MASS CLASSES DETERMINED FROM TOTAL RATINGS

Rating	100 - 81	80 - 61	60 - 41	40 - 21	< 20
Class No.	I	II	III	IV	V
Description	VERY GOOD	GOOD	FAIR	POOR	VERY POOR

D. MEANING OF ROCK MASS CLASSES

Class No.	I	II	III	IV	V
Average stand-up time	10 years for 15 m span	6 months for 8 m span	1 week for 5 m span	10 hours for 2.5 m span	30 minutes for 1 m span
Cohesion of the rock mass	> 400 kPa	300 - 400 kPa	200 - 300 kPa	100 - 200 kPa	< 100 kPa
Friction angle of the rock mass	< 45°	35 - 45°	25 - 35°	15 - 25°	< 15°

2.2.4 Rock Mass Index (RMi)

The RMi was developed by Palmstrom between 1986 and 1995 to characterise the rock mass strength of a material. It demonstrates the discount in inherent strength of the rock mass on account of the effects of joints (Singh & Goel, 1999). Equation 2.2 expresses the RMi in terms of the unconfined uniaxial compression test of the intact rock and the joint parameter:

$$RMi = \sigma_c \cdot JP \qquad 2.2$$

Where σ_c is the unconfined uniaxial compression test of the intact rock and JP is the jointing parameter with values ranging between 1 for an intact rock material and 0 for a crushed rock material.

Equation 2.3 illustrates the calculation for the joint parameter (JP) factor:

$$JP = 0.2\sqrt{jC} \cdot V_b^D \qquad 2.3$$

Where jC is the joint condition factor and V_b is the block volume measured in m^3, and D is a parameter derived from the joint condition jC using equation 2.4.

$$D = 0.37jC^{-0.2} \qquad 2.4$$

Figure 4 can be used to obtain the joint parameter JP from the block volume Vb and joint condition factor jC. As can be seen from the upper left part of Figure 4, the volumetric joint count (Jv) for numerous joint sets (or block shapes) might be used as an alternative to the block quantity (Vb), in addition to the RQD, however its incapability to characterise huge rock or extremely jointed rocks results in a decreased quality of JP (Palmstrom, 1996).

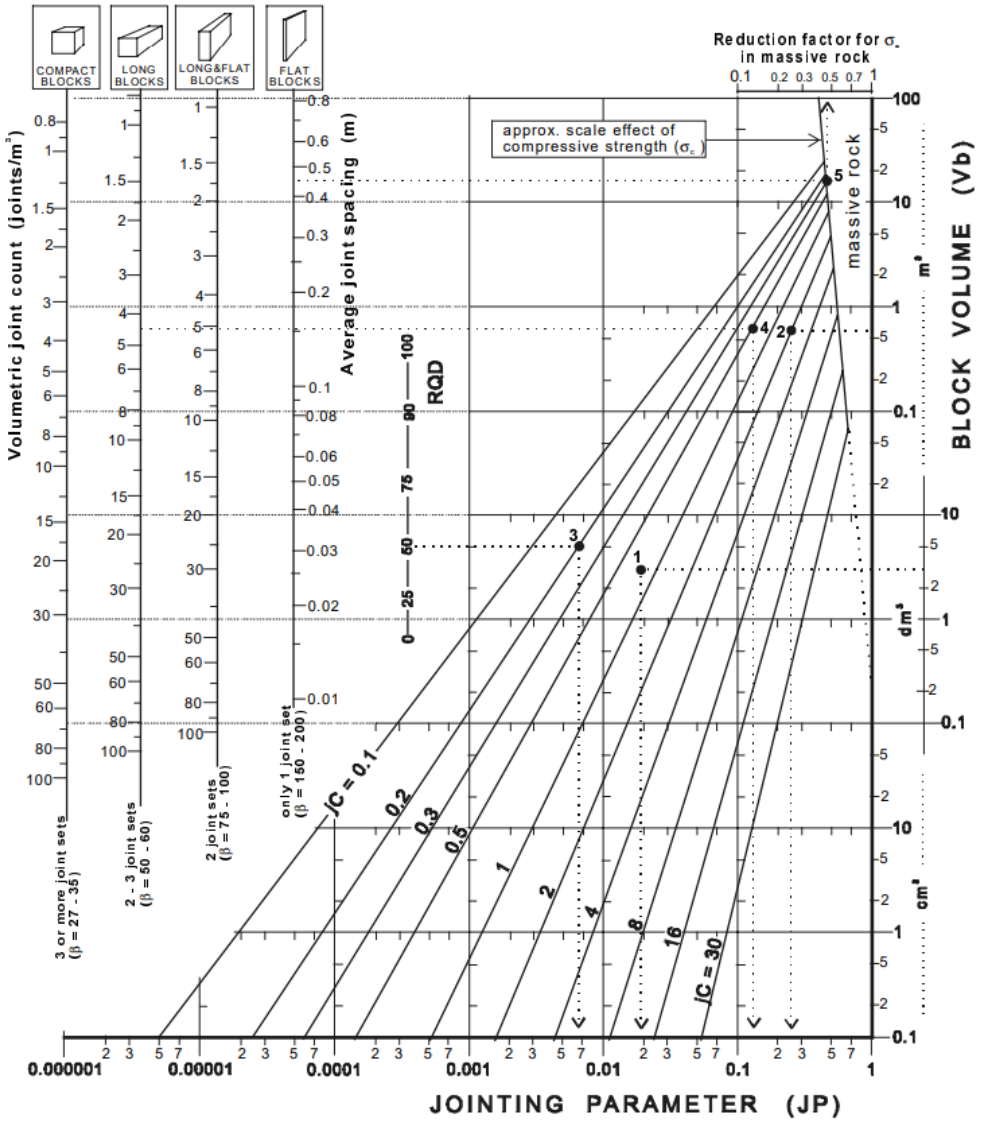


Figure 4. The joint parameter (JP) found from the joint condition factor (jC) and various measurements of jointing intensity (Vb, Jv, RQD). (Palmstrom, 1995).

The joint condition factor is related to jL, jR and jA, as can be seen in equation 2.5 (Singh & Goel, 1999):

$$jC = jL(\frac{jR}{jA}) \qquad 2.5$$

Where jC is the joint condition factor, jR is the joint roughness factor, jA is the joint alteration factor, and jL is a joint length and continuity factor. Table 2 can be used to determine the above-mentioned parameters:

Table 2. Input parameters to RMi (Palmstrom, 2014).

Uniaxial compressive strength of rock (UCS or σ_c)			**value** in MPa (from lab. tests or assumed from handbook tables)			
Block volume (Vb)			**value** in m³ (from observations at site or on drill cores, etc.)			
Joint condition factor (jC)			**jC = jR x jL / jA** (ratings of jR, jA and jL from the tables below)			
Joint roughness factor (jR) composed of large scale and small scale undulations (The ratings in ***bold italic*** are similar to Jr in Q-system)			**Large scale waviness of joint plane**			
			Planar	Slightly undulating	Undulating	Strongly undulating	Stepped or interlocking
Small scale smoothness of joint surface	Very rough		2	3	4	6	6
	Rough		***1.5***	2	***3***	4.5	6
	Smooth		***1***	1.5	***2***	3	4
	Polished or slickensided*)		***0.5***	1	***1.5***	2	3
For filled joints jR = 1 For irregular joints a rating of jR = 6 is suggested							
*) *For slickensided surfaces the ratings apply to possible movement along the lineations*							
Joint alteration factor (jA) (the ratings are based on Ja in the Q-system)							
Contact between joint walls	CLEAN JOINTS:	Healed or welded joints	filling of quartz, epidote, etc.				jA = 0.75
		Fresh joint walls	no coating or filling, except from staining (rust)				1
		Altered joint walls	- one grade higher alteration than the rock				2
			- two grades higher alteration than the rock				4
	COATING or THIN FILLING OF:	Frictional materials	sand, silt calcite, etc. without content of clay				3
		Cohesive materials	clay, chlorite, talc, etc.				4
						Thin filling (< 5mm)	Thick filling
Partly or no wall contact	THICK FILLING OF:	Frictional materials	sand, silt calcite, etc. (non-softening			jA = 4	8
		Hard, cohesive materials	clay, chlorite, talc, etc.			6	5 - 10
		Soft, cohesive materials	clay, chlorite, talc, etc.			8	12
		Swelling clay materials	material exhibits swelling properties			8 - 12	13 - 20
Joint size factor (jL) composed of the length and continuity of the joint						Continuous joints	Discont. joints*)
Bedding or foliation partings		length < 0.5 m				jL = 3	jL = 6
Joints		with length 0.1 - 1 m				2	4
		with length 1 - 10 m				1	2
		with length 10 - 30 m				0.75	1.5
(Filled) joint, seam or shear **)		length > 30 m				0.5	1
*) *Discontinuous joints end in massive rock* **) *Often a singularity and should in these cases be treated separately*							
Interlocking of rockmass structure (IL) (the ratings are based on the interlocking used in the GSI system)							
Very tight structure		undisturbed rock mass, well interlocked					IL = 1.3
Tight structure		undisturbed rock mass with some joint sets					**1**
Disturbed / open		folded / faulted with angular blocks					0.8
Poorly interlocked		broken with angular and rounded blocks					0.5

The RMi scheme shares some options just like these of the Q-system, akin to jR and jA, that are similar to the Jr and Ja within the Q-system (Palmstrom, 2014). According to Palmstrom (1996), the "RMi can easily be used for rough estimates in the early stages of a feasibility design of a project." Palmstrom (2014) further expanded the RMi for support estimation in various ground conditions from blocks to weak rock masses. By

using the RMi parameter JP, the s factor from the Hoek–Brown Criterion can be derived using the formula $s = JP^2$, and since the RMi includes a wide range of rock mass variations it has a wider application than other rock mass classification systems (Abbas & Heinz, 2015).

2.2.5 Rock Tunnelling Quality Index (Q-system)

According to Barton et al., (1974) "the Q-system was developed in 1974 by Barton, Lien and Lunde at the Norwegian Geotechnical Institute, Norway, for determining rock mass characteristics and tunnel support requirements." The Q-system is formulated using 212 case records from Scandinavia (Bieniawski, 1989).

The Q-system is formulated by assigning values using Tables 3 - 8 for the six parameters that are outlined into three quotients. The numerical value of Q varies from 0.001 for poor rock masses to 1000 for very high quality unjointed rock masses (Barton et al., 1974).

The following 6 parameters are used for the Q-system, as shown in equation 2.6:

$$Q = \left(\frac{RQD}{Jn}\right)\left(\frac{Jr}{Ja}\right)\left(\frac{Jw}{SRF}\right) \qquad 2.6$$

Where:

- RQD is the Rock Quality Designation
- Jn is the joint set number
- Jr is the joint roughness coefficient
- Ja is the joint alteration number
- Jw is the joint water reduction factor
- SRF is the stress reduction factor.

The initial quotient (RQD/Jn) is a representative of the crude measure of the block or particle size. The second quotient (Jr/Ja) is a representative of the roughness and frictional characteristics of the joint wall interfaces, as well as joint infill material. The third quotient (Jw/SRF) is regarded as the active stress component, where Jw is a

measure of water pressure and SRF is considered as the total stress parameter. Each of these parameters can be determined according to the descriptions found in Tables 3–8

Table 3. RQD- Rock Quality Designation (NGI, 2014).

Very poor	RQD = 0 - 25%
Poor	25 - 50
Fair	50 - 75
Good	75 - 90
Excellent	90 - 100
Notes: *(i) Where RQD is reported or measured as < 10 (including 0), a nominal value of 10 is used to evaluate Q* *(ii) RQD intervals of 5, i.e. 100, 95, 90, etc. are sufficiently accurate*	

Table 4. In-Joint set number (NGI, 2014).

Massive, no or few joints	Jn = 0.5 - 1
One joint set	2
One joint set plus random joints	3
Two joint sets	4
Two joint sets plus random joints	6
Three joint sets	9
Three joint sets plus random joints	12
Four or more joint sets, heavily jointed, "sugar-cube", etc.	15
Crushed rock, earthlike	20
Notes: *(i) For tunnel intersections, use (3.0 x Jn); (ii) For portals, use (2.0 x Jn)*	

Table 5. Jr-Joint set-roughness number (NGI, 2014).

a) Rock-wall contact, b) rock-wall contact before 10 cm shear		**c) No rock-wall contact when sheared**	
Discontinuous joints	Jr = 4	Zone containing clay minerals thick enough to prevent rock-wall contact	Jr = 1.0
Rough or irregular, undulating	3	Sandy, gravelly or crushed zone thick enough to prevent rock-wall contact	1.0
Smooth, undulating	2		
Slickensided, undulating	1.5		
Rough or irregular, planar	1.5	***Notes:*** *i) Add 1.0 if the mean spacing of the relevant joint set is greater than 3 m* *ii) Jr = 0.5 can be used for planar, slickensided joints having lineations, provided the lineations are oriented for minimum strength*	
Smooth, planar	1.0		
Slickensided, planar	0.5		
***Note**: i) Descriptions refer to small scale features, and intermediate scale features, in that order*			

Table 6. Ja-Joint alteration number (NGI, 2014).

	JOINT WALL CHARACTER		Condition	Wall contact
Contact between joint walls	CLEAN JOINTS	Healed or welded joints:	filling of quartz, epidote, etc.	Ja = 0.75
		Fresh joint walls:	no coating or filling, except from staining (rust)	1
		Slightly altered joint walls:	non-softening mineral coatings, clay-free particles, etc.	2
	COATING OR THIN FILLING	Friction materials:	sand, silt, calcite, etc. (non-softening)	3
		Cohesive materials:	clay, chlorite, talc, etc. (softening)	4

	FILLING OF:	Type	*Some wall contact* *Thin filling (< 5 mm)*	*No wall contact* *Thick filling*
Some or no wall contact	Friction materials	sand, silt calcite, etc. (non-softening)	Ja = 4	Ja = 8
	Hard cohesive materials	compacted filling of clay, chlorite, talc, etc.	6	5 - 10
	Soft cohesive materials	medium to low overconsolidated clay, chlorite, talc,	8	12
	Swelling clay materials	filling material exhibits swelling properties	8 - 12	13 - 20

Table 7. Jw-Joint water reduction factor (NGI, 2014).

Dry excavations or minor inflow, i.e. < 5 l/min locally	p_w < 1 kg/cm^2	Jw = 1
Medium inflow or pressure, occasional outwash of joint fillings	1 - 2.5	0.66
Large inflow or high pressure in competent rock with unfilled joints	2.5 - 10	0.5
Large inflow or high pressure, considerable outwash of joint fillings	2.5 - 10	0.3
Exceptionally high inflow or water pressure at blasting, decaying with time	> 10	0.2 - 0.1
Exceptionally high inflow or water pressure continuing without noticeable decay	> 10	0.1 - 0.05
Note: *(i) The last four factors are crude estimates. Increase Jw if drainage measures are installed* *(ii) Special problems caused by ice formation are not considered*		

Table 8. SRF-Stress reduction factor (NGI, 2014).

Weakness zones intersecting excavation	Multiple weakness zones with clay or chemically disintegrated rock, very loose surrounding rock (any depth)		SRF = 10
	Single weakness zones containing clay or chemically disintegrated rock (depth of excavation < 50 m)		5
	Single weakness zones containing clay or chemically disintegrated rock (depth of excavation > 50 m)		2.5
	Multiple shear zones in competent rock (clay-free), loose surrounding rock (any depth)		7.5
	Single shear zones in competent rock (clay-free), loose surrounding rock (depth of excavation < 50 m)		5
	Single shear zones in competent rock (clay-free), loose surrounding rock (depth of excavation > 50 m)		2.5
	Loose, open joints, heavily jointed or "sugar-cube", etc. (any depth)		5
Note: *(i) Reduce these SRF values by 25 - 50% if the relevant shear zones only influence, but do not intersect the excavation.*			
		σ_c / σ_1	σ_θ / σ_c SRF
Competent rock, rock stress problems	Low stress, near surface, open joints	> 200	< 0.01 2.5
	Medium stress, favourable stress condition	200 - 10	0.01 - 0.3 1
	High stress, very tight structure. Usually favourable to stability, may be except for walls	10 - 5	0.3 - 0.4 0.5 - 2
	Moderate slabbing after > 1 hour in massive rock	5 - 3	0.5 - 0.65 5 - 50
	Slabbing and rock burst after a few minutes in massive rock	3 - 2	0.65 - 1 50 - 200
	Heavy rock burst (strain burst) and immediate dynamic deformation in massive rock	< 2	> 1 200 - 400
Notes: *(ii) For strongly anisotropic stress field (if measured): when 5 < σ_1/σ_3 <10, reduce σ_c to 0.75 σ_c. When $\sigma 1/\sigma 3$ > 10, reduce σ_c to 0.5 σ_c* *(iii) Few case records available where depth of crown below surface is less than span width. Suggest SRF increase from 2.5 to 5 for low stress cases*			
			σ_θ / σ_c SRF
Squeezing rock	*Plastic flow of incompetent rock under the influence of high pressure*	Mild squeezing rock pressure	1 - 5 5 - 10
		Heavy squeezing rock pressure	> 5 10 - 20
Swelling rock	*Chemical swelling activity depending on presence of water*	Mild swelling rock pressure	5 - 10
		Heavy swelling rock pressure	10 - 15

The Q-system can be used to estimate the support requirements of excavations and to estimate the rock mass properties (Abbas & Heinz, 2015).

2.3 Using empirical methods to estimate dilution

The most common form of empirical method for dilution estimation was proposed by Pakalnis (2015). The method was developed in a joint collaboration between the Department of Mines of Manitoba, CANMET, and Rutton Mine of Hudson Bay Mining and Smelting Inc.

Clarke (1998) later expanded the concept of empirical stability methods using a database consisting of 43 stopes at various stages of mining – to compile the Equivalent Linear Overbreak Slough (ELOS). Information such as historical observation, in situ-stress, structural mapping and deformation monitoring were recorded. Another stope dilution method was proposed by O'Hara (1980), which was based on data collected from Canadian and international mines.

2.3.1 O'Hara's Dilution Method

One of the earliest methods to predict dilution was proposed by O'Hara (1980). The method compared stope width, stope wall sloughage against the stoping method, wall competence, and dip angle of stope. Three mining methods were used in the dilution estimate method: cut and fill, shrinkage stoping, and blasthole stoping.

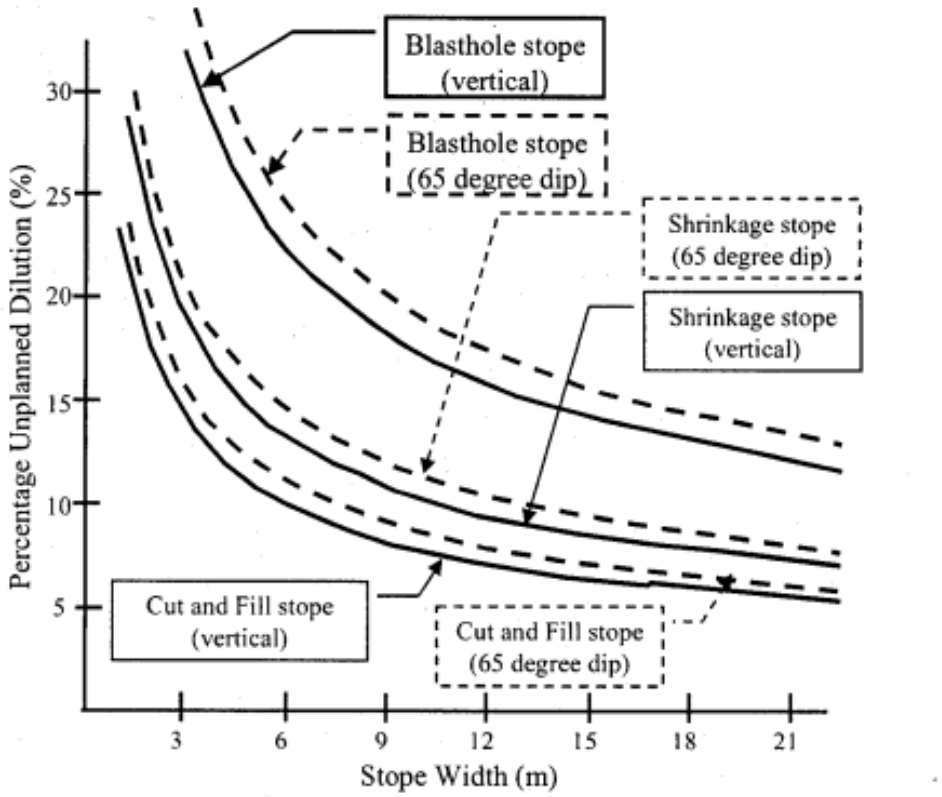


Figure 5. Waste rock dilution estimate (O'Hara, 1980).

Equation 2.7 was used to predict the dilution for blast hole stoping:

$$\%\ Dilution = \frac{100}{W^{0.5} sin A^{\circ}} \qquad 2.7$$

Where: W is the stope width in m and A is the orebody dip angle in degrees.

From Figure 5, it can be seen that dilution increases when the stope is at an angle away from the vertical. The percentage of unplanned dilution increases with an increase in

the width of the stope. Hence, from Figure 5, unplanned dilution is higher in the blast hole stoping mining method compared to the cut and fill method.

There are, however, a few shortcomings from O'Hara's dilution estimate method, such that there is no quantitative method assigned to the competence of the rock mass, e.g. the method on frequently used rock mass classification to quantify dilution. Furthermore, there is no clear information on how the method was formulated.

2.3.2 Dilution graph ELOS method

The ELOS is an empirical method using the Mathews stability number N', as well as the hydraulic radius (HR) that was developed by Clark and Pakalnis (1997). According to Woodward (2017), "the financial value of a stope is intrinsically linked to the success of the ore recovery, but it is also related to the amount of unintentional dilution." The ELOS is used to quantify the dilution of individual stopes – as well as the ultimate stope after the entire orebody has been mined. Figure 6 shows the illustration of ELOS and how it can be calculated using both the Cavity Monitoring System (CMS) and designed stope shape.

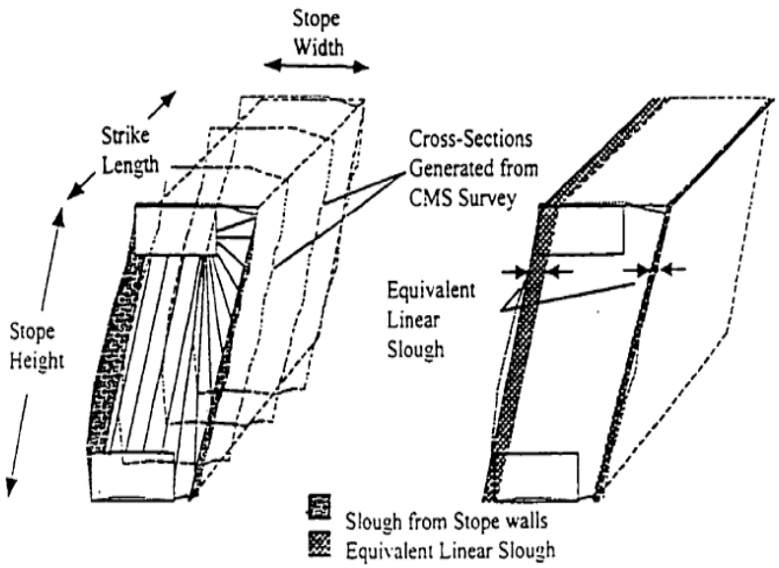


Figure 6. Equivalent Linear Overbreak Slough (ELOS) (Pakalnis & Clarke, 1994).

Equation 2.8 is used to determine the ELOS:

$$ELOS = \frac{Volume\ of\ slough}{Stope\ wall\ surface\ area} \qquad 2.8$$

According to Cepuritis (2014), inherent uncertainty associated with empirical methods implies that there is always a chance that designs will not perform as intended – resulting in adverse economic and safety implications.

Figure 7 shows the relationship between the N' stability number, hydraulic radius, and the equivalent linear overbreak slough.

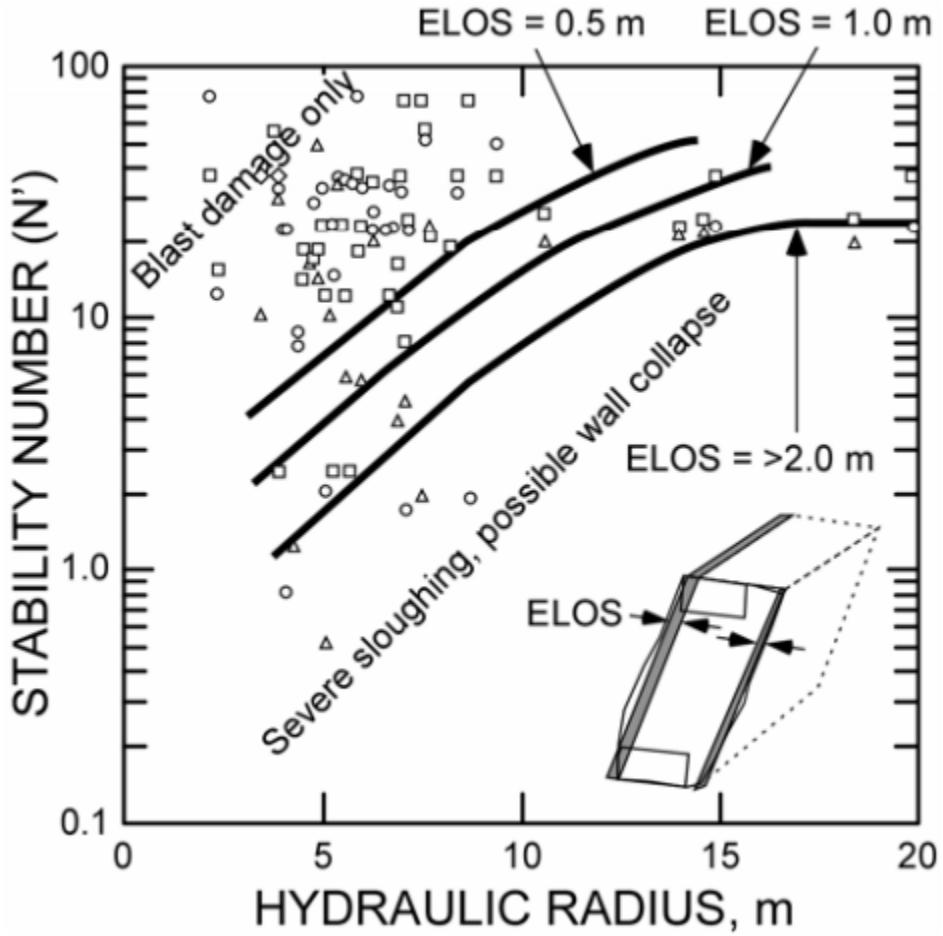


Figure 7. Stability graph (Clark, 1998).

According to Le Roux (2015), dilution can be estimated by plotting the modified stability number N' vs the hydraulic radius of stopes walls being assessed. Table 9

shows categorical descriptions of the severity of overbreak versus ELOS, where an ELOS of greater than 2 m indicates a possibility of unacceptable overbreak.

Table 9. ELOS categories (Pakalnis et al., 1996)

ELOS Value (m)	Category Description
0-0.5	Stable
0.5-2	Overbreak
>2	Significant overbreak

Cepuritis (2014) noted that Empirical open stope design strategies depend on categorised efficiency of open stope case histories and comparing this to the geometry of specific excavation and the perceived rock mass high quality. Some of the shortcomings of the ELOS method are that it does not include structural influence arising from faults and dykes around the orebody stope walls.

2.3.3 Stability graph method

According to Mawdesley et al. (2001), the "Mathews stability number N represents the ability of the rock mass to stand up under a given stress condition and the shape factor, S, or hydraulic radius accounts for the geometry of the surface." Potvin (1988) furthermore expanded the unique stability graph with a further 175 case histories and formulated the modified stability number, N', in the place of the Mathews' stability number, and these cases were primarily from Canadian mines. In 2014, Suorineni emphasised that the empirical methods should not be applied beyond the limits of their databases or be extrapolated. Suorineni (2014) further illustrated that the stability graph method was also created with the assumption of good ground conditions, as well as good blasting practices, and that the stopes are isolated with no nearby excavations. Equation 2.9 illustrates the modified stability number, which also incorporates a modified form of the Q system by excluding the third quotient as shown in Equation 2.10.

$$N' = Q'ABC \qquad 2.9$$

Where:

N' is the stability number

Q' is the modified Q

A is the factor that account for induced stress

B is the factor that accounts for orientation of joints with respect to stope surface

C is the factor that accounts for measure of influence of gravity

$$Q' = \left(\frac{RQD}{Jn}\right)\left(\frac{Jr}{Ja}\right) \qquad 2.10$$

Where *RQD* is referred to as the Rock Quality Designation of the rock mass, *Jn* is the joint set number, *Jr* is the joint roughness co-efficient, and *Ja* is the joint alteration number. These parameters can be obtained from face mapping as well as core logging.

A: ***Stress to strength effect factor***

The stress to strength ratio considers the induced stresses around the stope, and the strength of an intact rock sample. The assumption is that under low stress environments, there is low confinement and hence instability of stopes is likely to occur as opposed to high stresses.

The A factor can be obtained from equation 2.11:

$$A = 1.125R - 0.125 \qquad 1 > A > 0.1 \qquad 2.11$$

The value of A can be obtained more readily by calculating the ratio between the UCS and the maximum induced stress, as shown in Figure 8. The maximum induced stress can be obtained from numerical modelling.

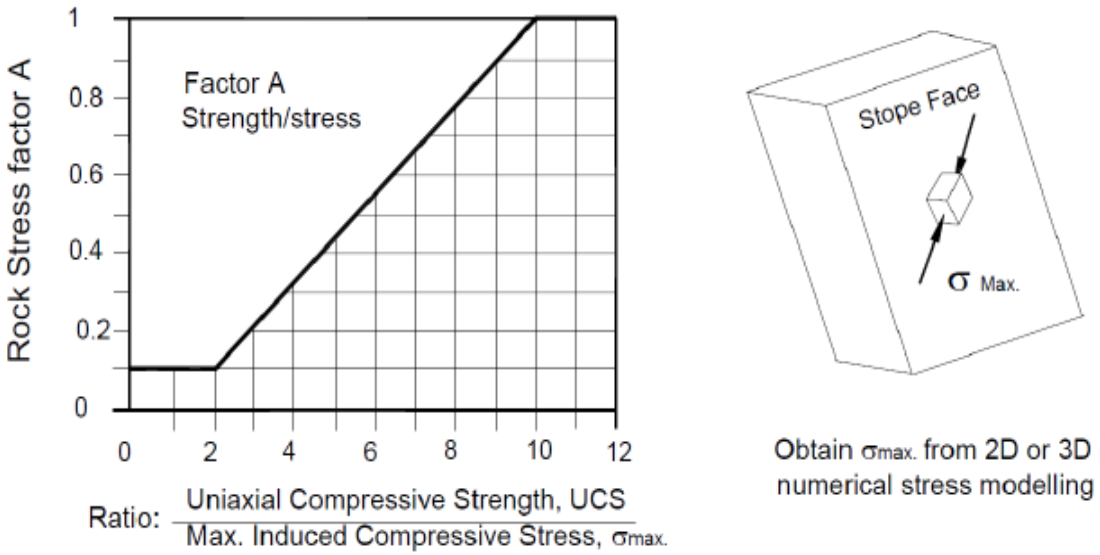


Figure 8. Stability Graph Factor A (Potvin, 1988).

B: ***Ease of block fallout factor***

Orientation of joint can be obtained from kinematic analysis, in order to obtain the dip of the critical joint that will be the joint with a steep dip. The most critical joint set can then be used to obtain the value of B. According to Brady et al. (2005), "the B factor looks at the influence of the orientation of discontinuities with respect to the surface analysed and states that joints oriented at 90° to a surface do not create stability problems." Equations 2.12 to 2.15 are used to calculate the B factor using α, which is the angle between the face pole and joint pole, as can be seen in Figure 9.

$B = 0.3 - 0.01$	$\alpha < 10$	2.12
$B = 0.2$	$10 < \alpha < 30$	2.13
$B = 0.02\alpha - 0.4$	$30 < \alpha < 60$	2.14
$B = 0.0067\alpha - 0.4$	$60 < \alpha < 90$	2.15

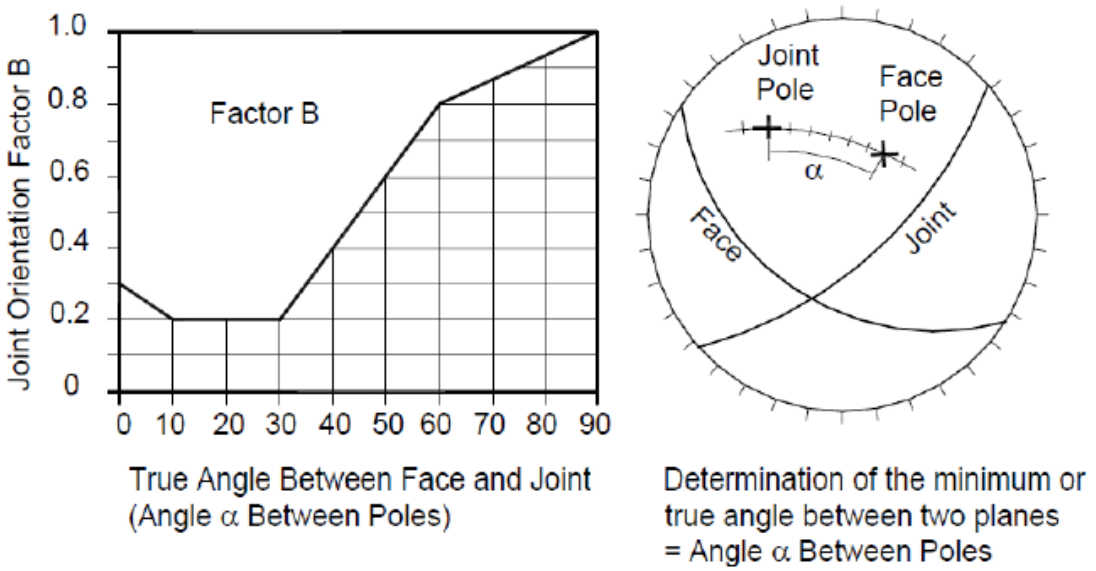


Figure 9. Stability Graph Factor B (Potvin, 1988).

C: ***Gravity adjustment factor***

According to Villaescusa (2014), the gravity adjustment factor – as can be seen in Figure 10 – is based mostly on the belief that due to gravity, a vertical stope wall is extra secure than a horizontal stope crown. The gravity adjustment factor can be obtained from the dip of the stope face by identifying the most likely structural failure mechanism.

In the instance where there is no joint sliding, the gravity factor C can be obtained from Equation 2.16:

$$C = 8 - 6\cos(Dip\ of\ stope\ face) \qquad 2.16$$

Where there is a possibility of joint sliding, Equations 2.17 and 2.18 can be used:

$$C = 8 \qquad Dip\ of\ critical\ joint < 30° \qquad 2.17$$

$$C = 11 - 0.1\ (Dip\ of\ the\ critical\ joint) \qquad Dip\ of\ critical\ joint > 30° \qquad 2.18$$

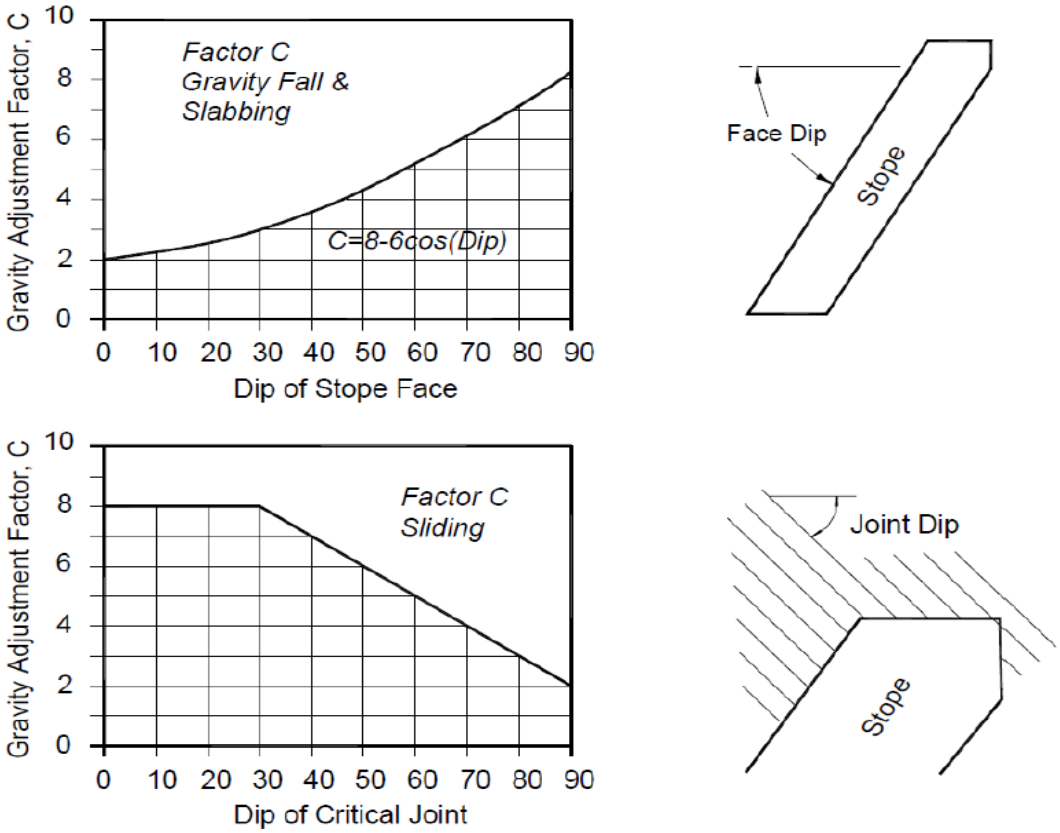


Figure 10. Stability Graph Factor C (Potvin, 1988).

The above parameters are obtained from field mapping as well as from intact laboratory testing.

The hydraulic radius, – as can be seen in Figure 11, – is usually utilised in massive mining methods as a size factor of an area to be mined. It is used in conjunction with the modified stability number N' to determine the stability of an open stope. Equation 2.19 shows how the hydraulic radius can be formulated:

$$HR = \frac{Area}{Perimeter} \qquad 2.19$$

Where the area can be obtained by multiplying the length and the width of the open stope, as well as obtaining the perimeter from the given stope dimensions.

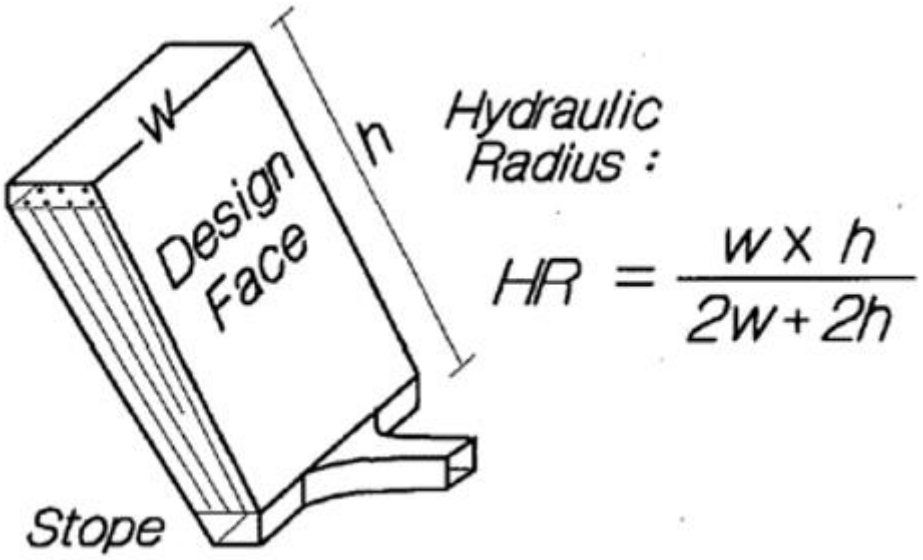


Figure 11. Hydraulic Radius, HR (Hutchinson & Diederichs, 1996).

The average expected dilution to be obtained by using the stability graph number, as well as the hydraulic radius, can be estimated by using a site-specific, calibrated dilution-based graph such as that shown in Figure 12. According to Papaioanou and Suorineni (2016), care should be used when using these stability graph methods, as they have been developed in narrow vein mining environments. The use of these graphs, however, can guide the user to make informed decisions during feasibility studies of mining projects.

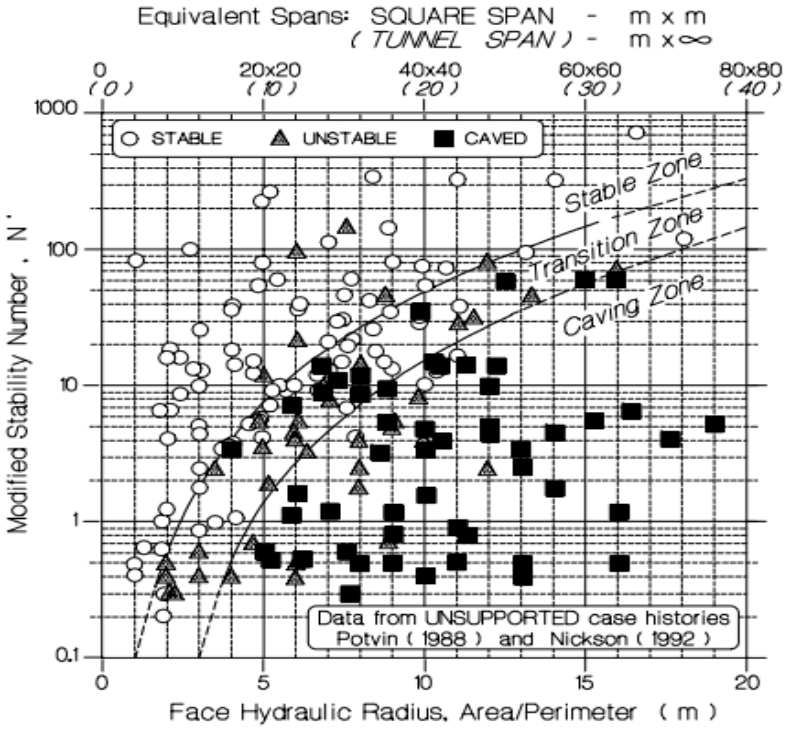


Figure 12. Database of unsupported stope (Potvin, 1988; Nickson, 1992).

2.4 Cable bolt support

In an effort to minimise dilution, cable bolting is currently used in most underground mining methods around the world. According to Hutchinson and Diederichs (1996), "a cable bolt is a flexible tendon consisting of a number of steel wires wound into a strand, which is grouted into a borehole." Cable bolts are generally grouted in the boreholes and can be tensioned, but are generally left un-tensioned as they are typically installed prior to the opening of the stope or sequentially during the stoping operations (Urli, 2015).

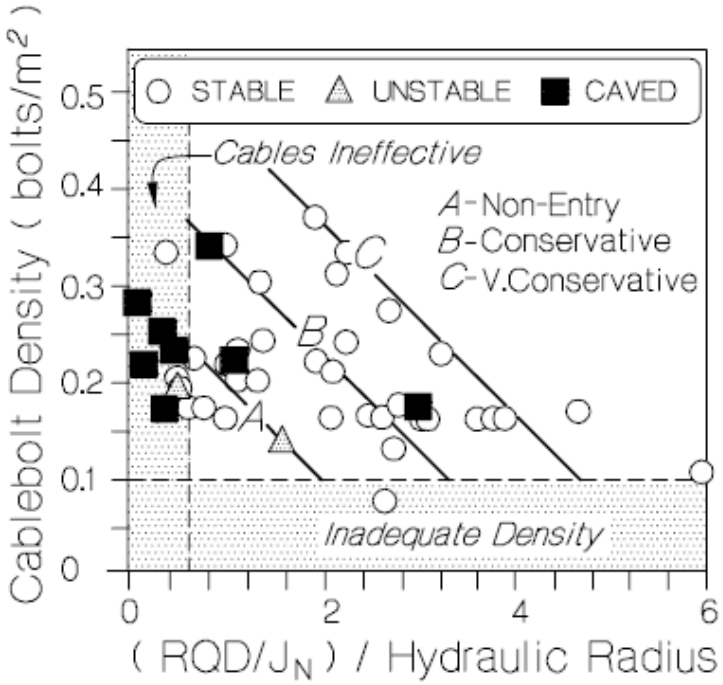


Figure 13. Cable bolt density chart (Potvin, 1988).

Several methods for estimating the cable bolt density were proposed by Potvin (1988) and Nickson (1992). For the design of cable bolt density, Potvin used the (RQD/Jn) to represent the relative block size factor divided by the excavation dimensions. From Figure 13 (above) values for (RQD/Jn)/HR less than 0.6 would mean that cable bolts would be ineffective. Hence, installing cable bolts will not prevent caving of the stope face. This can be attributed to a small block size or large hydraulic radius, as shown in Figure 13, where there is a relatively large number of caved areas for values less than 0.6 of the (RQD/Jn)/HR. A minimum cable bolt density of 0.1 is shown in Figure 13,

which roughly corresponds to a value of 3×3 m. The region below this value is not recommended for design purposes.

Furthermore, Nickson (1992) showed a good correlation between cable bolt density as well as N'/HR. The assumption is that by using the N' stability number, stress-related fracturing as well as joint orientation are considered. From Figure 14, the graph is divided into two zones: the caved zone and the stable zone. Design is either based on the conservative or non-conservative approach. The conservative zone is used in stope backs above drilling horizons or in areas where entry is permitted, whereas the non-conservative approach is based on areas were entry is not permitted (Hutchinson & Diederich, 1996).

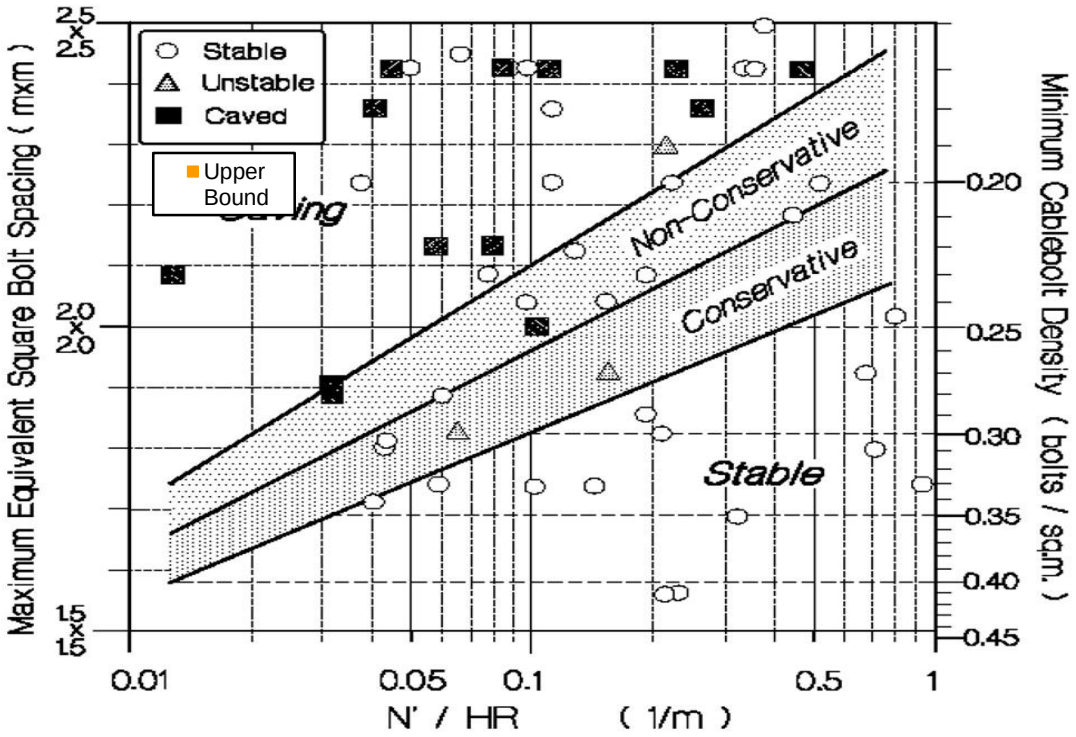


Figure 14. Guidelines for cable spacing and density - overall stope face stability (Nickson, 1992).

2.5 Numerical Modelling

Any underground opening creates a varied degree and magnitude of stress in both the near and far field area (Diakite, 1998). Empirical and theoretical models are not able to thoroughly analyse the behaviour of a rock mass, and cannot effectively relate the variations in stress and displacement inside the rock mass (Tavakoli, 1994). This section explores the theory behind numerical modelling using constitutive laws, as a way to perceive the behaviour of the rock mass.

Tavakoli (1994), noted that "umerical analysis is divided into two methods: the continuum approach which considers the rock mass as a continuum block with a number of discontinuities, and discontinuum which considers the rock mass as a group of independent blocks." Figure 15 includes a schematic of both these analysis methods.

Example of continuum models are finite and boundary element models. Examples of continuum-based models are *inter alia* Phase 2D, Examine 2D, 3D and Map 3D. Figure 15 provides a guideline using the Q-system for which continuum models are applicable where the overall rock mass is considered isotropic and homogeneous. According to Barla and Barla (2000), the "most common way to solve this problem, which seems to have gained wide acceptance, is to scale the intact rock properties down to the rock mass properties by using empirically defined relationships – such as those given by Hoek and Brown (1997)."

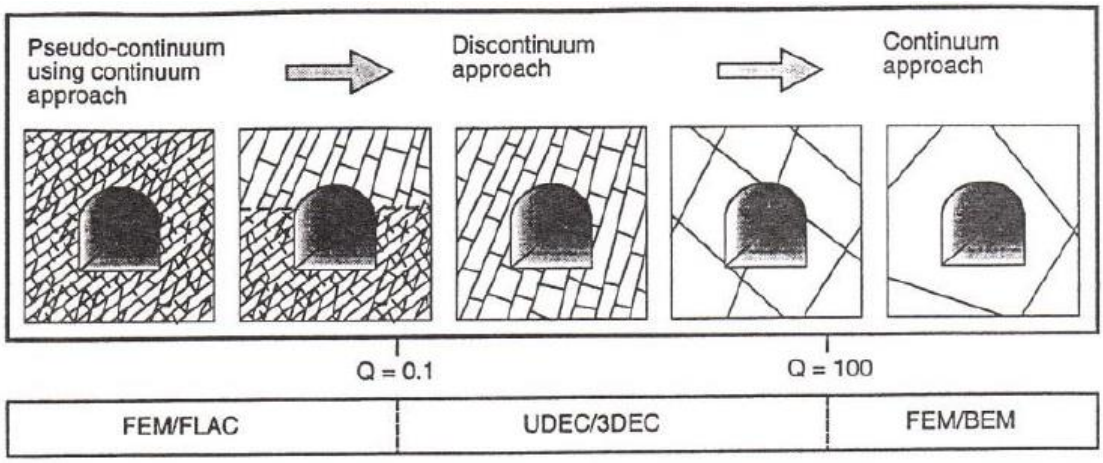


Figure 15. Schematic diagram suggesting the range of application of continuum and discontinuum modelling in relation to the Q-value (modified from Barton, 1998).

According to Barla and Barla (2000), “rock joints and discontinuities in a rock mass play a key role in the response of a tunnel to excavation.” Hence the use of discontinuous modelling has been gaining progressive attention in rock mechanics. In discontinuum modelling, the rock mass is represented as an assemblage of discrete blocks that are either assigned properties for deformable or non-deformable material, and interact with each other on surfaces regarded as joints. An example of software codes for discontinuum models include Universal Distinct Element Code (UDEC), as well as 3DEC. Figure 15 illustrates typical values of the Q-system ranging between Q = 0.1 and 100 for which the discontinuum modelling codes can be considered.

2.5.1 Mohr–Coulomb failure criteria

According to Labuz and Zang, 2012 “the Mohr–Coulomb (MC) failure criterion can described as a set of linear equations in principal stress space that are able to describe the conditions for which an isotropic material will fail, with the intermediate principal stress σ2 being neglected.” Mohr–Coulomb failure criteria can also be written in terms of major σ1 and minor σ3 principal stresses or in terms of normal and shear stress on the failure plane (Jaeger & Cook, 1979). Figure 16 illustrates the representation of the Mohr–Coulomb failure criteria in terms of principal stresses and normal and shear stresses.

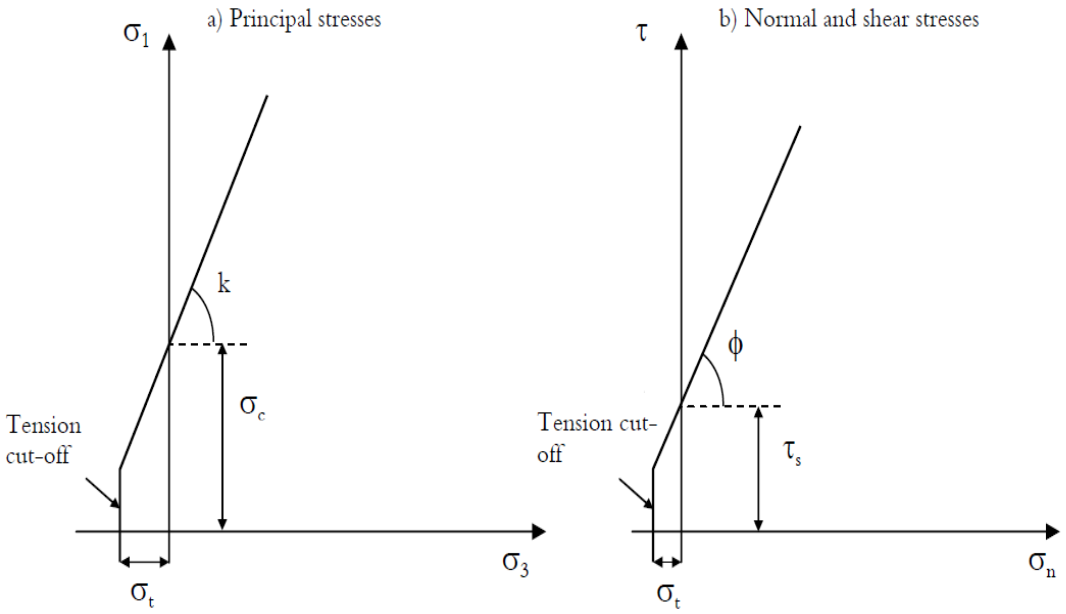


Figure 16. Mohr–Coulomb failure criterion in terms of: a) principal stresses; b) normal and shear stresses (Edelbro, 2004).

Equation 2.20 illustrates the Mohr-Coulomb failure criteria in terms of principal stresses:

$$\sigma_1' = \sigma_c + \beta_0{}'\sigma_3 \qquad 2.20$$

Where σ_1 and σ_3 is the maximum and minimum principal stresses. The β_0 is the function related to the angle of internal friction that is obtained from the slope of best fit line, and σ_c is the uniaxial compression test and is related to the cohesion – as shown in equations 2.21 and 2.22:

$$\sigma_c = \frac{2c\ cos\phi}{1 - sin\phi} \qquad 2.21$$

$$\beta_0 = \frac{1 + sin\phi}{1 - sin\phi} \qquad 2.22$$

Most geotechnical softwares are still written in terms of the Mohr-Coulomb failure criterion, however it is possible to obtain equivalent angles for both friction and cohesive strengths, as shown in equations 2.23 and 2.24 for each rock mass and stress range (Hoek et al., 2002):

$$\phi' = sin^{-1}\left[\frac{6am_b(s + m_b\sigma'_{3n})^{a-1}}{2(1+a)(2+a) + 6am_b(s + m_b\sigma'_{3n})^{a-1}}\right] \quad 2.23$$

$$\beta_0 = \frac{ci[\,(1+sa)s+(1-a)m_b\sigma'_{3n}](s+m_b\sigma'_{3n})^{a-1}}{(1+a)(2+a)\sqrt{1+(6am_b}(s+ m_b\sigma'_{3n})^{a-1}/((1+a)(2+a))} \quad 2.24$$

Where ϕ' is the angle of friction and β_0 is the cohesive strength.

The Mohr–Coulomb failure criterion can be expressed in terms of normal and shear stress. Equation 2.25 illustrates the Mohr–Coulomb shear strength criteria:

$$\tau = c + \sigma_n \tan\varphi \quad 2.25$$

Where τ is known as the shear strength and σ_n is the effective normal stress resolved on the eventual fracture plane, c is cohesion, and φ is the angle of internal friction (Lockner et al., 2002).

2.5.2 Hoek–Brown Failure Criterion

According to Le Roux (2015). The "Hoek–Brown failure criterion follows a non-linear parabolic form that separates it from the Mohr–Coulomb failure criterion." According to Hoek et al. (2002), the criterion was formulated to cater for a lack of knowned empirical strength criteria, however it was not unique since an identical equation had been utilised for describing the failure of concrete and associated materials. Hoek and Brown used a various number of experiments of parabolic curves to formulate one that gave good correlated with the Griffith theory and which fitted the observed failure conditions for brittle rock subjected to compressive stresses (Edelbro, 2004). Equation 2.26 represents the Hoek–Brown non-linear equation for intact rock and was introduced in 1980 by Hoek and Brown (1980):

$$\sigma_1 = \sigma_3 + \sqrt{m\,\sigma_3\sigma_{ci} + s\,\sigma_{ci}{}^2} \quad 2.26$$

Where m and s are dimensionless empirical constants that depend on the properties of the rock material and the extent to which it weakened before being subjected to stress σ_1 and σ_3, which are the maximum and minimum principal stresses. The uniaxial compressive strength of the intact rock is represented by σ_{ci}. The parameter m can be compared to the frictional strength characteristic of the rock material and s illustrates the degree fractures a rock is and can be related to the rock mass cohesion (Ulusay & Hudson, 2007).

In 2002, a Generalised Hoek–Brown failure criterion for jointed rock mass was defined using Equation 2.27 as follows:

$$\sigma_1' = \sigma_3' + \sigma_{ci}(m_b \frac{\sigma_3'}{\sigma_{ci}} + s)^a \quad 2.27$$

Where σ_1' and σ_3' is the maximum and minimum effective principal stresses. The uniaxial compressive strength of an intact rock is given by σ_{ci}. The m_b is a reduced value of m_i, which depends on how severely the rock is broken. The original m_i value was re-examined and was found to depend on the mineralogy, composition as well as the size of grains in the intact rock (Hoek et al., 2002). The following set of equations (2.28 to 2.30) illustrates how the empirical constant m_b , s and a can be obtained:

$$m_b = m_i \, exp\left(\frac{GSI - 100}{28 - 14D}\right) \quad 2.28$$

$$s = exp\left(\frac{GSI - 100}{9 - 3D}\right) \quad 2.29$$

$$a = \frac{1}{2} + \frac{1}{6}\left(e^{-\frac{GSI}{15}} + e^{-\frac{20}{3}}\right) \quad 2.30$$

According to Hoek et al.,(2002), "the exponential term a was added to address the system's bias towards hard rock and to better account for poorer quality rock masses,

by enabling the curvature of the failure envelope to be adjusted – particularly under very low normal stresses."

Based on the Hoek–Brown envelope defined by the above parameters, the unconfined compressive as well as the tensile strength of a given rock mass can be expressed from equations 2.31 and 2.32 below:

$$\sigma_c = \sigma_{ci} s^a \qquad 2.31$$

$$\sigma_t = \frac{s\sigma_{ci}}{m_b} \qquad 2.32$$

Where σ_c is the unconfined compressive strength, and σ_t is the tensile strength of the rock mass.

The global rock mass strength, σ_{cm}, can be estimated based on the laboratory unconfined compressive strength, σ_{ci}, and the other Hoek–Brown parameters, using equation 2.33 (Hoek et al., 2002).

$$\sigma_{cm} = \sigma_{ci} \frac{(m_b + 4s - a(m_b - 8s))(\frac{m_b}{4+s})^{a-1}}{2(1+a)(2+a)} \qquad 2.33$$

The Hoek–Brown failure criteria, like the Mohr–Coulomb criteria, is a shear-based criterion, and hence brittle failure may not be appropriately modelled. Both the Hoek–Brown and the Mohr–Coulomb failure criteria ignore the intermediate principal stress, σ_2, when it varies from the minimum principal stress. Furthermore, the Hoek–Brown failure criterion can only be applied to weak rock masses where behaviour of the rock mass is controlled by joints, rather than individual failure planes or the rock mass material. Furthermore, the Hoek–Brown criterion fits the laboratory low-stress (including tensile stress) regimes reasonably well, but sometimes tends to over-estimate the downward curvature of the strength for strength characteristics at high confining stresses (Ryder & Jager, 2002).

2.5.3 Improved Unified Constitutive Model

Numerical modelling was conducted using the Improved Unified Constitutive Model (IUCM) formulated by Vakili (2016). According to Vakili (2017), "the Improved Unified Constitutive Model (IUCM) is a result of collating the most notable recent research in the area of rock mechanics and extensive back-analysis of mining case histories together, into a unified material model." Vakili (2016) further emphasised that the IUCM was developed from well proven methods of determining the strength of the rock mass. The IUCM can be used in a variety of ground conditions, ranging from intact brittle rocks to extremely weak and ductile rocks, as well as anisotropic rocks Vakili (2016).

The input parameters used for the IUCM model are:

- Unconfined intact rock strength (σ_{ci})
- Intact Young's Modulus
- Density
- Hoek–Brown constant m_i
- GSI.

In addition, the post peak properties of a material in the IUCM can be predicted using a linear Mohr–Coulomb criterion. The default values used are such that the cohesion is zero, as well as the tensile values at residual state of stress. However, these values can be varied. The frictional angle is assumed to be 45°. Vakili (2016) presents a detailed description of the IUCM components. This includes systematic instructions on the processes that were formulated in the models' algorithms.

Vakili (2016), further noted that "one of the main emphases during the development of the IUCM was to establish a unified model that could capture the more complex failure mechanisms and still require minimum additional input properties, which could also be obtained through conventional data-collection procedures." Table 10 shows input parameters used in the IUCM model:

Table 10. Input parameters used in the IUCM (Vakili, 2016)

Property	Description	Required/Optional	Used for isotropic Rock	Used for anisotropic rock
Density	Density of the rock mass	Required	Yes	Yes
Sigci	Uniaxial Compressive Strength of the intact rock	Required	Yes	Yes
GSI	Geological Strength Index of the rock mass	Required	Yes	Yes
m_{iMax}	Hoek-Brown constant m_i for the intact rock matrix	Required	Yes	Yes
E_i	Elastic Modulus of intact rock	Required	Yes	Yes
m_{iMin}	Hoek-Brown constant m_i for the plane of anisotropy of the intact rock	Required for anisotropic rock	No	Yes
$Aniso_{Fac}$	Anisotropy Factor	Required for anisotropic rock	No	Yes
$Aniso_{Dip}$	Dip angle of the plane of anisotropy	Required for anisotropic rock	No	Yes
$Aniso_{DipD}$	Dip direction angle of the plane of anisotropy	Required for anisotropic rock	No	Yes
Dis_{Fac}	Disturbance factor	Optional	Yes	Yes
C_{Res}	Residual Cohesion of the rock mass	Optional	Yes	Yes
$Fric_{Res}$	Residual Friction Angle of the rock mass	Optional	Yes	Yes
Ten_{Res}	Residual Tensile Strength of the rock mass	Optional	Yes	Yes
$Crit_{Red}$	Reduction factor for critical strain	Optional	Yes	Yes

2.5.3.1 Unconfined compressive strength and elastic modulus

In the IUCM model, the unconfined compressive strength is represented by Sigci property (Vakili, 2016). In a rock mass with a GSI lower than 65, the intact laboratory unconfined strength can be directly assigned for Sigci. Vakili (2016) noted that "this is because for these rock masses, the size of the intact blocks, bounded by the discontinuities is close enough to the laboratory samples that the effect of increasing sample size on the strength of the intact rock can be neglected".

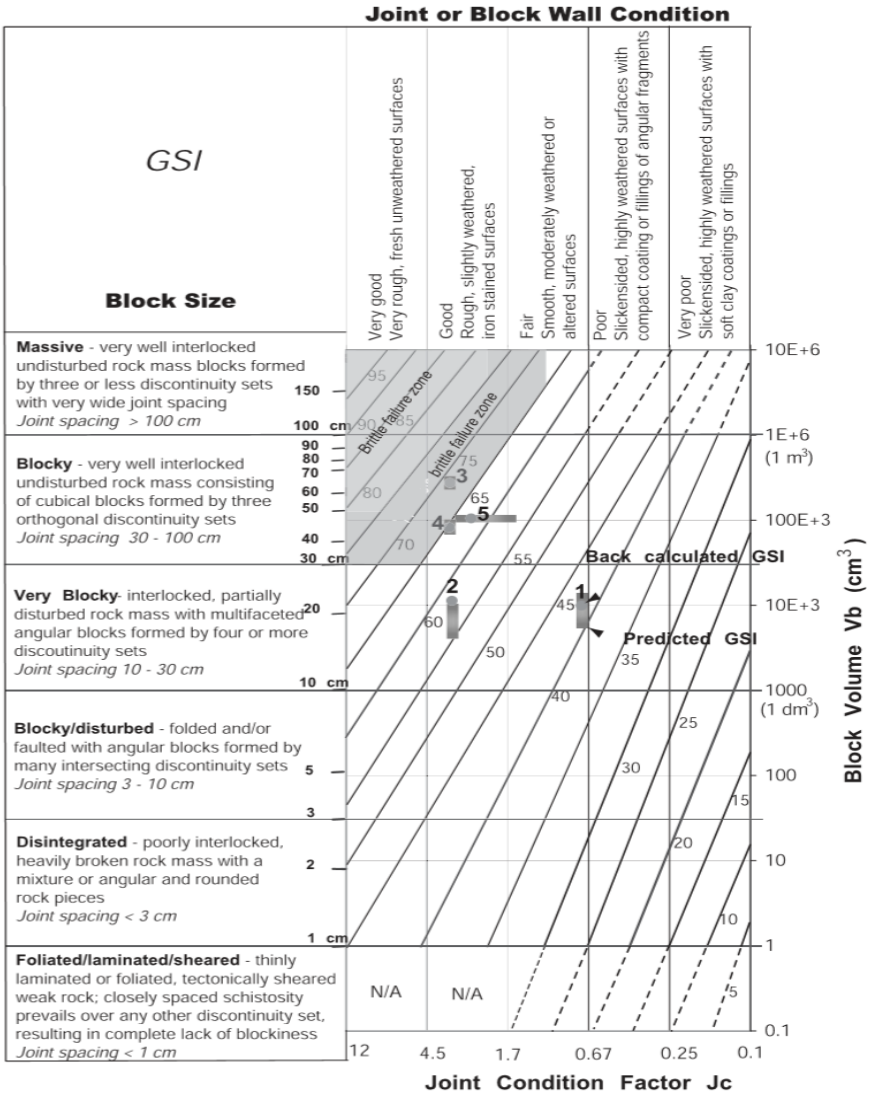


Figure 17. Quantification of GSI chart (Cai et al., 2003).

The unconfined strength of an intact rock for a rock mass with a high GSI value above 65 should be reduced according to the methods provided in the literature by Hoek and Brown (1980) and Cai et al. (2007).

The unconfined intact rock strength for rock masses with a GSI greater than 65 can be reduced using Figure 17 by approximating the average joint spacing of the joint sets of the rock mass and with its respective GSI value. Using the average joint spacing obtained and its respective GSI, Figure 18 can then be used to reduce the intact rock strength. This can be achieved by obtaining the strength ratio, with which the lab scale unconfined intact rock strength is multiplied to obtain the reduced unconfined intact rock strength.

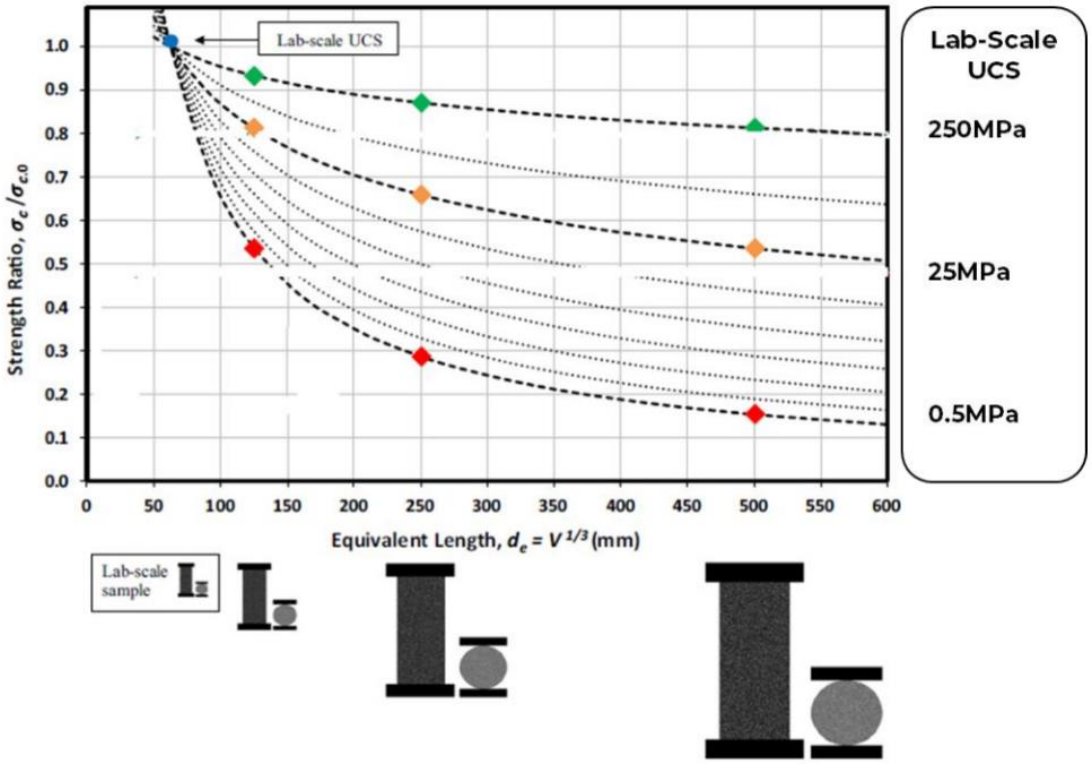


Figure 18. Scale effect relations for intact rock UCS (Yoshinaka et al., 2008).

2.5.3.2 Elastic properties

One of the important parameters in assessing the behaviour of the rock mass is the deformation modulus (Hoek & Diederichs, 2006). The elastic modulus can be calculated from the Hoek and Diederichs' equation (Equation 2.34) provided below, using in situ rock mass deformation from various countries including China and Taiwan:

$$Em = Ei\left(0.02 + \frac{1-D/2}{1+e^{(60+15D-GSI)/11}}\right) \quad 2.34$$

Where Ei is the modulus of the intact rock, GSI is the Geological Strength Index, and D is the disturbance factor. The value of Ei is estimated using Equation 2.35 as proposed by Deere (1968):

$$Ei = (MR)\sigma ci \quad 2.35$$

Where the Ei is the modulus of the intact rock, MR is the modulus ratio and σci is the intact rock strength. Equation 2.35 is used when no direct data of the intact modulus E_i are available or where undisturbed sampling for measurements of E_i has proven to be difficult (Hoek & Diederichs, 2006).

Table 11 illustrates different methods of obtaining MR from different rock types, with the earliest work on MR carried out by Malik and Rashid (1997). Wang & Aledejare (2016) stated that "the UCS and E data obtained for a project site are generally limited, and the sparse number of UCS and E data often obtained is insufficient to provide joint probability distribution of UCS and E and to estimate their correlation coefficient." Hence it is important that Ei is estimated from an intact rock sample to obtain a reliable Ei value.

Table 11. Modulus ratio MR (E and UCS in MPa) (Malkowski et al., 2018)

Rock type	Reference	Number of samples	*MR* (range)
Claystone	Hoek & Diederichs, 2006	nda	(200–300)
	Malik & Rashid, 1997	30	141 (87–228)
	Małkowski & Ostrowski, 2017 (Carboniferous)	**81**	**E_{tan} 274 (118–657)**
			E_{av} 276 (77–606)
			E_{sec} 269 (79–616)
Siltstone	Hoek & Diederichs, 2006	nda	(350–400)
	Malik & Rashid, 1997	30	137 (79–190)
Mudstone	Małkowski & Ostrowski, 2017 (Carboniferous)	**70**	**E_{tan} 232 (59–421)**
			E_{av} 242 (61–500)
			E_{sec} 203 (45–436)
Sandstone	Hoek & Diederichs, 2006	nda	(200–350)
	Bell & Lindsay, 1999	27	372 (141–680)
	Malik & Rashid, 1997	30	119 (76–157)
	Sabatakakis et al., 2008	36	303 (120–727)
	Małkowski & Ostrowski, 2017 (Carboniferous)	**86**	**E_{tan} 223 (139–381)**
			E_{av} 236 (141–491)
			E_{sec} 187 (82–379)

2.5.3.3 Rock strength anisotropy

In rock mechanics, the term rock anisotropy is a mechanical property of rock that makes the strength of rocks directional dependent. Rock anisotropy can be classified into two forms: intact rock anisotropy as well as rock mass anisotropy. Intact rock anisotropy results from natural fractures that constitute the rock, which result in directional dependency for intact anisotropic rocks (Vakili et al., 2014). On the other hand, rock mass anisotropy occurs due to occurrences of geological structures. The anisotropy of the rock is a very important mechanical property of a rock and it influences the amount of deformation. Watson et al. (2015) suggested that "the effect of rock strength anisotropy must be taken into account when assessing the rock mass response to mining in anisotropic rock conditions." In most cases – there is a tendency to ignore anisotropic factors of the rock mass in order to simplify the design process.

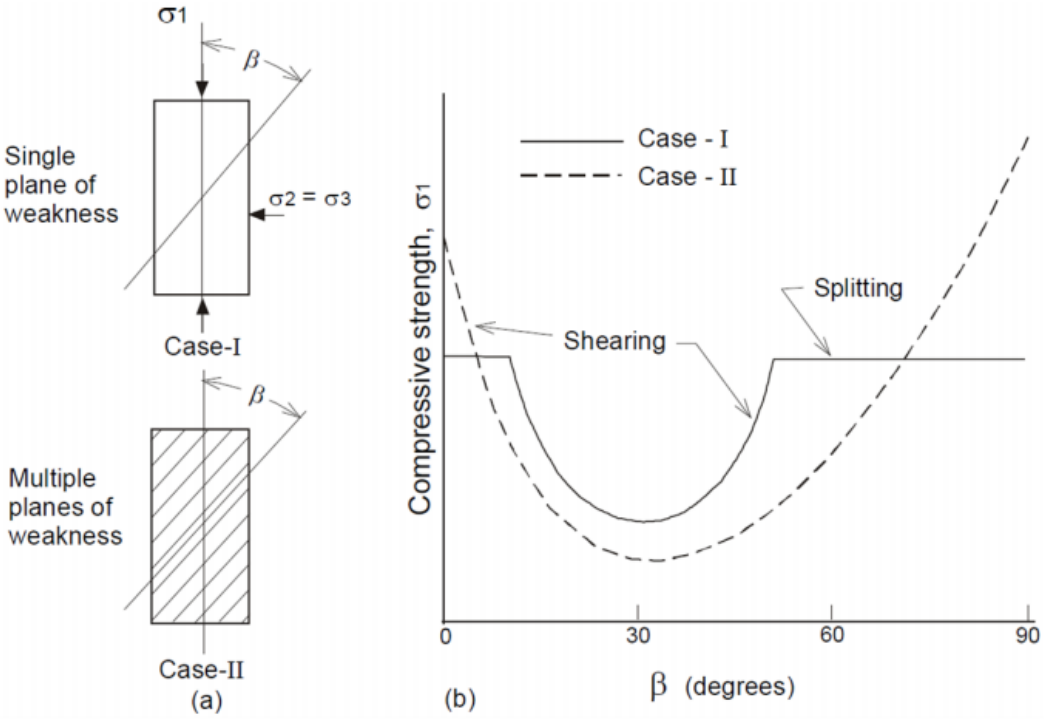


Figure 19. Theoretical variation of uniaxial compressive strength depending on orientation with respect to anisotropy plane (Ramamurthy et al, 1993, as referenced by Palmstrom, 1994).

Figure 19 indicates the compressive strength vs β angle results, were β is the angle of the foliation with respect to the direction of the applied load. The highest value $\sigma_{c\ max}$ is obtained when β is either 0° or 90°. The lowest $\sigma_{c\ min}$ occurs between 30° and 45°. The ratio between $\sigma_{c\ max}$ and $\sigma_{c\ min}$ is known as the anisotropic factor and can be estimated from Figure 18.

Table 12 can be used to assign anisotropic factors of rocks in the case were no available laboratory intact rock test results for anisotropic rocks. Guidelines for data collection and selection of input parameters are summarised by Vakili et al. (2014).

Table 11. Classification of anisotropy intensity in various rocks (modified from Tsidzi, 1990; Singh et al, 1989; Ramamurthy et al, 1993; Palmstrom, 1994).

Anisotropic classification	Example rock types	Anisotropy factor
Isotropic	Quartzite, hornfels, granulites	1-1.1
Low anisotropy	Quartzofeltspatic gneiss, mylonite, migmatite, shale	1.1 2.0
Medium anistropy	Schistose gneiss, quartz schist	2.0 - 4.0
High anisotropy	Mica schist, hornblende schist	4.0 - 6.0
Very high anistropy	Slate, phyllite	>6.0

2.5.3.4 Hoek-Brown material constant m_i

The Hoek–Brown constant mi for the intact rock matrix can control how damage starts and progresses in a numerical model hence it is an important parameter. According to Vakili (2016) “this constant can control the confinement dependency of the modelled rock under high stress conditions.”

The estimates of the m_i can be obtained using triaxial test results, and this method is the most reliable method of obtaining the constant m_i. The second method involves the use of tensile strength test, if available, and the ratio Sigci/UTS can be used where the UTS is the Uniaxial Tensile Test. The third method to estimate the value of m_i can be used when no laboratory tests have been conducted, and values from Table 12 can be used.

Table 12. Values of the constant mi for intact rock by group (Hoek & Brown, 1997).

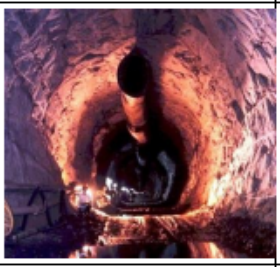
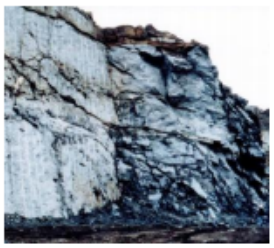
Rock type	Class	Group	Texture			
			Coarse	Medium	Fine	Very fine
SEDIMENTARY	Clastic		Conglomerate* (22±3) Breccias (19±5)	Sandstone 17±4	Siltstone 7±2 Greywacke (18±3)	Claystone 4±2 Shales (6±2) Marls (7±2)
	Non-Clastic	Organic				Chalk 7±2
		Carbonates	Crystalline Limestone (12±3)	Sparitic Limestone (10±2)	Micritic Limestone (9±2)	Dolomites (9±3)
		Evaporites		Gypsum 8±2	Anhydrite 12±2	
METAMORPHIC	Non Foliated		Marble 9±3	Hornfels (19±4) Metasandstones 26±6	Quartzites 20±3	
	Slightly foliated		Migmatite (29±3)	Amphibolites 26±6		
	Foliated*		Gneiss 28±5	Schists 12±3	Phyllites (7±3)	Slates 7±4
IGNEOUS	Plutonic	Light	Granite 32±3	Diorite 25±5		
			Granodiorite (29±3)			
		Dark	Gabbro 27±3	Dolerite (16±5)		
			Norite 20±5			
	Hypabyssal		Porphyries (20±5)		Diabase (15±5)	Peridotite (25±5)
	Volcanic	Lava		Rhyolite (25±5) Andesite 25±5	Dacite (25±3) Basalt (25±5)	Obsidian (19±3)
		Pyroclastic	Agglomerate (19±3)	Breccia (19±5)	Tuff (13±5)	

The use of Table 12 to estimate the values of m_i should be used for preliminary design purposes. However, for detailed design studies, laboratory tests should be carried out to obtain values that are more reliable (Hoek & Brown, 1997).

2.5.3.5 Disturbance factor (D)

The disturbance factor was proposed in order to downgrade the rock mass properties after blasting and stress changes have taken place. Hoek et al. (2002) noted that the "effects of heavy blast damage as well as stress relief due to removal of the overburden results in disturbance of the rock mass." The disturbance factor has a large influence on both the frictional angle and cohesion. The disturbance factor varies from D=0 for undisturbed to D=1 for highly disturbed rock masses – as shown in Table 13.

Table 13. Guidelines for estimating the disturbance factor D (Hoek et al., 2002)

Appearance of rock mass	Description of rock mass	Suggested value of D
	Excellent quality controlled blasting or excavation by Tunnel Boring Machine results in minimal disturbance to the confined rock mass surrounding a tunnel.	$D = 0$
	Mechanical or hand excavation in poor quality rock masses (no blasting) results in minimal disturbance to the surrounding rock mass. Where squeezing problems result in significant floor heave, disturbance can be severe unless a temporary invert, as shown in the photograph, is placed.	$D = 0$ $D = 0.5$ No invert
	Very poor quality blasting in a hard rock tunnel results in severe local damage, extending 2 or 3 m, in the surrounding rock mass.	$D = 0.8$
	Small scale blasting in civil engineering slopes results in modest rock mass damage, particularly if controlled blasting is used as shown on the left hand side of the photograph. However, stress relief results in some disturbance.	$D = 0.7$ Good blasting $D = 1.0$ Poor blasting
	Very large open pit mine slopes suffer significant disturbance due to heavy production blasting and also due to stress relief from overburden removal. In some softer rocks excavation can be carried out by ripping and dozing and the degree of damage to the slopes is less.	$D = 1.0$ Production blasting $D = 0.7$ Mechanical excavation

2.5.4 Peak failure criteria

The IUCM used the curve-fitting approach in order to estimate the rock mass strength over varying stress levels. Hence a Hoek–Brown criterion was used in the IUCM to calculate the Mohr–Coulomb parameters for all stress increments. The approach used for estimating the Mohr–Coulomb criteria is outlined in the work done by Vakili (2016).

Vakili (2016) outlines the following steps that the IUCM computes in order to obtain the Mohr–Coulomb parameters:

- Firstly initialise the pre-mining stresses in the model.
- Secondly obtain the current minor and major principal stresses for each finite difference zone (or element in the finite element method).
- Obtain the minor principal stress increment ($\Delta\sigma_3$) by adding and subtracting 0.1% of the current σ_3 of the current σ_3 magnitude, as depicted in equations 2.36 and 2.37.

$$\sigma_3^1 = \sigma_3 - 0.001\sigma_3 \quad (2.36)$$

$$\sigma_3^2 = \sigma_3 - 0.001\sigma_3 \quad (2.37)$$

- Calculate constants for the Hoek–Brown criteria based on equations 2.38 to 2.40, provided by Hoek et al. (2002):

$$m_b = m_i \exp\left(\frac{GSI-100}{28-14D}\right) \quad (2.38)$$

$$s = \exp\left(\frac{GSI-100}{9-3D}\right) \quad (2.39)$$

$$a = \frac{1}{2} + \frac{1}{6}\left(e^{-\frac{GSI}{15}} + e^{-\frac{20}{3}}\right) \quad (2.40)$$

- Obtain the major principal stress increment ($\Delta\sigma_1$) from the generalised Hoek–Brown failure criteria and from the measured change in the minor principal stress ($\Delta\sigma_3$) – as shown by equation 2.41 to 2.42:

$$\sigma_1^1 = \sigma_3^1 - \sigma_c \left(m_b \frac{\sigma_3^1}{\sigma_c} + s \right)^a \quad 2.41$$

$$\sigma_1^2 = \sigma_3^2 - \sigma_c \left(m_b \frac{\sigma_3^2}{\sigma_c} + s \right)^a \quad 2.42$$

- Obtain the slope of the incremental stress envelope – as shown in equation 2.43.

$$tan\varphi = \frac{\sigma_1^1 - \sigma_1^2}{\sigma_3^1 - \sigma_3^2} \quad 2.43$$

- Calculate the instantaneous friction angle (∅) from (φ), as shown in equation 2.44:

$$\varphi = sin^{-1} \left(\frac{\tan \varphi - 1}{\tan \varphi + 1} \right) \quad 2.44$$

- Calculate the instantaneous cohesion, as shown in equation 2.45:

$$c = \frac{\sigma_1^1 (1 - sin\varphi) - \sigma_3^1 (1 + sin\varphi)}{2cos\varphi} \quad 2.45$$

- Calculate uniaxial tensile strength, as shown in equation 2.46:

$$\sigma_t = \frac{s\sigma_c}{m_b} \quad 2.46$$

In order to prevent the tensile strength from exceeding the value of σ_3, which is related to the apex limit of the Mohr-Coulomb relation, a comparison of the tensile strength value derived from equation 2.45 and that from the maximum limit (c/tan∅) is used and the lower value of the two is used.

2.5.5 Post peak failure criteria

The IUCM uses the linear Mohr–Coulomb failure criterion for the post peak properties of a completely broken rock, with a cohesion of zero and a frictional angle of 35-55°,

which can be specified by the user. The criteria used for the IUCM implies that after a prolonged deformation of the rock mass, the rock will later exhibit soil-like properties.

The residual strength of a rock mass has an important role in the process of failure propagation of the rock mass, since in this region the rock mass strength has been exceeded by the stress in the surrounding rock mass. Cai et al. (2007) noted that "the determination of the global mechanical properties of jointed rock masses remains one of the most difficult tasks in rock mechanics." Few notable methods for estimating the residual strength of the rock mass were presented by Cai et al. (2007), by using the peak GSI and converting it to a residual GSI (GSI_r) to calculate the residual block volume, V_b^r, and the residual joint condition factor J_c^r. Lorig and Varona (2013) further researched downgrading the peak strength of a rock mass by using the disturbance factor proposed by Hoek. An alternative method proposed by Vakili (2016), was the use of cohesion-softening and friction-hardening linear Mohr–Coulomb criterion.

2.6 Summary

Open stoping mining methods are widely used for the extraction of massive ore bodies. The use of rock mass classification systems to estimate support requirements forms the foundation of open stope span design. There are a variety of rock mass classification systems that are used to quantify the strength of the rock mass.

Advances in research has made it possible for the use of numerical modelling in open stoping design. The use of failures criteria such as the Hoek-Brown and Mohr-Coulomb Failure Criteria allows numerical models to predict the behaviour of a rock mass using intact rock properties. Lastly the IUCM constitutive model was discussed in detail.

3 Review of Rosh Pinah Zinc Mine

3.1 Rosh Pinah Zinc mining history

Rosh Pinah Zine Mine is located in south-western Namibia in the Karas Region, as shown in Figure 20:



Figure 20. Location of Rosh Pinah Zinc Mine (Google Maps, 2019)

Discovery of Rosh Pinah dates back to 1963. This makes it one of the oldest mines in Namibia. Prior to the discovery, there were no mining activities in the area. A major discovery was also made approximately 25 km west of Rosh Pinah, in an area known as the Skorpion deposit.

In 1969, mining started at the Rosh Pinah Mine with an open pit above the current orebody. The first owners of the mine were Imcor Zinc, which was formed via a joint venture between Iscor and Molly Copper. The decision to mine at the time was based on 23 boreholes and exploration thereafter continued until now. Between 1993 and 1995 the mine was liquidated, and the new mining right was awarded to PE Minerals Pty (Ltd). In 1998, Rosh Pinah Zinc Mine Corporation was formed, with a joint venture between Iscor and PE Minerals. Between 2001 and 2006, Iscor became Kumba and then Exxaro. On 1 May 2012, Glencore purchased the majority shareholder in Rosh Pinah Zinc Mine from Exxaro worth 80.08%, with the remaining shares owned by Black Economic Empowerment and PE Minerals. From September 2017, Trevali Mining acquired 80.08% of Rosh Pinah Zinc Mine from Glencore and subsequently increased their interest to 90% from mid-2018.

3.2 Regional geology of Rosh Pinah Mine

According to Frimmel (2008), the Rosh Pinah ore deposit is hosted in a thick package of turbidites comprising both hinterland and contemporaneous-volcanic, clastic provenance, which was deposited in a Neoproterozoic rift basin during the early part of the evolution of the Gariep Terrance of southern Namibia – as shown in Figure 21. Research shows that due to intense folding, thrusting and wrench faulting are all direct evidence of the original extent, depth and structure of the Gariep Basin has been obliterated. The belt records a series of tectonic stages, from crustal thinning which occurred during the preparation of the breakup of the supercontinent Rodinia, to subsequent continental rifting, opening of an oceanic basin and closure – as well as continent to continent collision during the amalgamation of west Gonwana (Frimmel, 2008).

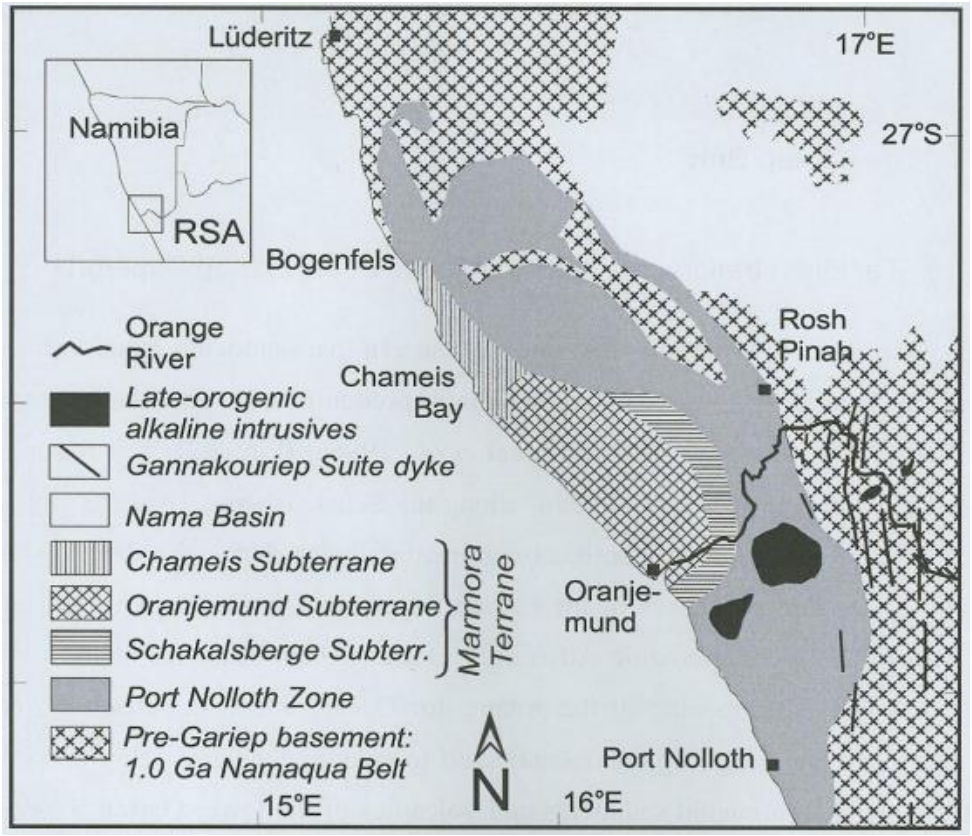


Figure 21. Tectonic subdivision of the Gariep Belt (modified from Frimmel, 2000a)

Stratigraphically, the Gariep belt has been divided into two main zones: the continental Port Nolloth Zone in the east and the largely oceanic Marmora Terrane in the west. The two zones are separated by a major thrust fault, the Schakalsberg Thrust.

3.3 Mining geology

The surrounding area where the Rosh Pinah deposit occurs is an anticlinorium, divided into a western domain (WD) and an eastern domain (ED). The Ore Equivalent Horizon (OEH) consists of massive, argillitic, microquarzitic and carbonate ore. According to Flavianu (2010), the lithological units of the ore zone comprise microquartzite and carbonate and massive ore. The host rock is mostly arkose.

Due to several deformation episodes, the Rosh Pinah deposit occurs as lenses located in fold hinges (e.g. EF1, EF2, AME) and along tightly folded limbs bounded or truncated by major shear zones – e.g. S1N, S1S, SF3 against the SF fault and WF3 against the Northern Fault (NF).

The geometry of the SF3 deposit is shown in the section in Figure 22. The SF3 orebody is hosted in Arkose rock, with carbonates as the rock type that contains the ore equivalent horizon. The orebody has a strike length of 170 m in the upper levels and reduces to 90 m at the lower levels of the orebody. The width of the orebody is about 7 m on the upper levels and increases to an average of 25 m on the lower levels. The upper levels were mined at a depth of 270 m and the lower level *in situ* ore will be mined at a depth of 495 m.

The dominant ore types in the SF3 orebody are mainly carbonates as well as brecciated arkoses, with the carbonate ore in the upper levels of the orebody. At the lower levels, the orebody is hosted within mostly the arkose.

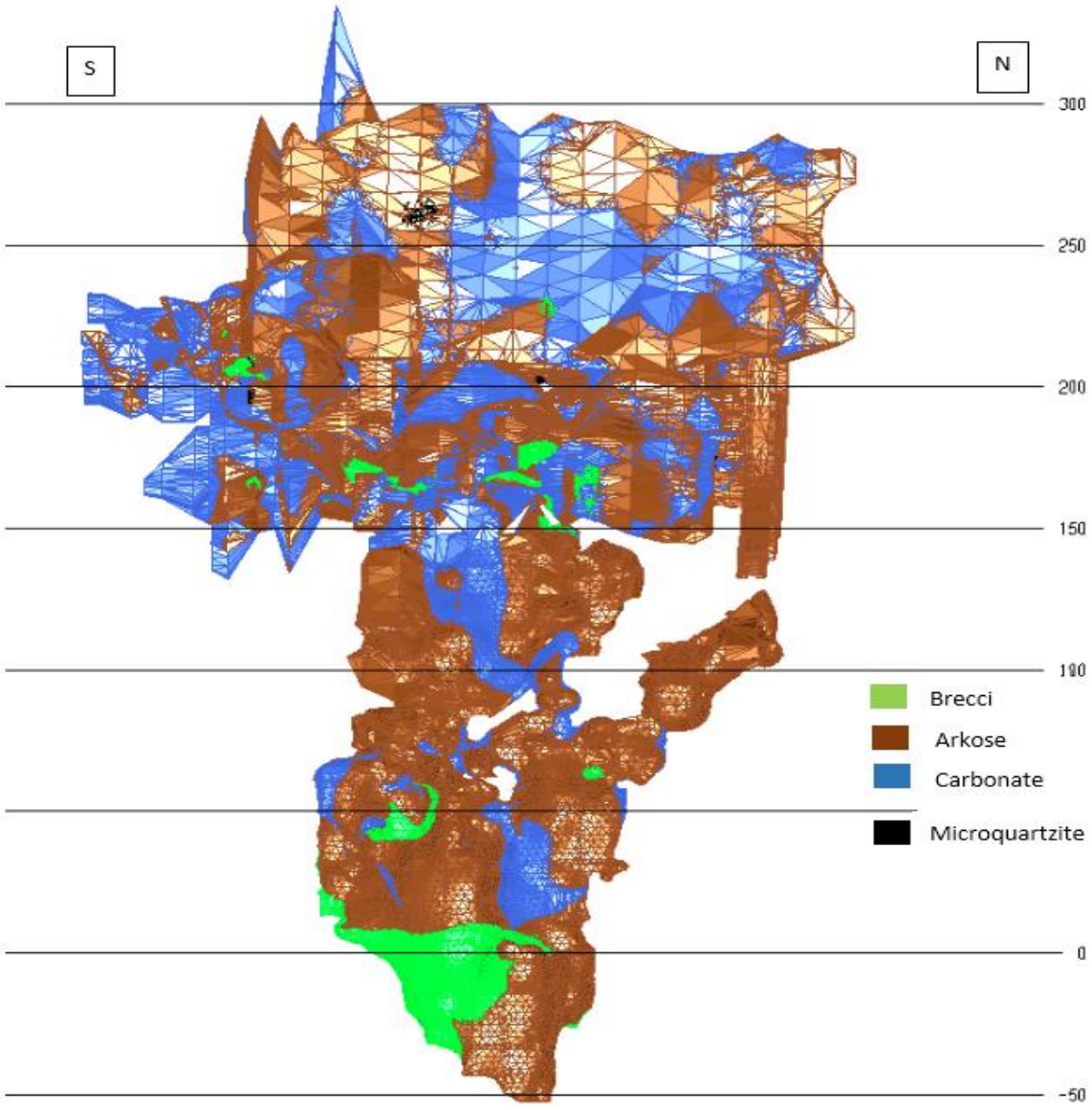


Figure 22. Simplified geological map of the SF3 orebody.

Arkose: A feldspar rich sandstone or grit coarse-grained, with angular to sub-rounded clasts, substantially smaller than 4 mm (Torben, et al., 2018). Figure 23 shows a typical drill core of arkose.



Figure 23. An example of arkose drill core.

Microquartzite: Is a local name used at the mine to represent a more silicified shale or mudstone. An example of microquartzite drill core is shown in Figure 24.



Figure 24. An example of a microquartzite drill core.

Carbonates: At Rosh Pinah any rock consisting predominantly of carbonate minerals (e.g calcite, dolomite and siderite) is referred to as a carbonate. Carbonate is described as a fine to coarse grained, with a mottled texture containing mainly honey coloured sphalerite, minor galena, pyrite and occasional chalcopyrite (Torben et al., 2018). An example of carbonate ore which is dominant in the SF3 orebody is shown in Figure 25.

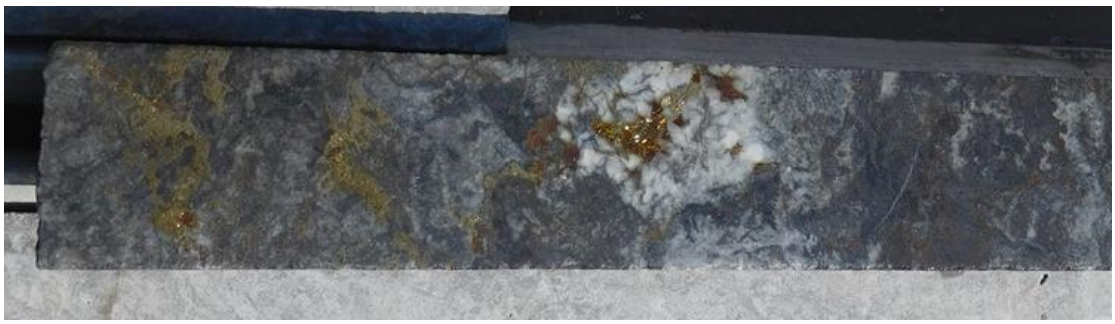


Figure 25. An example of a carbonate drill core.

Breccia: is an altered or silicified arkose, with fractures and veins filled by mainly pyrite, minor sphalerite and chalcopyrite. An example of breccia is shown in Figure 26.

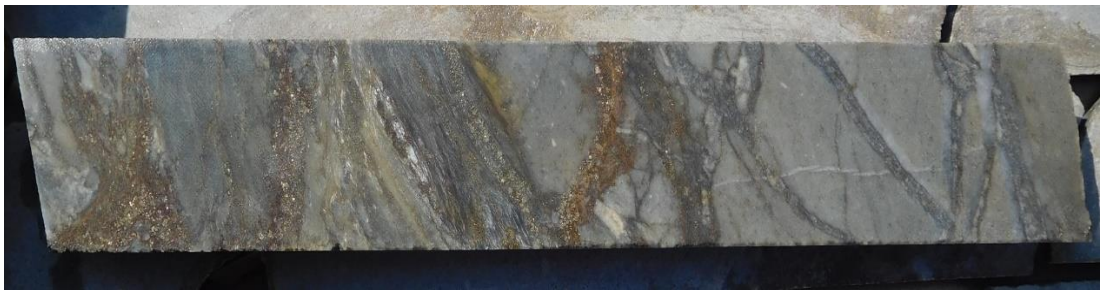


Figure 26. An example of a breccia drill core.

The SF3 orebody is sandwiched between the Northern Fault as well as the SF3 Fault. The hanging wall is bounded by the SF3 Fault, while the footwall is bounded by the Northern Fault. Geological mapping as well as borehole data were used to create the (3D dimensional) structures in Leapfrog. More refined structures with the aid of level maps from the geologists, provided an improved structural model for the SF3 orebody. The structures were mapped and interpreted over at least one mine level to determine the continuity of the structures. Figure 27 shows the structural model of the SF3 orebody.

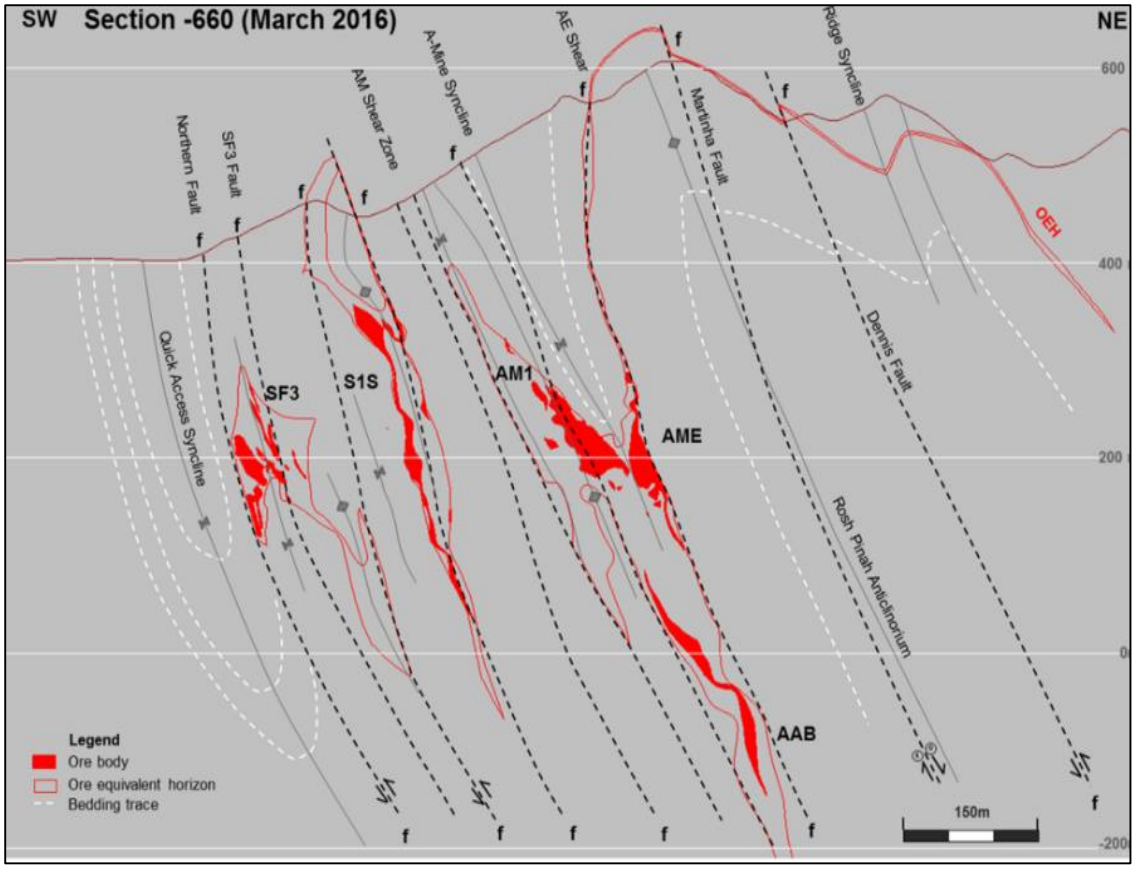


Figure 27. A section showing faults in the Rosh Pinah Mine area (Flavianu, 2015).

3.4 Mining Method

The main stoping method currently used at Rosh Pinah Zinc is the Sublevel Open Stoping mining method. Sublevel open stoping comprises of a cut-off raise first drilled and excavated, and then opening the cut-off slot and finally blasting the main rings in a retreat manner. A raise is excavated with a raise bore with a diameter of 1.5 m, and easer holes are drilled by the Simba with a hole diameter of 7.6 cm, through which charging of the raise will take place.

Remote loading is carried out with LHD scoops at draw points that are either located transversely or longitudinally to the orebody. The typical width of the orebody is 7 m to 15 m and the in ore development is excavated along the strike of the orebody.

3.4.1 In situ stress regime and measurement

The importance of reliable *in situ* stress measurements cannot be overemphasised. *In situ* stress measurements were completed at the Rosh Pinah Mine in 2014 at the Western Orefield at -030 level. No *in situ* stress measurements were done on the SF3 orebody.

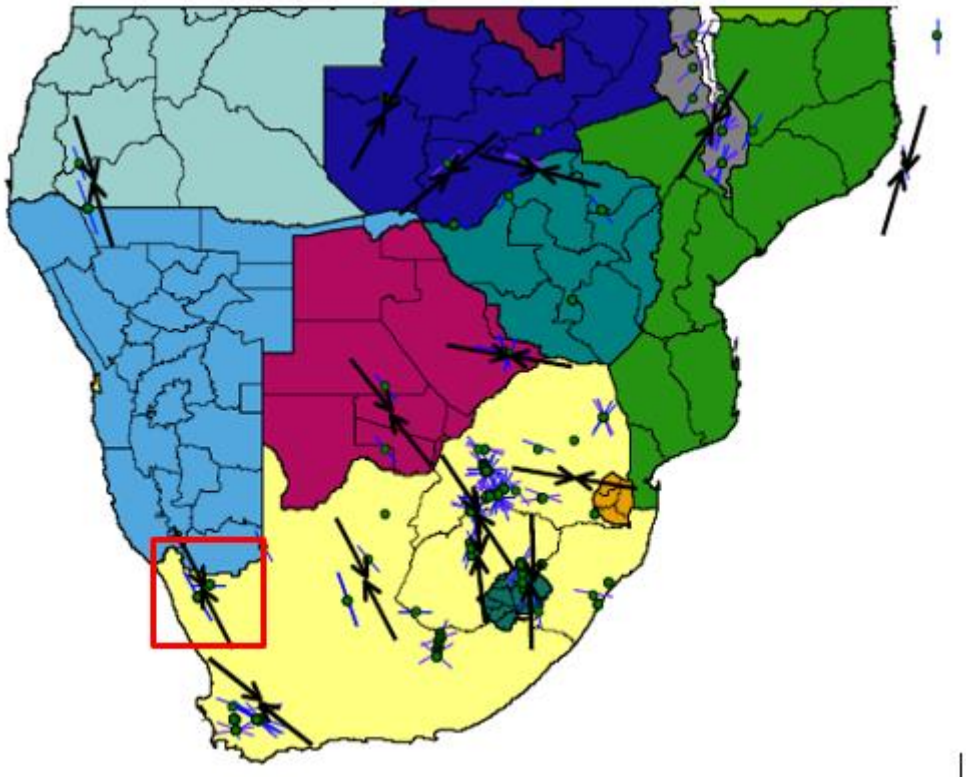


Figure 28. Orientation of horizontal *in situ* stresses (Stacey & Swart, 2001).

According to Handley and Piper (2014), the purpose of *in situ* measurements is to determine the state of stress in a specific area of interest on a mine, with view to allowing credible and representative numerical modelling of the induced stresses around planned stopping and geological structures in the Western Orefield. *In situ* stress measurements will also be used to explain stope failures previously encountered on the mine.

Previous numerical modelling undertaken at Rosh Pinah Mine prior to the stress measurements carried out on site were based on the South African stress measurement database (Wesseloo & Stacey, 1998). The magnitudes of stress and their orientation were based on the results of Black Mountain and O' Okiep Mine – as shown in Figure 28. According to Stacey and Wesseloo (1998), most "horizontal secondary principal stresses tend to be aligned approximately in the NW-SE and NE-SW directions in most locations."

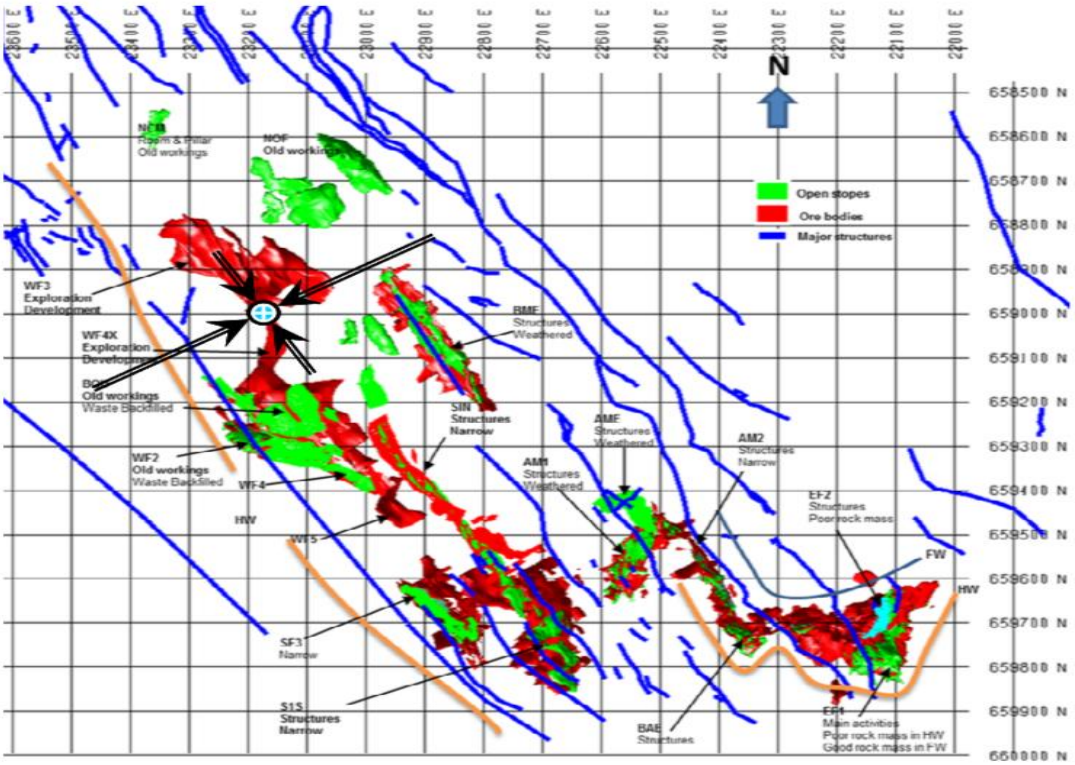


Figure 29. A plan showing the location of measurements in relation to the orebody mined out stopes (Handley & Piper, 2014).

Two stress measurements were carried out in the Western Orefield at a depth of 10 m and 12 m from the collar. The depth at which stress measurements were taken was approximately 495 m. Figure 29 indicates the locality of the test site where the two measurements were done.

By comparing Figure 28 for the orientation of major horizontal stress fields in Southern Africa to that of the Western Orefield in Figure 29, there is an agreement in terms of the orientation of stress measurement one.

Worotniki (1993) stated that "the CSIRO hollow inclusion (HI) stress cell is one of the most widely used devices for measurement of *in situ* rock stresses, by the stress relief over coring method." The HI stress cell was used at the Rosh Pinah Mine. The location of stress measurements was chosen to obtain reliable results.

The site should be located (in):

- Fine grained homogenous rock.
- Intact and isotropic rock.
- Away from geological structures such as shear zones.
- Isolation from other existing excavation.

The site chosen at WF3 -030 has a massive arkose with small isolated pepples and grits with minor brecciated zones. The UCS of the rock was about 200 MPa. The test site was placed further away from excavations that could have an influence on the results. The bearing for the hole was 243.6° and had an inclination of 29.6° upwards. Two stress measurements were taken. The first measurement was taken at 10.39 m depth, and the second measurement was taken at 11.6 m. From Figure 30, it can be seen that there is a joint structure in measurement one behind the strain cell. However, the structure, according to GroundWorks consultant, did not influence the direction of the principal stresses as the structure was intact at the time of stress measurement (Handley & Piper, 2014).



Figure 30. Sections of over core showing strain cells (Handley & Piper, 2014).

The results from the two stress measurements in Table 14 show a large variation of all three principal stresses. The major principal stress for stress one measurement is twice than that of stress measurement two. According to Handley and Piper (2014), both measurements are considered to be of good quality and reliable, although they are different in magnitude. Both measurement results will be used for numerical modelling and their results will be compared.

Table 14. Stress measurement readings at WF3 – 030.

Stress Measurement One			
Stress Components	Gradient (MPa)	Plunge (°)	Trend (°)
σ_1	0.117	34	342
σ_2	0.069	39	106
σ_3	0.026	32	227
σv	0.073		
Stress Measurement Two			
Stress Components	Gradient (MPa)	Plunge (°)	Trend (°)
σ_1	0.044	14	135
σ_2	0.029	59	21
σ_3	0.018	27	232
σv	0.028		

Both these measurements were taken into account and plotted against the Southern African stress measurement database. A qualitative way to assess the results from measurements one and two is to plot them against a background of crustal stress measurements made in Southern Africa over the last 40 years (Handley, 2013). In Figure 31, the two measurements were plotted on the Southern African stress measurement database and the results are within the limits of the two Hoek–Brown Minimum and Maximum best fit lines as shown.

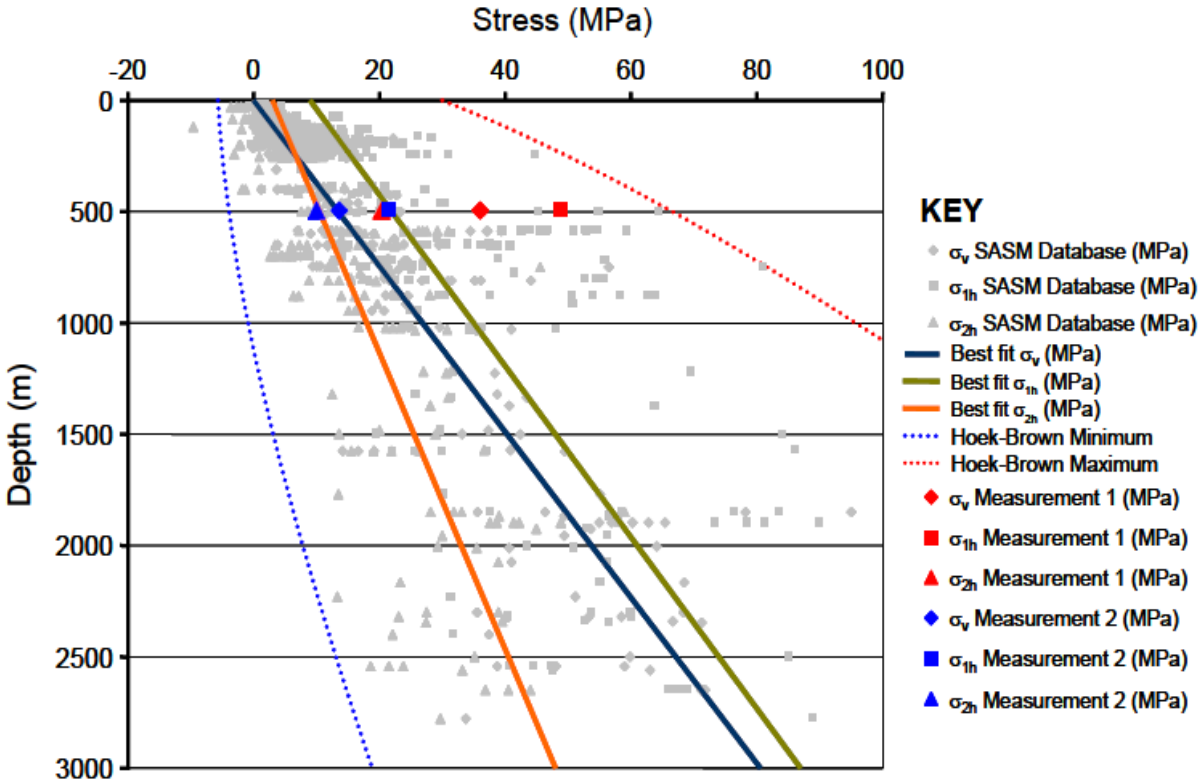


Figure 31. A plot of stress vs depth for both measurement one and two.

The k-ratio for the two measurements also showed a good agreement, as they lie close to the best fit lines as indicated in Figure 32. Handley and Piper (2014) noted that although these plots cannot be used as a test of quality of the measurements, they do confirm that the measurements make sense, and that all the efforts to ensure good quality measurements at Rosh Pinah were largely successful.

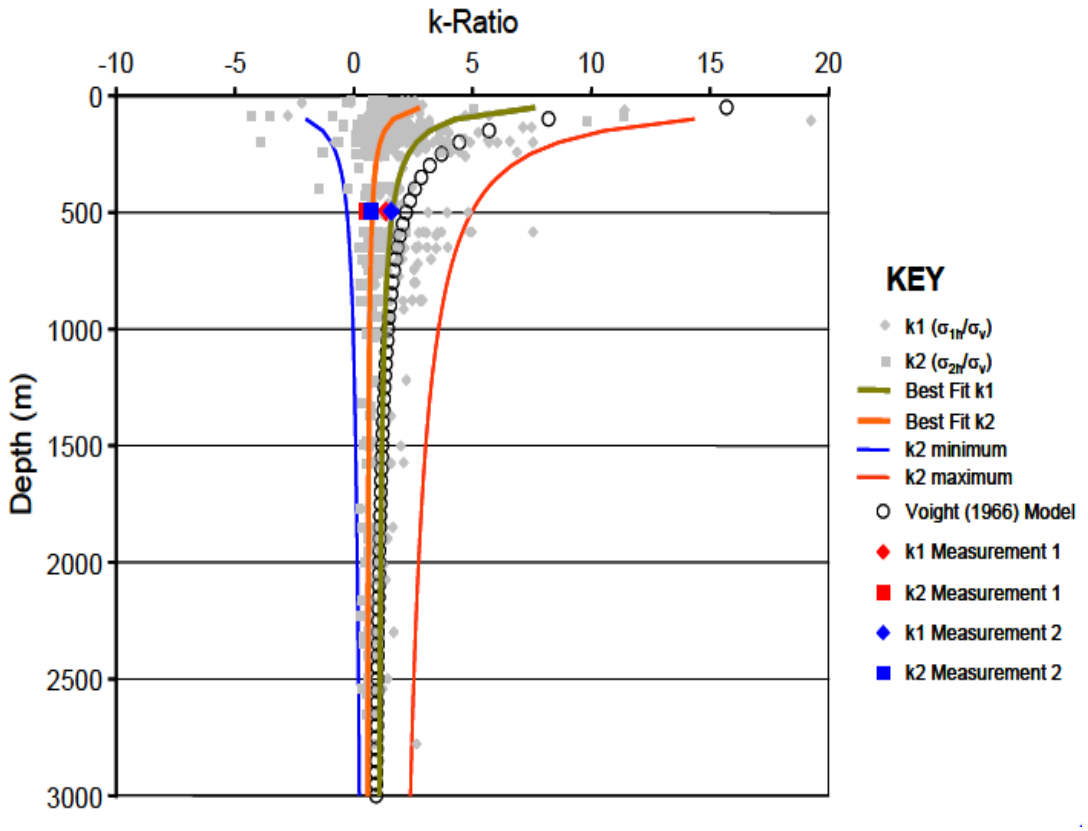


Figure 32. A plot of the K ratio for both measurement one and two.

The stress measurement two was used for the project because of its virgin stress corresponding to that of the expected virgin stress of 13 MPa. The bearing of the stress measurement two also corresponds to that of the bearing of sigma one stress field, which was estimated in the SRK report to be 142.6°, as derived from the O'Okiep measurements near Black Mountain in the Western Cape, South Africa. Underground observations on site indicate a low stress environment at current depths for the SF3 orebody and no signs of stress damage were reported.

3.4.2 Design of open stopes

In order to predict stope stability, there are certain geotechnical parameters that need to be obtained. Core logging as well as underground mapping was carried out for the SF3 orebody. These parameters were derived from statistical distribution and are represented in Table 15.

Table 15. Joint properties from core logging

	Ja	Jr	RQD	GSI
Arkose	5	2.5	80	67
Carbonate	1	3	100	89
Argillite	1	2	100	84
Breccia	1	3	100	89

3.4.3 Rock Mass Model

A geotechnical rock mass model was constructed in Leapfrog using geotechnical-logged boreholes for understanding the geotechnical domains of the SF3 orebody. As can be seen in Figure 33, the RQD values of the SF3 orebody are lower in the upper mined out portions of the orebody from level 140 to 230, with a range of 40-60 RQD. The lower portion of the orebody is characterised by more ideal ground characteristics, with an average RQD of 90%. It is important to obtain the correct parameters for the design of stope stabilities, and so far the only geotechnical mapping that was performed for the SF3 orebody was between the 110-030 levels.

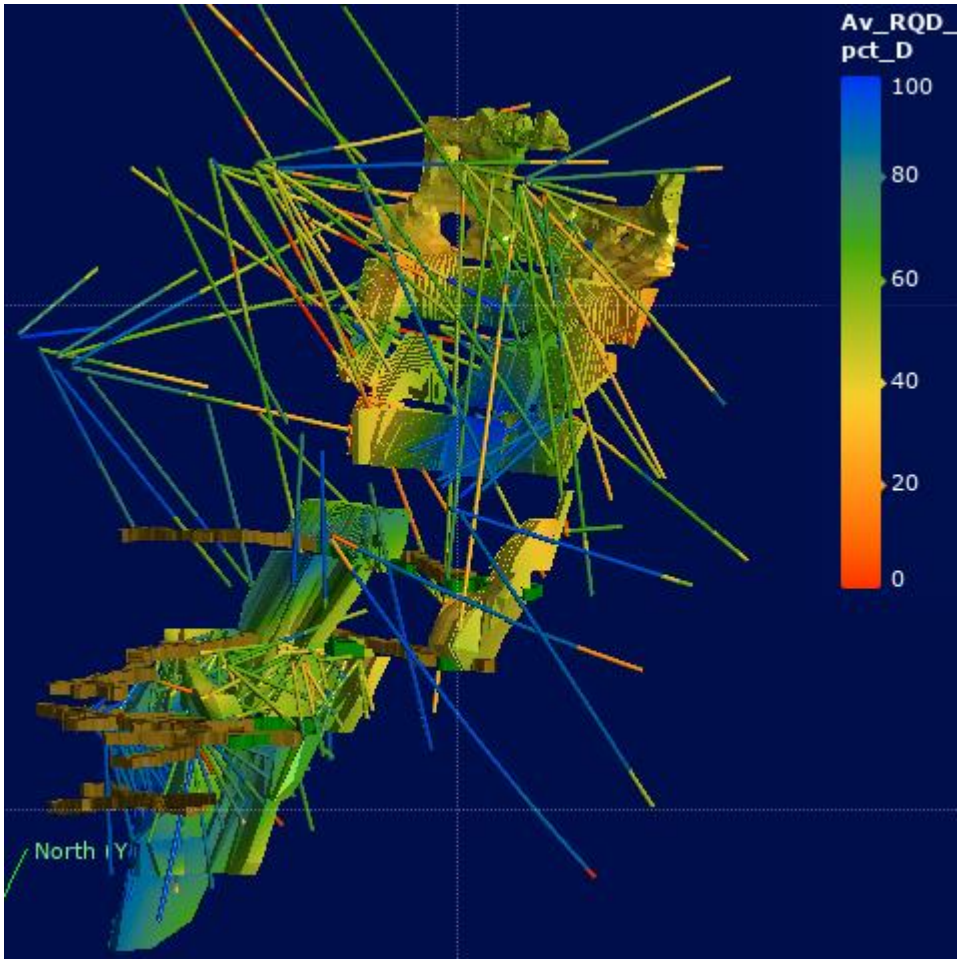


Figure 33. Rock mass model depicting RQD for SF3 orebody.

3.4.4 Rock Quality Designation

According to Tommila (2014), the concept of RQD is used as a measure of the fracture spacing and has a strong influence on both the Q' and GSI. The RQD values used for the SF3 orebody were estimated from core logging, as well as face mapping, especially on the upper levels of the orebody where sill access drives have been developed. Figure 34 shows the average RQD of the SF3 orebody, which is in the range of 95-98%.

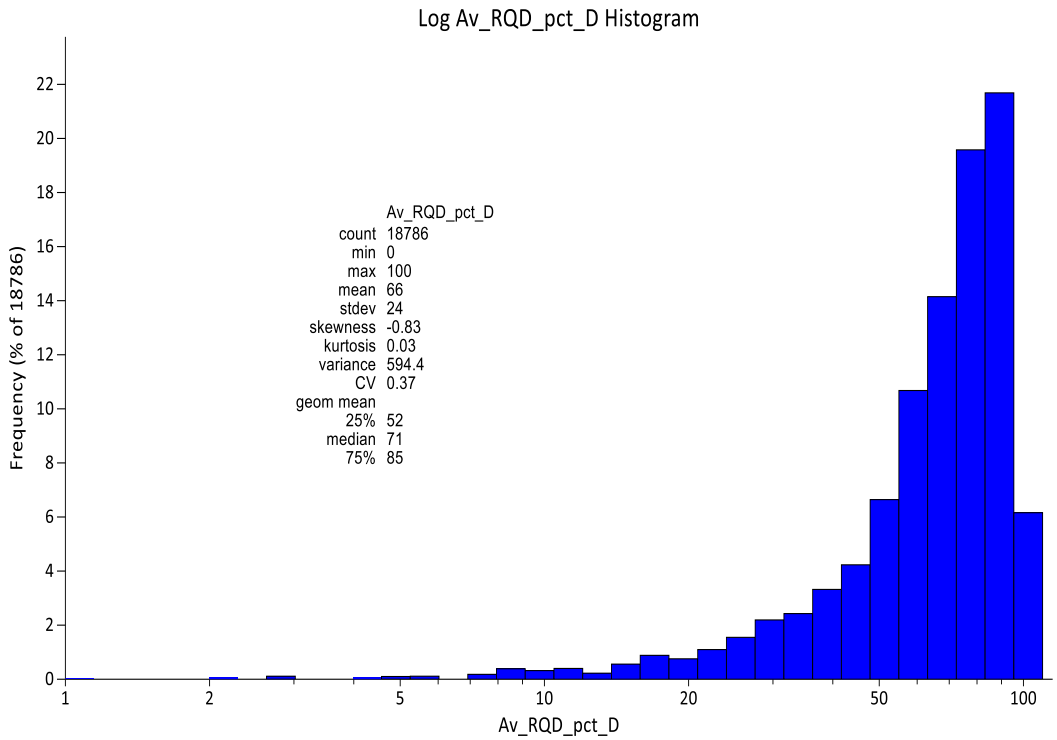


Figure 34. A histogram showing the log average RQD.

3.4.5 Geological Strength Index (GSI)

The GSI was first introduced by Hoek (1994) and was developed to account for the discontinuity or joint rock mass conditions that affect the deformation and strength of the rock mass. The GSI is a very important parameter in the use of numerical modelling when using constitutive models that incorporate the use of the Hoek–Brown failure criteria. Equation 3.1 is used to derive the GSI, as proposed by Hoek et al. (2013):

$$GSI = \frac{52Jr/Ja}{(1+\frac{Jr}{Ja})} + RQD/2 \qquad 3.1$$

Where Jr is the joint roughness coefficient, Ja is the joint alteration and RQD is the rock quality designation. Table 16 shows the GSI values of different lithological units, as calculated from the core. The carbonate unit has the highest GSI value of 89, as carbonate is comprised of massive lithological units with few jointing.

3.5 Rock Mass Classification

A detailed rock mass classification was carried out using bore hole data as well as mapping data. All the infill-drilled holes from the geological drilling programme are geotechnically logged by the geotechnical engineers at the mine. The table below shows the summary of the rock mass classification parameters derived from geotechnical-logged boreholes used in the designs of the SF3 orebody.

Table 16. Lithological domains and geotechnical rock mass parameters.

Domain	Ja	Jr	RQD	GSI
Arkose	5	2.5	80	67
Carbonate	1	3	100	89
Argillite	1	2	100	84
Breccia	1	3	100	89

Table 16 indicates that the host rock (arkose) is competent and has a RQD value of 80 and a GSI of 67. The UCS of the host rock mass was estimated to be 139 MPa.

3.6 Empirical stope design methods

The empirical stope design method used at Rosh Pinah Mine to help determine the stability of open stopes follows that proposed by Potvin 1988 and Nickson 1992.

The N' stability number is derived from the factor A which is the stress factor, B which is the joint adjustment factor, C which is the gravity factor, and the Q' which is the modified Q.

Table 17. Stability graph parameter estimates

SHAPE AND GEOMETRY									
Segment	**HW Dip**	**STRIKE LENGTH (m)**	**TRUE H/W HEIGHT (m)**	**H/W PERIMETER (m)**	**H/W SURFACE AREA (m^2)**	**HR**	**N'**	**Stability**	**Mining Levels**
HW	60	60	21	162	1260	7.8	1.1	Yes	Level 110
SW	90	7	21	56	147	2.6	2.9	Yes	
Backs	0	60	7	134	420	3.1	0.7	Yes	
HW	60	20	24	88	480	5.5	6.8	Yes	Level 110-2
SW	89	9	24	66	216	3.3	14.4	Yes	
Backs	19	20	9	58	180	3.1	2.8	Yes	
HW	57	62	54	231	3323	14.4	8.2	No	Level 080
SW	90	57	6	126	342	2.7	16.3	Yes	
Backs	0	62	7	138	434	3.1	4.1	Yes	
HW	67	62	67	258	4154	16.1	9.2	No	Level 050
SW	90	62	6	136	372	2.7	16.6	Yes	
Backs	0	6	67	146	402	2.8	4.6	Yes	
HW	57	55	127	364	6985	19.2	11.3	No	Level 020-1
SW	90	27	127	308	3429	11.1	30	Yes	
Backs	0	55	27	164	1485	9.1	7.5	Yes	

Table 17 (contd) Stability graph parameter estimates.

SHAPE AND GEOMETRY									
Segment	**HW Dip**	**STRIKE LENGTH (m)**	**TRUE H/W HEIGHT (m)**	**H/W PERIMETER (m)**	**H/W SURFACE AREA (m^2)**	**HR**	**N'**	**Stability**	**Mining Levels**
HW	57	31	60	182	1860	10.2	16.2	Yes	Level 020-2
SW	90	6	60	132	360	2.7	27.4	Yes	
Backs	0	35	6	82	210	2.6	18.3	Yes	
HW	57	80	166	492	13280	27	16.2	No	Level -010
SW	90	8	166	348	1328	3.8	27.4	Yes	
Backs	0	80	8	176	640	3.6	18.3	Yes	

According to Villaescusa (2014), the stability graph method is used as a design tool. However, the system has a number of limitations that must be understood in order to assess its applicability in any particular geotechnical environment. The HR values of the designed stopes were measured by accumulating the stope dimensions as mining descends downwards. The HR was found to be somewhat difficult to measure accurately because of the irregular orebody geometry. Mining has taken place at the upper stopes from Level 230 to Level 140. Hence Table 17 only indicate stopes from Level 110 -010.

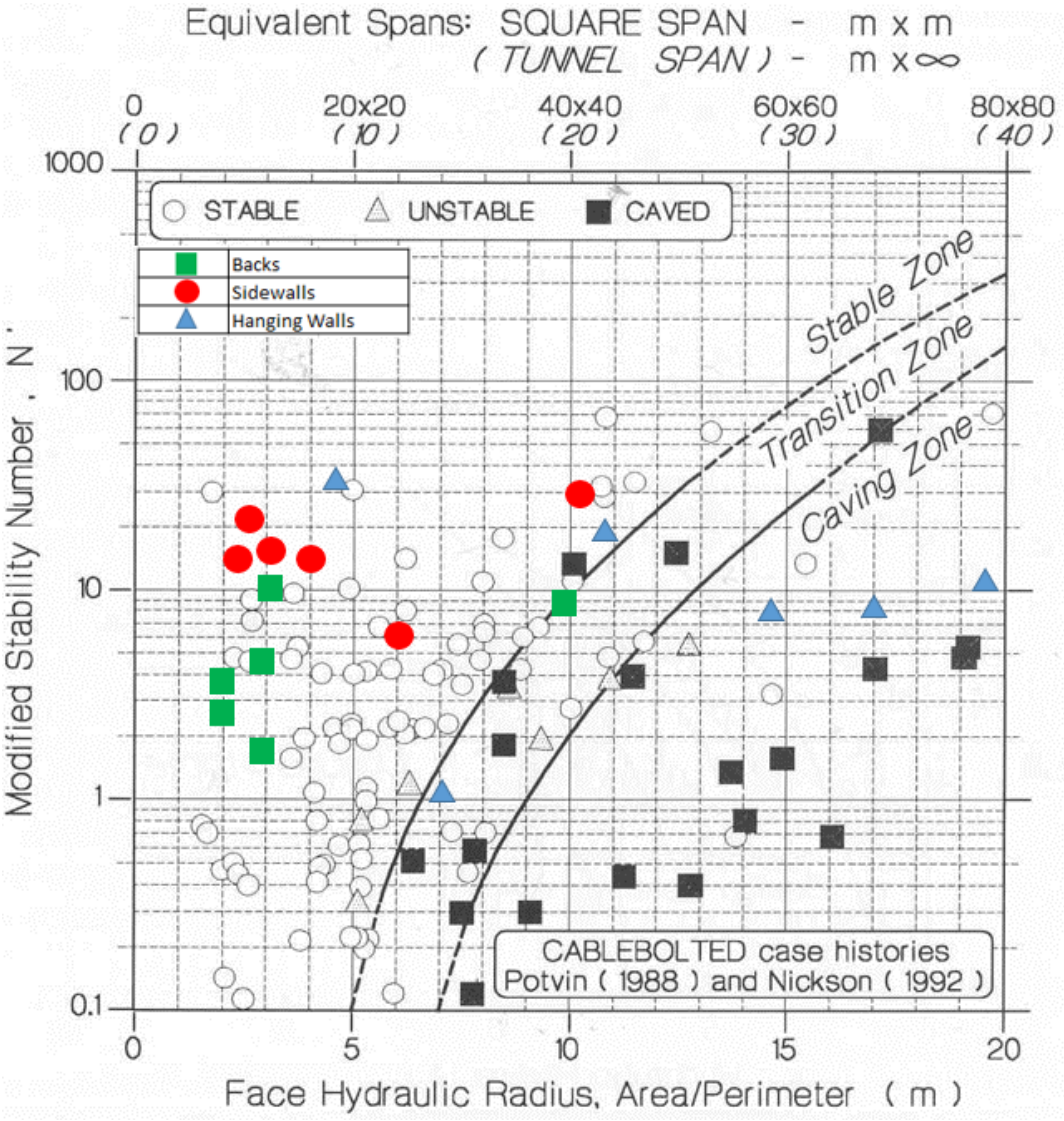


Figure 35. Stability graph for unmined stopes (Hutchinson & Diederichs, 1996).

Mining of Level 110 is expected to be stable before the mining of the levels beneath. However, support will be required in the form of cable anchors. As indicated in Figure 35 on the stability graph, mining Level 080 by undercutting Level 110 will result in an

unstable hanging wall, owing to an increased hydraulic radius, changing from 7.8 to 14.4m respectively. As indicated in Figure 36 the hanging wall is compromised when mining from Level 080 to 010, taking into consideration that no backfill will be used to compartmentalise the mine to increase the extraction ratio. It is expected that dilution will occur when mining from Level 080, and it is expected to increase with an increase in HR as mining of deeper levels occurs. It is recommended that a regular stope scan be carried out to determine the overbreak of the stope and to validate the design assumptions.

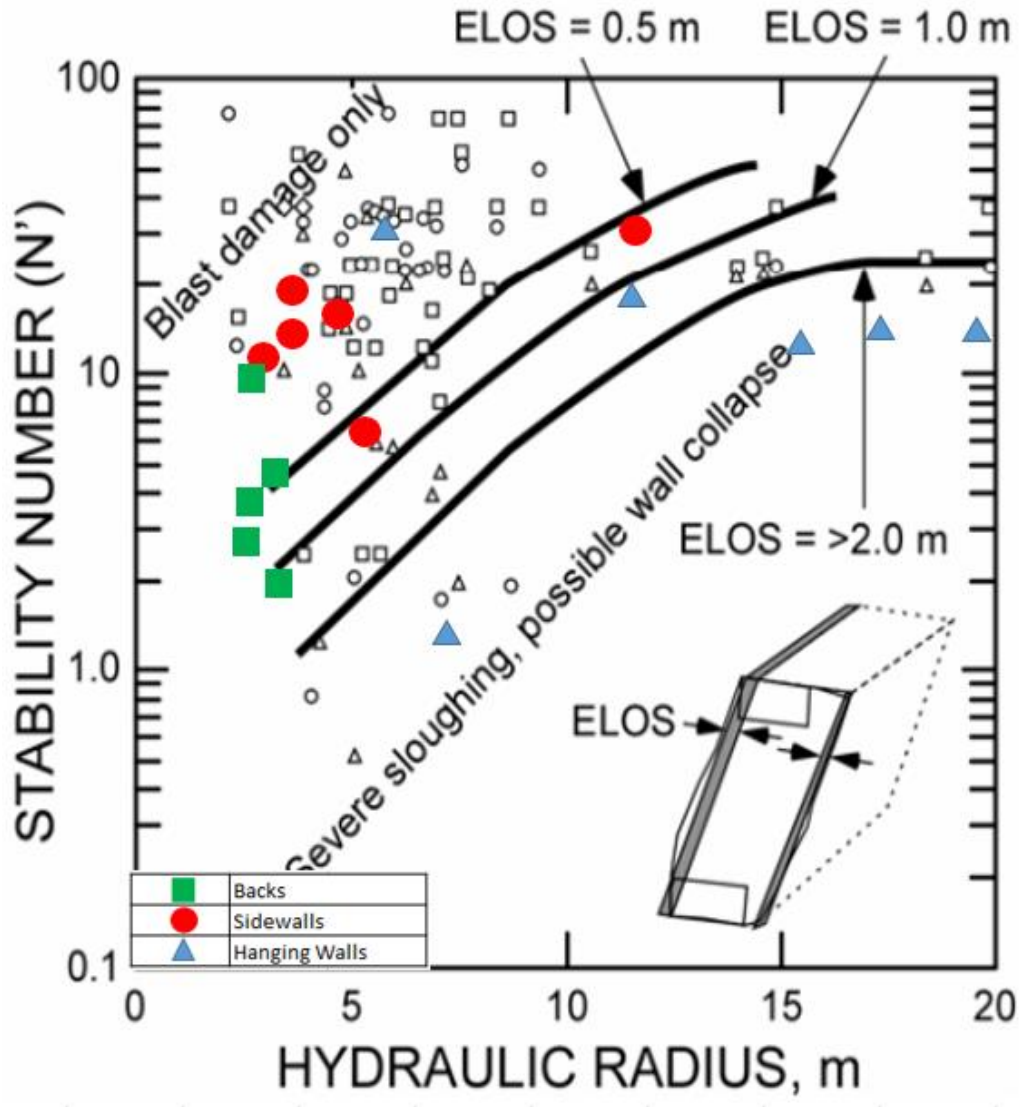


Figure 36. A graph showing the Equivalent Linear Overbreak Slough (ELOS) (Brady et al., 2005).

The Equivalent Linear Overbreak Slough was included in Figure 36, and indicates that the Level 110 is <0.5 m, which is within the limits of acceptable overbreak. Mining Level 080 and 050 are beyond an ELOS of 4 m. An ELOS greater than 4 m indicates a major overbreak is likely to occur and in most cases an overbreak beyond an ELOS of 4 m does not justify designing a stope of such a dimension.

The following categories have been used to determine stope performance:

- Stable – depth of failure 0.0 to 2.5 m
- Transition – depth of failure 2.5 to 4.0 m
- Unstable – depth of failure >4 m.

The results from Figure 36 indicate that an ELOS of greater than 4 m is expected when mining level 80 with a stope height of 30 m cumulatively, as mining progresses downwards. Further representation of stopes mined to level 20 with a cumulative height of 90 m shows a much larger ELOS greater than 4 m. Hence, a pillar can be left at 50 level in order to reduce the HR – which improves the stability.

3.7 Stope excavation support

Cable bolting at Rosh Pinah Zinc Mine is carried out by a five men cable bolting crew, which installs cable bolts into 51 mm holes that are drilled by an air buggy drill machine. Twin strand bulbed cable bolts, each with a diameter of 15.8 mm, are inserted into holes and grouted with a 42.5N Portland cement, with a water to cement ratio of 0.35–0.40 as requested by the rock mechanic engineer. A ChemGrout CG-500/3*8-grout pump is used to pump grout into the holes. A black breather tube with a diameter of 10 mm is inserted into up holes, with the cables to act as an air release hose during the grouting process as well signalling the crew that enough grout has been pumped into the hole once it overflows. Grout is pumped with a tube slightly larger than the breather tube and is inserted through a paste retainer and tied to the cable bolt just 15 cm from the collar of the hole.

Routine Quality Control and Quality Assurance is carried out by the rock mechanic engineer to ensure that the support installed abides with the standards of the Rosh Pinah Zinc Mine. Frequent observational tests are done in order to assess the mixing ratio of

grout, to ensure that good quality cement is inserted into the hole. Post observations are also done by the rock mechanic engineer on face plates, wedge and barrels, to ensure that the faceplate fits snuggly onto the OSRO strap and the excavation of the surface.

3.8 Support requirements for SF3 stopes

Figure 37 indicates estimations for the cable densities in the hanging walls of the SF3 orebody. By using the block size factor (RQD/Jn)/HR, individual stopes were assessed for the suitability of cables and estimation of the cable bolt density. Cable bolting studies are important as total extraction of stopes will be carried out. The estimation for cable bolt density indicates that the first two lifts level 110 and 080 are likely to be conservative owing to a larger (RQD/Jn)/HR factor. Mining Level 050 to -010 lie in the range of 0.2 cable density. Table 18 outlines the relative block size factors for the hanging walls of all levels of the SF3 orebody.

Table 18. Relative block size factor for hanging walls

Mining Level	RQD	Jn	(RQD/Jn)	(RQD/Jn)/HR
Level 110	75	4	18.8	2.4
Level 110-2	45	4	11.3	2
Level 080	68	5	13.6	0.9
Level 050	77	5	15.4	1
Level 020-1	75	4	18.8	1
Level 020-1	68	6	11.3	1.1
Level -010	68	6	11.3	0.4

Figure 37 shows that the cable bolting of stopes appears in a non-entry zone. As the stopes get larger, this results in more unstable hanging walls.

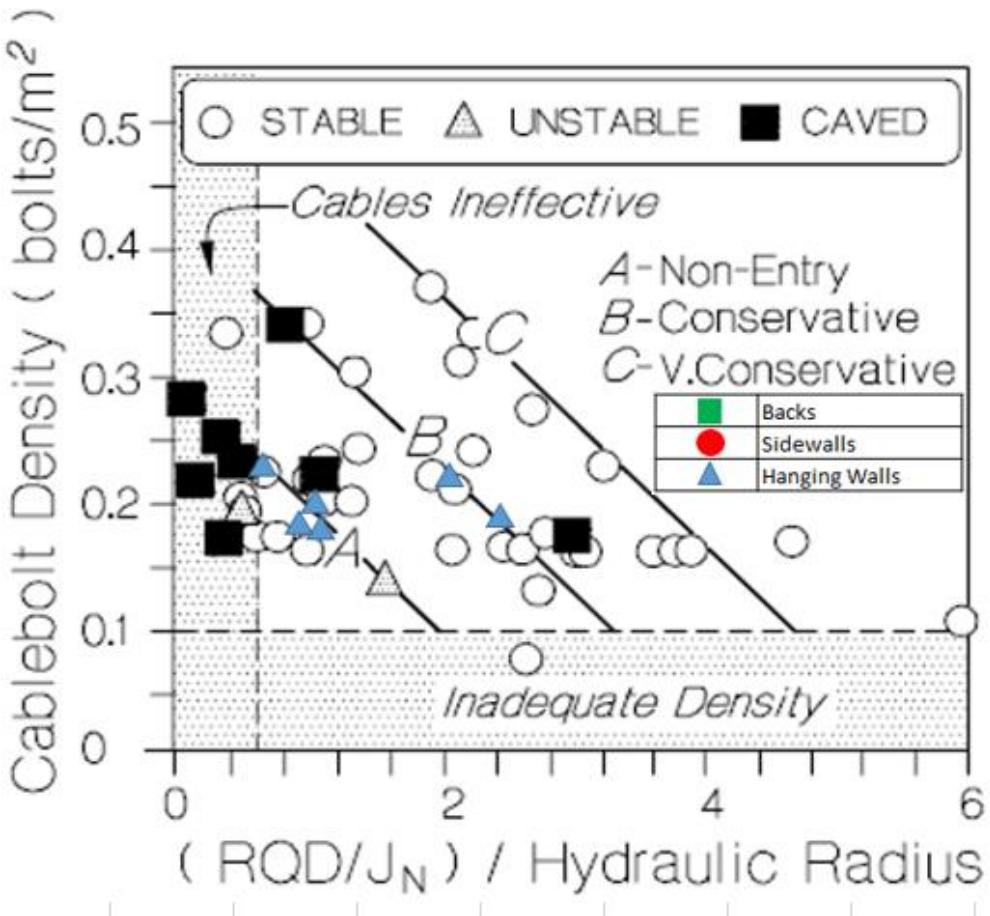


Figure 37. Design chart for cable bolt density (cable bolt/m^2)(Potvin,1988).

Stope hanging walls need to be supported to reduce dilution. The sidewalls gradually would require support as mining progresses deeper. This is a result of increased hydraulic radius. Figure 38 indicates that the hanging wall towards the end of mining will cave irrespective of the cable bolting. The larger the stope becomes, the larger the HR, and hence an increase in relaxation zones surrounding the excavation boundaries.

Figure 38 also indicates that initial stoping at Level 110 would not require cable bolting. However, as the stope size increases, cable bolting would be required. The last three mining Levels from 20 to -040 would require cable bolts with an average length greater than 18 m. Furthermore, the initial stages of mining at Level 110, hanging walls can be installed with longer cables than estimated from Figure 38.This will ensure that a conservative design is attained in order to have a more uniform cable bolt length in the hanging wall.

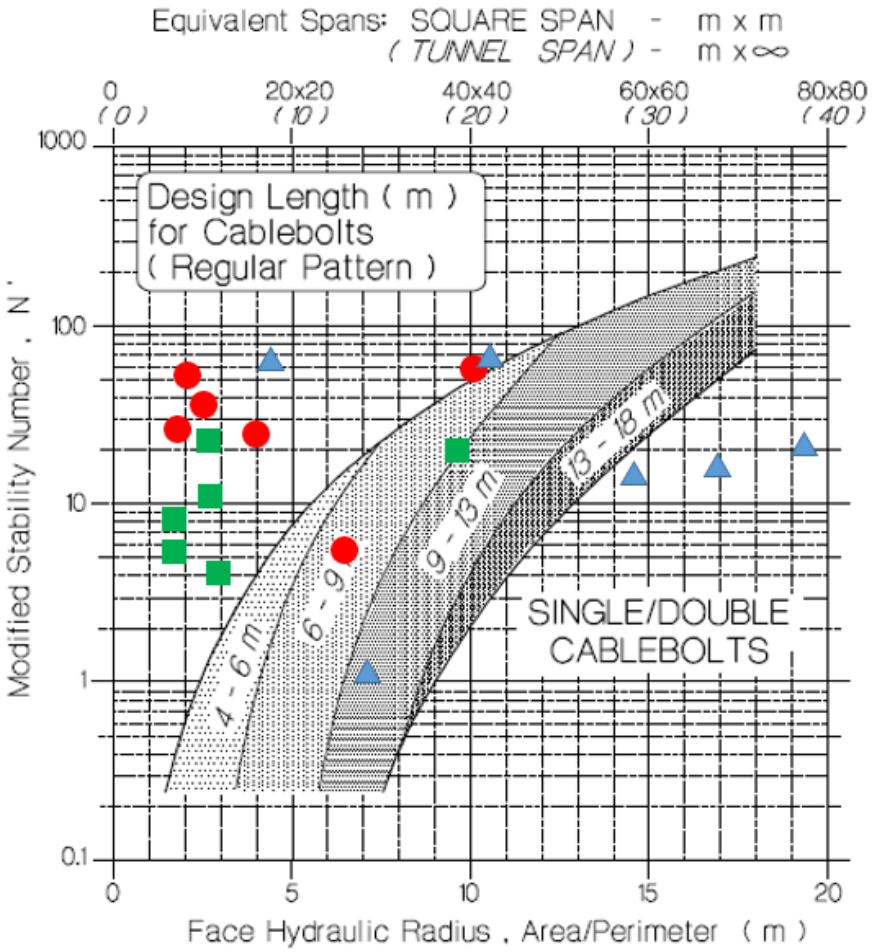


Figure 38. A graph showing estimates of cable bolt lengths (Hutchinson & Diederichs, 1996).

3.9 Summary

In this chapter brief overviews of the history of mining at Rosh Pinah Zinc Mine, the geological setting of the Rosh Pinah orebody, and the background on the SF3 Ore body were highlighted. Furthermore, the chapter also discussed the outcomes of potential stability and dilution of the SF3 orebody by making use of empirical methods such as the N' and ELOS. The results were plotted on a modified stability diagram after Brady et al. (2005).

The chapter concluded with the formulation of support requirement for the hanging walls for each level of stoping.

4 Numerical modelling of the SF3 orebody

Numerical modelling was carried out using the IUCM constitutive model proposed by Vakili (2016), which attempts to address the limitations of current material models used in rock mechanics.

4.1 Conceptual rock mass for SF3 orebody

Four domains have been chosen to represent the rock mass. The input parameters are shown in Table 19. As shown in the table, the classification of these rock masses is massive according to the GSI, with a lowest value 65 found in microquartzite, and a largest value of 89 for both the breccia and carbonate rock mass domains. The following summarises the four rock mass domains used in the model:

- Rock Mass – Arkose. The arkose rock mass can be considered moderate, with a GSI value of 67.
- Rock Mass – Breccia. The breccia rock mass can be considered massive, with a GSI value of 89 and a high UCS value as can be seen in Table 19.
- Rock Mass – Carbonate. The carbonate rock mass which hosts the mineralisation is characterised by a lower UCS value compared to other rock masses. However, it is considered massive with a GSI value of 89.
- Rock Mass – Microquartzite. The microquartzite rock mass has the lowest GSI value of 65. This rock mass is anisotropic and has a lower UCS value.

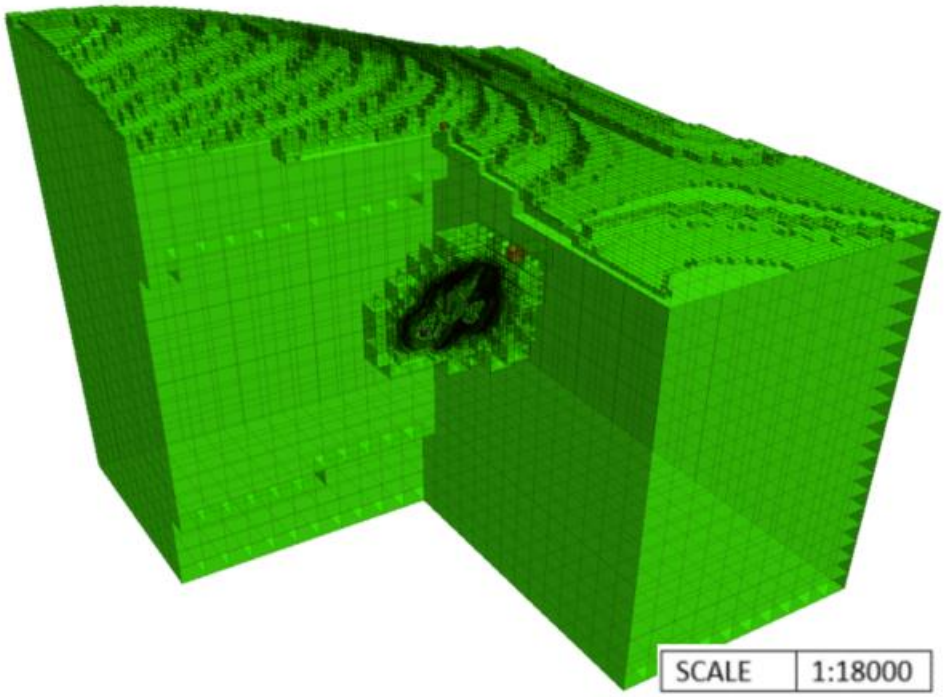
Table 19. Input parameters used for forward analysis for the SF3 orebody.

Rock Strength Properties									
Rock Unit	**IUCM Input Parameters**								
	Density (t/m^3)	**E_i (GPa)**	**Sig_{ci} (MPa)**	**mi_{Max}**	**mi_{Min}**	**Anisotropy Factor**	**Dip (°)**	**Dip Direction (°)**	**GSI**
Arkose	2.69	72	292	15	7.5	-	-	-	67
Breccia	3	72	232	15	7.5	-	-	-	89
Carbonate	3.83	62	139	20	10	-	-	-	89
Microquartzite	2.76	58	163	12	6	1.4	75	235	65

4.2 Modelling construction and approach

The geometry of the model indicating the topography, as well as the orebody geometry, is indicated in Figure 39. The topographic surface, geotechnical domains and orebody geometries were included in the model. A mesh of 3 m ×3 m ×3 m was used to envelop the orebody. The far field zone size of 48 m was used, which is the largest far field in the model. These parameters were considered to minimise the run time of the model, while taking into consideration the level of accuracy required to run the model.

a) Topographical view of SF3 orebody



b) Cross sectional view of the SF3 Orebody

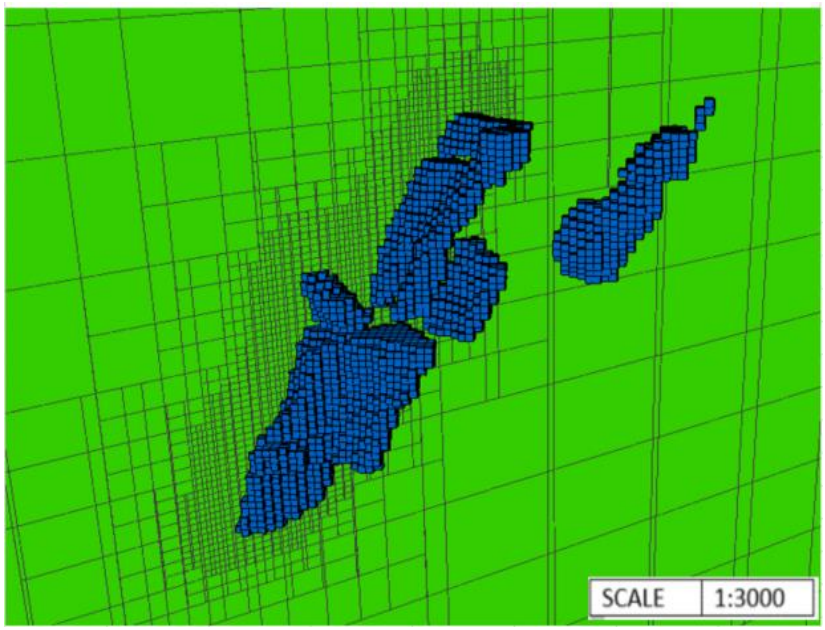


Figure 39. Geometry of a model indicating the topography as well as the orebody geometry.

Numerical modelling was undertaken in 10 different phases – as shown in Figure 40. The model sequence used is the top-down approach to replicate the actual method at the mine. No backfill is currently used at the mine, since mining is carried out as a total extraction and a natural pillar was left between level 140 and 110. The orebody geometry, together with the main lithologies such as arkose, micro quartzite and breccia, were included in the model.

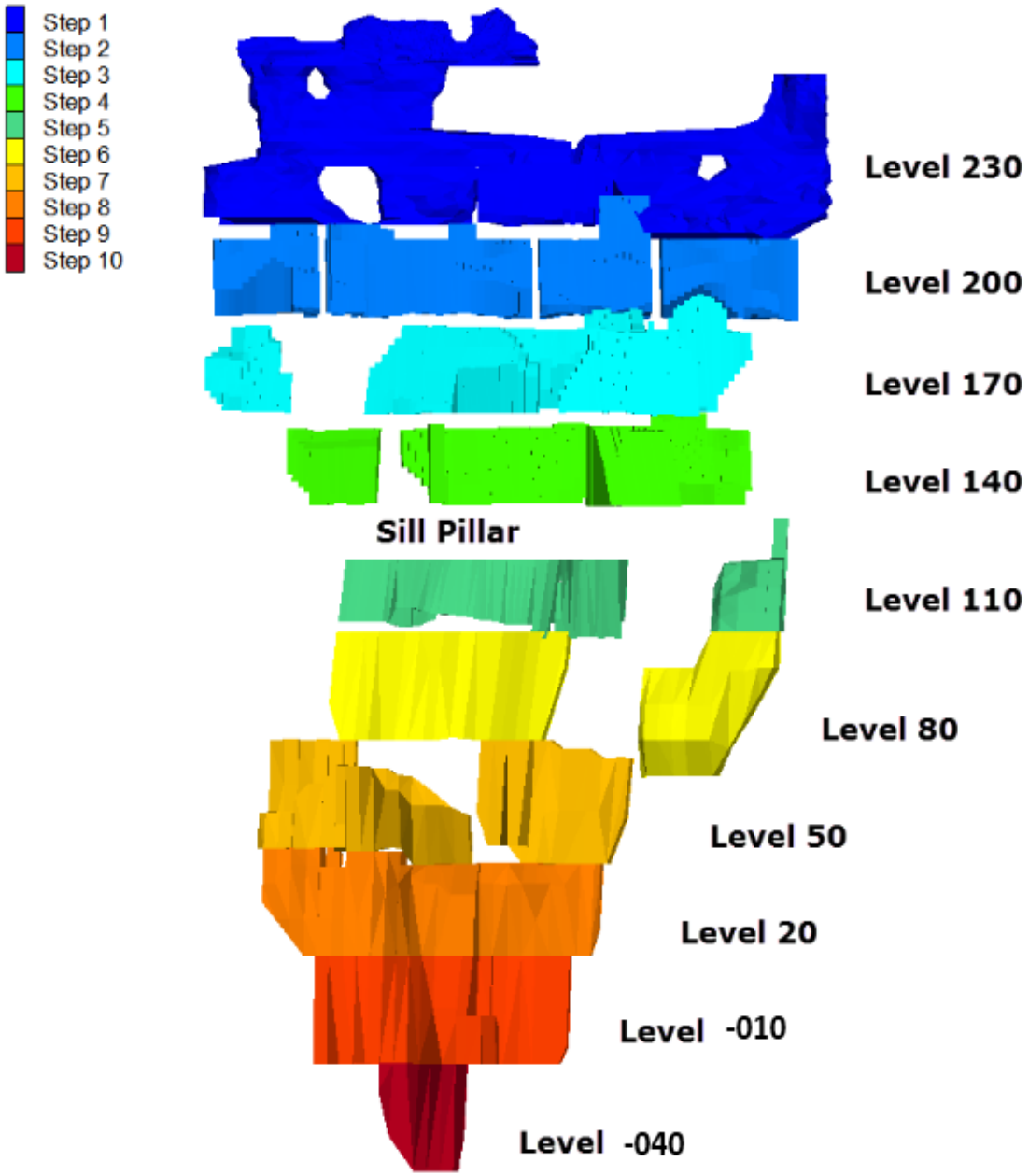


Figure 40. Front view, showing the model sequence (Shali & Vakili, 2019).

4.3 *Numerical modelling results and interpretation*

The volumetric strain and stress factors were used in the interpretation of numerical modelling results for the SF3 orebody.

4.3.1 Volumetric strain

The IUCM uses volumetric strain to represent the damage severity and degree of disintegration within the rock mass. Volumetric strain was calculated by summing the major, minor and intermediate strains – as shown in equation 4.1.

$$\frac{\Delta V}{V0} = \varepsilon 1 + \varepsilon 2 + \varepsilon 3 \qquad 4.1$$

A positive value for volumetric strain indicates dilution, while a negative value indicates contraction. Contraction occurs at high confinement levels as opposed to dilation – which happens in lower confinement zones such as near the boundary of the excavation. According to Vakili (2016), the "rock mass damage is mostly controlled by dilational volumetric strain induced at low confinement levels." However, in cases of high confinement levels, the rock can still become highly damaged and pulverised while undergoing contraction (negative volumetric strain).

	Class I	Class II	Class III	Class IV
Volumetric Strain	0.5%	1.0%	2.0%	5.0%
Visual Appearance				
Conditions in Massive Rock Mass	– Onset of cracking – Less than 20% of blocks mobilised – Probability of failure is less than 20% – Less than 5% Cohesion Loss – Rock bridges exist along 80% of cracks	– Intermediate cracking – Around 50% of blocks mobilised – Probability of failure is around 50% – Around 20% Cohesion Loss – Rock bridges exist along 50% of cracks	– Extensive cracking – Around 80% of blocks mobilised – Probability of failure is around 80% – Around 50% Cohesion Loss – Rock bridges exist along 20% of cracks	– Very extensive cracking – More than 80% of blocks mobilised – Probability of failure is more than 80% – More than 50% Cohesion Loss – Minimum Rock bridges existing
Conditions in Highly Jointed Rock Mass and in high confinement	– cracking and joint opening – Less than 50% of blocks mobilised – Probability of failure is less than 20% – Less than 5% Cohesion Loss	– Around 80% of blocks mobilised – Probability of failure is around 50% – Around 20% Cohesion Loss	– Most blocks are mobilised – Probability of failure is around 80% – Around 50% Cohesion Loss	– Most blocks are mobilised – Probability of failure is more than 80% – More than 5% Cohesion Loss
Conditions in Highly Jointed Rock Mass and in low confinement	– Deep cracking and joint opening – Less than 50% of blocks mobilised – Probability of failure is less than 50% – Less than 5% Cohesion Loss	– Around 80% of blocks mobilised – Probability of failure is around 80% – Around 20% Cohesion Loss	– Most blocks are mobilised – Probability of failure is more than 80% – Around 50% Cohesion Loss	– About 80% of blocks mobilised – Probability of failure is more than 80% – More than 5% Cohesion Loss

Figure 41. Visual representation of the degree of rock disintegration at various levels of volumetric strains (Vakili et al., 2012).

The results in Figure 42 show volumetric strain of the SF3 orebody. The orebody has been cut into three horizontal cross sections, as indicated. The iso-surface for volumetric strain of 0.5, 1 and 3%, shows that the severity of the degree of disintegration is minimal at stopes above level 110, whereas a higher degree of rock mass damage is expected at levels between level 080 and -040. With a total extraction

method employed for the SF3 orebody, higher dilution is expected to occur when mining at these levels.

The vertical cross section (a) in Figure 42 on level 050 indicates a large area from the stope boundary that falls within the volumetric strain of 2-3%, which, according to Figure 41, shows a class III and class IV that illustrates extensive cracking – as well as mobilisation of 80% of the block.

Furthermore, Vakili (2016) emphasised that experience “in numerical back analysis at several mining operations showed that a model volumetric strain of 1% to 3% often generates similar or close to overbreak/breakout volumes to those obtained from actual underground excavations.” The volumetric stain of 0.5, 2 and 3% were calculated and estimated by volume comparison. It was found that more dilution was expected when a 1% volumetric strain is used, resulting in about 20.69% dilution. The lowest dilution was expected with a 3% volumetric strain of about 1.92% dilution. Figure 42 shows the isosurface volumetric strain of 1%, which resulted to the most dilution (20.962%). Figure 42 also indicates that most of the dilution will be occurring at the lower levels of the orebody towards the end of mining the SF3 030, as well as SF3 010 blocks.

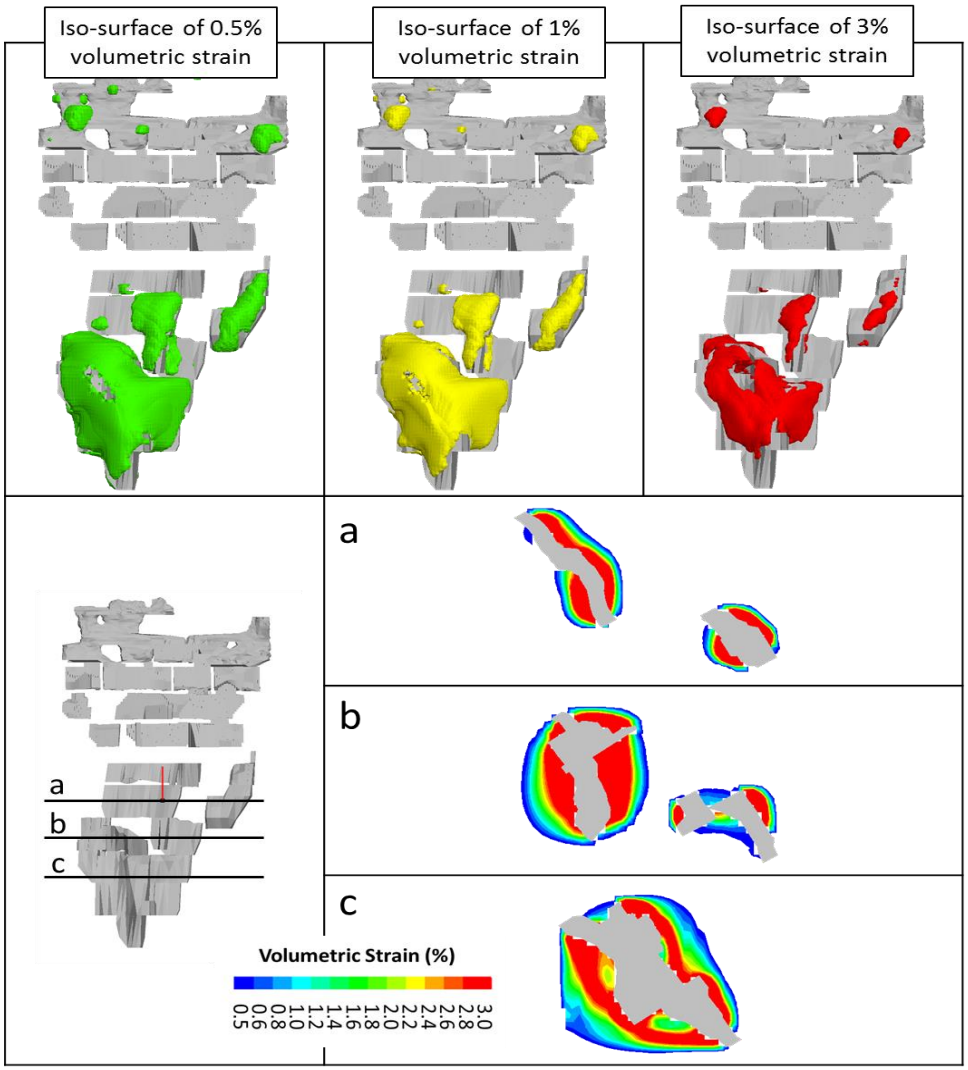


Figure 42. Isosurface of 0.5, 1 and 3% volumetric strain.

4.3.2 Stress factor

Another parameter that was used to assess the stability of the stopes was the minor principal stress. As the minor principal stress approached zero, the stope instability becomes prone to gravity since the rock mass is free to dilate. According to Martin et al. (1999), confining stress expressed as sigma three, may be a good indicator for predicting the amount of dilution. The zone surrounding the mined stope walls is close to zero, meaning that there are no confining stresses and rock may fall due to gravity. Figure 43 shows the possibility of high dilution – both as shown vertically and horizontally in cross sections of a and b for both the major and minor principal stress.

When mining commences, a CMS can be used to back analyse and calibrate the model with the volumetric strain by adjusting the percentage of volumetric strain and inferring a correlation.

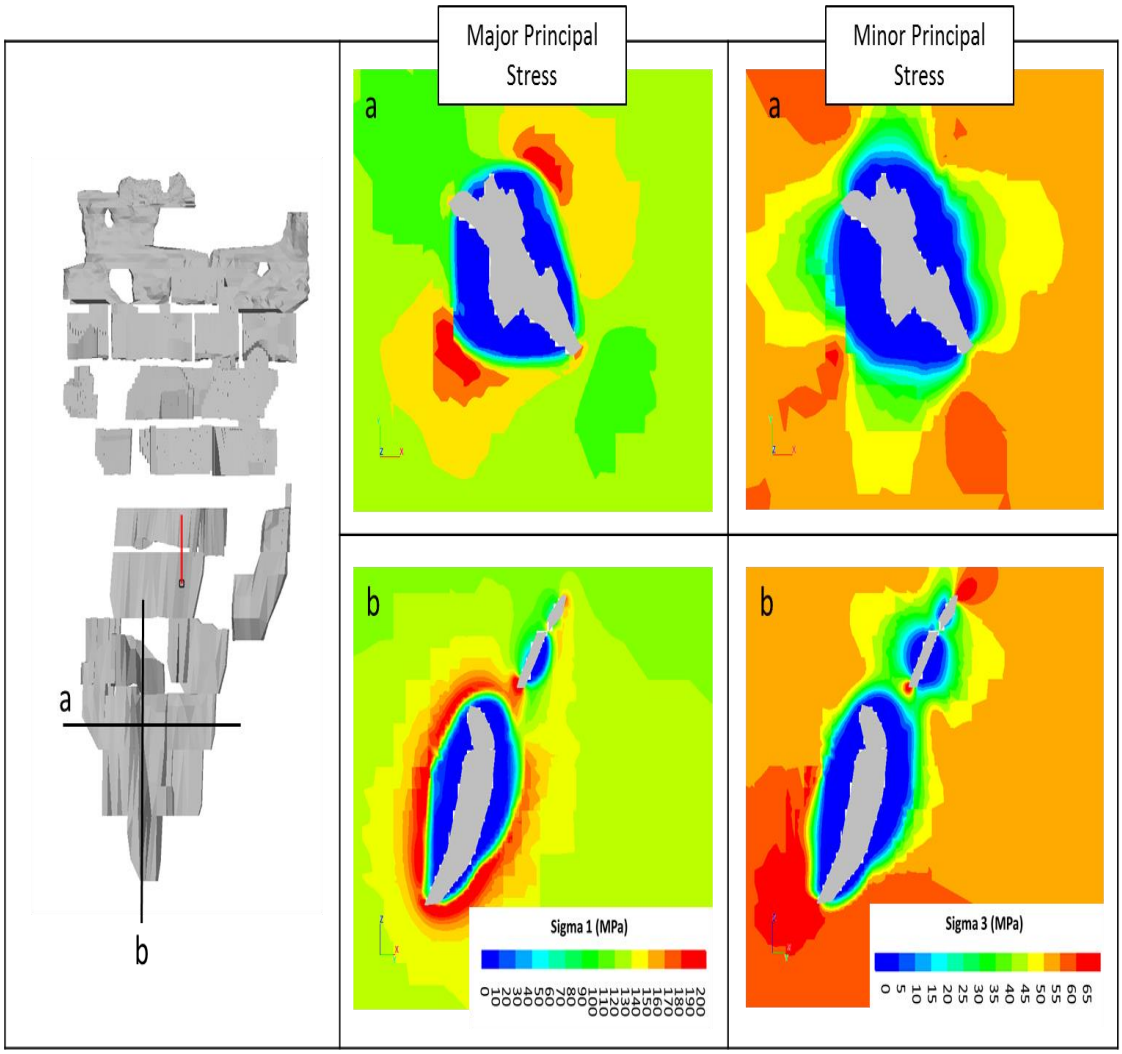


Figure 43. Visual representation of the minor and major principal stress.

4.4 Summary

The chapter discussed the results obtained from the IUCM constitutive model proposed by Vakili (2016) using FLAC. The influence of induced stress on both the hanging and footwall walls was investigated using the concept of volumetric strain. The IUCM model was used to plot the strain distribution around open stopes which translates to failure to evaluate the stability of the hangingwall and sidewalls of the excavations.

5 Conclusions and Recommendations

The rock mass of the orebody of the SF3 orebody is of good quality, and little dilution has been encountered at the upper levels of the orebody between the 140 and 280 levels. The use of empirical modelling shows that the lower portion of the orebody can be mined with a maximum HR of 13, comprising a stope width of 58 m and height of 30 m. The use of numerical modelling is co-related well with the observed dilution in the upper stopes at Level 230 to 200.

The major conclusion from the research is that dilution will increase as mining progresses to the lower levels. The study also assessed the need for cable bolting for hanging wall support, and it was concluded that the ultimate stope size will be too large for the cable to be effective. Furthermore, in future there should be a detailed analysis of Level 050 to incorporate it as a rib pillar that will reduce the span and lower dilution. The following is concluded with respect to the empirical and numerical models:

- Dilution is expected to adversely reduce the grade mined when Level 050 is mined. This is a result of an increase in HR.
- Assessment of cable bolting on the hanging walls using empirical models indicates a cable bolt density below 0.25 bolts/m^2 and a relative block size factor below 2.0, which indicates a potential or occasional fall of ground.

The following are recommended for the future, once mining commences for the SF3 orebody:

- More geotechnical data such as mapping should be carried out as development continues, in order to obtain more data for stability estimations. Furthermore, a sample of intact core should be gathered for laboratory testing from the SF3 orebody. The information used was based on the western orebody data.
- The use of the IUCM constitutive model should be calibrated and verified.
- The use of extensometers in the hanging wall at 110 level will allow the geotechnical engineer to monitor the hanging wall and calibrate the numerical model to assess if there is a need for cable bolting at lower levels.

- The use of CMS scans should be employed periodically, as stoping is progressing downwards. This will allow verification of overbreak or under break and can be compared to numerical modelling.
- Seismic data should be incorporated into the back analysis process, as soon as mining of the stopes commences.

6 References

ASTM D6032 ,1997, Standard testing method for determination of RQD of rock core, ASTM International, 100 Barr Harbor Dr., West Conshohocken, PA,1997, DOI: D6032-96.

Abbas, S. M. & Konietzky, H. (2017) 'Rock mass classification systems', in Introduction to Geomechanics. 09/2017 Ed. Freiberg: Technical University Freiberg, pp. 1–48.

Barla, G. & Barla, M., 2000. Continuum and discontinuum modeling in tunnel engineering. *Rudarsko-Geološko-Naftni Zbornik* 12:45–57.

Barton, N., Lien, R. & Lunde, J., 1974. Engineering classification of rock masses for the design of tunnel support. *Rock Mechanics* 6: 189–239.

Bieniawski, Z.T., 1989. Engineering rock mass classification: A complete manual for engineers and geologists in mining, civil, and petroleum engineering. New York City: John Wiley & Sons, Inc.

Bieniawski, Z.T., 1993. Classification of rock masses for engineering: The RMR system and future trends. In: Hudson, J.A., ed., Comprehensive rock engineering, Volume 3. Oxford, New York: Pergamon Press, pp. 553–573.

Brady, T., Martin, L. & Pakalnis, R., 2000. Empirical approaches for opening design in weak rock masses. Mining Technology, 114(1),13-20.

Brady, B.H.G. & Brown, E.T., 1988. Rock mechanic for underground mining. London: Allen & Unwin.

Brady, T., Pakalnis, R., & Clark, L. 2005. Design in weak rock masses, Nevada underground mining operations. Proceedings of the Annual General Meeting of the SME, Salt Lake City, pp. 9.

Cai, M., Kaiser, P.K., Tasaka, Y., & Minami, M., 2007. Determination of residual strength parameters of jointed rock masses using the GSI system. *International Journal and Mining Science* 44(2): 274–65.

Cai, M., Kaiser, P.K., Uno, H., Tasaka, Y., & Minami, M., 2004. Estimation of rock mass deformation modulus and strength of jointed hard rock masses using the GSI system. *International Journal and Mining Science* 41(1): 3–19.

Cepuritis, M.P., 2010. An integrated approach to span design in open stope mining. PhD Thesis, Western Australia School of Mines, Australia.

Cepuritis,M.P., 2014. Design reliability for open stope span using empirical methods. 1st International Conference on Applied Empirical Design Methods in Mining. Sheraton Lima Hotel Convention Center. June 2014. Lima

Clark, L., 1998. Minimizing dilution in open stope mining with a focus on stope design and narrow vein longhole blasting. Master of Science thesis, University of British Columbia, Canada.

Clark, L.M. & Pakalnis R.C., 1997. An empirical design approach for estimating unplanned dilution from open stope hangingwalls and footwalls. 99th CIM Annual General Meeting, Vancouver, Canada.

Crockford, A.M., 2012. Shallow urban tunnelling through heterogeneous rockmasses: Practical experience from scale tunnels in Calgary, Alberta and the influence of rockmass layering on excavation stability and support design. p. 11–30.

Deere, D.U., Hendron, A.J., Patton, F.D. & Cording, E.J. 1967. Design of surface and near surface construction in rock. Proceedings from the 8th U.S. Symposium on Rock Mechanics, Minneapolis, MN. 237-302.

Diakite' O., 1998. Ore dilution in sublevel stoping. Masters thesis, McGill University. McGill.

Edelbro, C., 2004. Evaluation of rock mass strength criteria. Lulea University of Technology.

Elbrond, J., 1994. Economic effects of ore loss and rock dilution. CIM Bulletin.

Flavianu, L.S., 2010. An investigation of exploration guides for Proterozoic Rosh Pinah type sediment-hosted massive sulphides ("SEDEX") lead-zinc deposits, Rosh Pinah, Namibia. Masters thesis, Rhodes University, Grahamstown.

Frimmel, H, E. (2008). Neoproterozoic Gariep Orogen. In; The Geology of Namibia, Volume 2: Neoproterozoic to Lower Palaeozoic by Miller, R, McG., 2008. Ministry of Mines and Energy, 14-1

Handley, M.F., 2013. Pre-mining stress model for subsurface excavations in Southern Africa. The Journal of The Southern African Institute of Mining and Metallurgy, Vol.113, June 2013, pp 449-471.

Handley, M.F. & Piper, P.S., 2014. In-situ stress measurement on -030 level, Rosh Pinah Zinc Mine. Unpublished.

Hoek, E., 2007. Practical rock engineering. Source, Hoeks's corner.

Hoek, E. & Brown, E.T., 1980a. Underground excavations in rock. London: Institute of Mining & Metallurgy.

Hoek, E., & Brown, E.T. 1980b. Empirical strength criterion for rock masses. *Journal of Geotechnical and Geoenvironmental Engineering. American Society of Civil Engineers* 106: 1013–1035.

Hoek, E. 1994. Strength of rock and rock masses. ISRM News Journal. 2(2): 4-16.

Hoek, E. & Brown, T., 1997. Practical estimates of rock strength. International Journal of Rock Mechanics and. Mining Sciences 34: 1156–1186.

Hoek, E., Carranza-Torres, C. & Corkum, B., 2002. Hoek–Brown failure criterion — 2002 edition, NARMS-TAC 2002: Mining and Tunnelling Innovation and Opportunity,

Hoek, E., Carter, T.G. & Diederichs, M.S., 2013. Quantification of the geological strength chart. American Rock Mechanic Association, San Francisco, pp. 5–6.

Hoek, E. & Diederichs, M.S., 2006. Empirical strength criterion for rock masses. *International Journal of Rock Mechanics and Mining Sciences* 43(2): 203–2015.

Hoek, E., Kaiser P.K. & Bawden W.F., 1995. Support of underground excavation in hard rock. Rotterdam, Netherlands: Balkema.

Hoek, E., Wood, D. & Shah, S., 1992. A modified Hoek–Brown criteria for jointed rock masses. Proceeding of the 20th Eurorock (International Society of Rock Mechanics), London, pp. 209–214.

Hustrulid W. A, Bullock R. L. Underground Mining Methods: Engineering Fundamentals and International Case Studies. United States: Society for Mining, Metallurgy, and Exploration Inc.; 2001.

Hutchinson, D.J. & Diederichs, M., 1996. Cable bolting in underground mines. Vancouver: Bitech.

Jaeger, J, C. & Cook, N, G, W., 1979. Fundamentals of rock mechanics. 3rd Edition. London.

Labuz, J.F. & Zang, A., 2015. Mohr–Coulomb failure criterion. Rock Mechanics & Rock Engineering 45(6): 975–979.

Le Roux, P.J., 2015. Measurement and prediction of dilution in a gold mine operating with open stoping mining methods. PhD thesis, University of the Witwatersrand, Johannesburg.

Lockner, D.A. & Beeler, N.M., 2002. Rock failure and earthquakes, International handbook of earthquake and engineering seismology, Eds. Lee, William H.K., Kanamori Hiroo, Jennings Paul C and Kisslinger Carl. Part A and B, Chap 32. Academic Press, pp. 505–537.

Lorig, L,J. & Varona, P., 2013. Guidelines for numerical modelling of rock support for mines. Key note lecture. 7th international symposium on ground support in mining and underground construction, pp. 13-15.

Malik, M.H. & Rashid, S., 1997. Correlation of some engineering geological properties of the Murree formation at lower Topa (Murree District), Pakistan. Geological Bulletin of University of Peshawar, pp. 69-81.

Martin, C.D., Tannant, D.D., Yazici, S. & Kaiser, P.K., 1999. Stress path and instability around mine opening. International Society of Rock Mechanics Congress. Paris, pp. 1–5.

Mateveke, R., 2019. Excavating through the Kalahari group rock masses: Practical experience from a small-scale shaft sinking project. Masters thesis, University of the Witwatersrand, South Africa.

Mawdesley, C., Trueman , R & Whiten, W.,2001. Extending the Mathews stability graph for open-stope design. Trans. IMM (Section A). Volume 110, p A27-39.

Nickson, S., 1992. Cable support guidelines for underground hard rock mine operations. Masters thesis, University of British Columbia, Canada.
NGI, 2014., Using the Q-system Handbook, Norwegian Geotechnical Institute, 2015.

O'Hara, T.A., 1980. Quick guides to the evaluation of orebodies. Canadian Institute of Mining Bulletin 73(814): 87–99.

Pakalnis, R., 2015. Empirical design methods in practice. Underground Mine Design Methods, Australian Centre of Geomechanics, pp. 37–56.

Pakalnis, R., Nickson, S., Lunder, P., Clark, L., Milne, D. & Mah, P., 1996. Empirical methods for the design of mine structure, 11th Colloquium on Ground Control, Mining Association of Quebec.

Pakalnis, R.T., Miller, H.D.S. & Madill, T. (1985) Open stope design - a dilution approach, Proc of the Symposium on Rock Mass Characterization, Randburg, South Africa, 8 Nov. 1985, pp. 93-98.

Palmstrom, A., 1996. Characterizing rock masses by the RMI for use in practical rock engineering – Part 1. Tunnelling and Underground Space Technology 11(2): 175–188.

Palmstrom, A., 2014. An introduction to the Rock Mass index (RMi) and its applications. www.rockmass.net

Papaioanou, A. & Suorineni F.T., 2016. Development of a generalised dilution-based stability graph for open stope design. *Mining Technology* 125(2): 121–128.

Ponierwierski, J., 2005. Effect of stope size on sustainable steady-state production rates in a sublevel open stoping system. *Transactions of the Institute of Mining and Metallurgy, Section A: Mining Technology* 114: 241–250.

Potvin, Y., 1988. Empirical open stope design in Canada. PhD thesis, University of British Columbia, Canada.

Ramamurthy, T., Venkatappa Rao, G., & Singh, J. (1993) Engineering behaviour of phyllites. Engineering Geology. 33:209-225.

Ryder, J.A. & Jager, A.J., 2002. A textbook on rock mechanics for tabular hard rock mines. The Safety in Mines Research Advisory Committee (SIMRAC), Johannesburg, South Africa

Shali, G.P. & Vakili, A., 2019. Geotechnical assessment of stope design for the SF3 Orebody at Rosh Pinah Zinc Mine. Deep Mining Conference, 2019. Johannesburg, South Africa.

Singh, B., & Goel, R.K., 1999. Rock mass classification: A practical approach in Civil Engineering. Amsterdam: Elsevier Science, 282 pp.

Stacey, T.R. & Swart, A.H. Booklet: Practical Rock Engineering Practice for Shallow and Opencast Mines, The Safety in Mines Research Advisory Committee (SIMRAC). 2001. pp. 66.

Suorineni, F.T.,2014. Reflections on Empirical Methods in Geomechanics – The Unmentionables and Hidden Risks. 3rd Australian Ground Control in Mining Conference. Sydney. Australia, pp. 143-156.

Tavakoli, M., 1994. Underground metal mine crown pillar stability analysis. Doctor of Philosophy thesis, University of Wollongong, Wollongong.

Tommila, E., 2014. Mining method evaluation and dilution control in Kittila mine. Masters thesis, Aalto University, Finland.

Torben, J., Blakely, I.T., Jacquemin, T. & Avakash, P.A., 2018. *Technical Report on The Rosh Pinah Mine, Namibia NI43-101 Report,*. Rock Solid Resources, Toronto.

Ulusay, R. & Hudson, J.A., 2007. The complete ISRM suggested method for rock characterization, testing and monitoring: 1974–2006.

Urli, V.,2015. Ore-Skin Design to Control Sloughage in Underground Open Stoping Mining. Masters thesis, University of Toronto, Toronto.

Vakili, A., 2016. An improved unified constitutive model for rock material and guidelines for its application in numerical modelling. *ScienceDirect*: 261–282.

Vakili, A., 2017. The improved unified constitutive model: A fine-tuned material model tailored for more challenging geotechnical conditions. Australian Centre of Geomechanics, Perth.

Vakili, A., Albrecht, J. & Sandy, M.P.,2014. Rock strength anisotropy and its importance in underground geotechnical design. 3rd Australasian control in mining conference. Sydney.

Vakili, A, Sandy, M & Albrecht, J, 2012. Interpretation of non-linear numerical models in geomechanics A case study in the application‒of numerical modelling for raise bored shaft design in a highly stressed and foliated rock mass, in Proceedings Massmin 2012 (The Canadian Institute of Mining, Metallurgy and Petroleum: Sudbury).

Vakili, A., Harvey, F. & Greaves, H., 2018. Forecasting mine seismicity – towards a more established methodology. The Fourth Australasian Ground Control in Mining Conference, Sydney, New South Wales, pp. 207–222.

Villaescusa, E., 2014. Geotechnical design for sublevel open stoping, Western Australia School of Mines, CRC Press.Australia.

Wang, Yu, & Aladejare, A.E., 2016. Bayesian characterization of correlation between uniaxial compressive strength and Young's modulus of rock. *International Journal of Rock Mechanics and Mining Sciences* 85: 10–19.

Watson, J.M., Jakubowski,M & Vakili, A ., (2015). Rock strength anisotropy in high stress conditions: A case study for application to shaft stability assessments Studia Geotechnica et Mechanica. pp. 115-125

Wesseloo, J. & Stacey, T.R. (1998) In situ stresses in mining areas in South Africa. Journal of the South African Institution of Mining and Metallurgy, vol.98.pp 365-368.

Woodward, K., 2017. Stope reconciliation. December 2017 Newsletter. Australian Centre of Geomechanics. Perth.

Appendix A

Mechanical properties of rock masses

a) Arkose

	Ja	Jr	RQD	GSI
Arkose	5	2.5	80	67

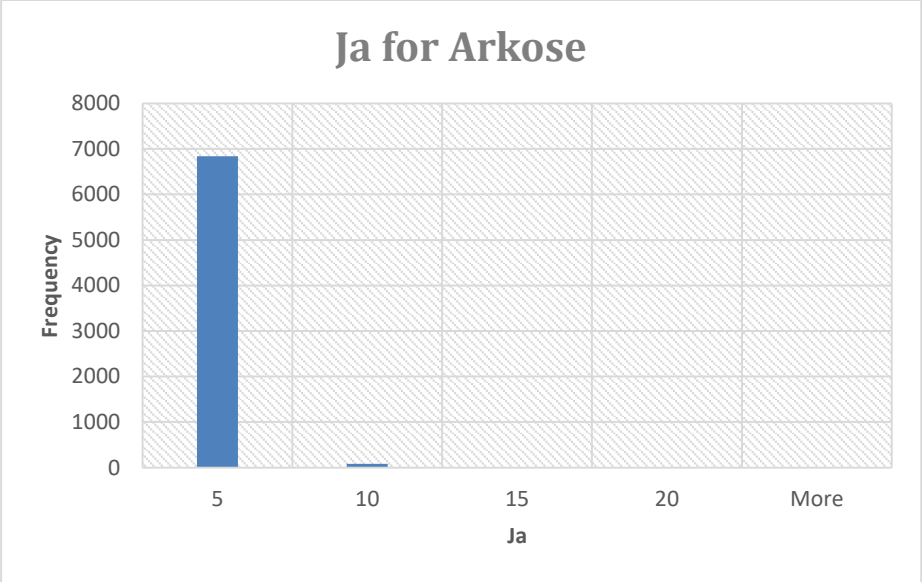


Figure A1. Histogram showing the joint alteration.

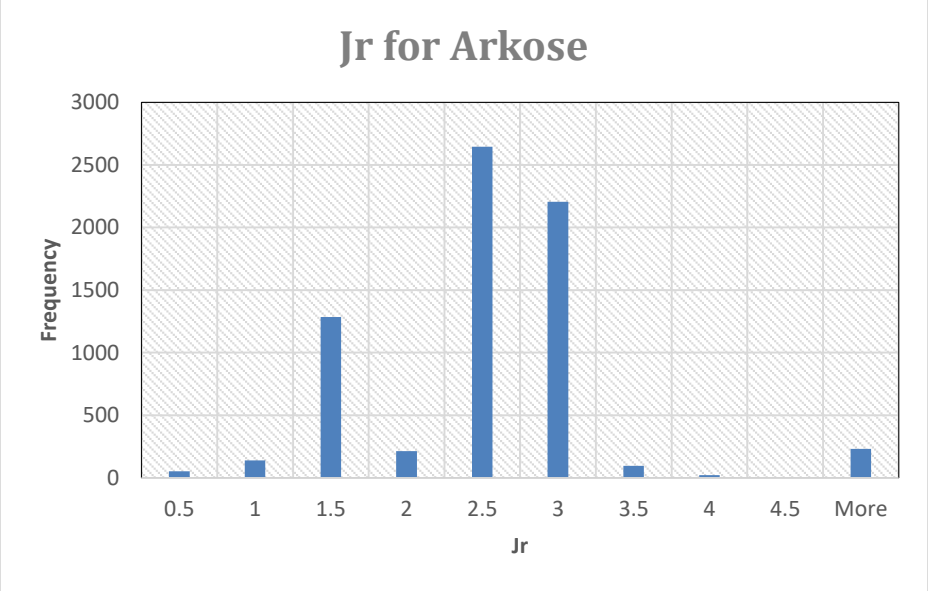


Figure A2. Histogram showing the joint roughness coefficient.

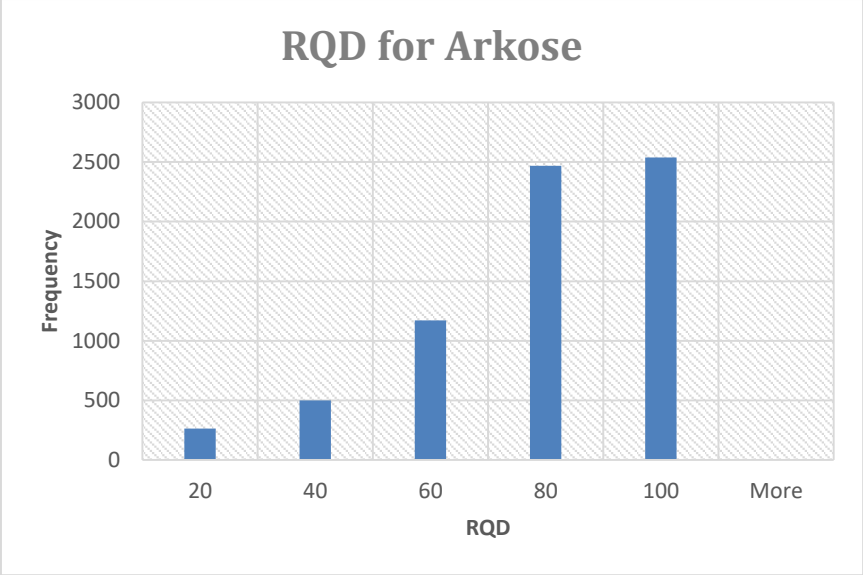


Figure A3. Histogram showing the joint roughness coefficient.

b) Carbonate

	Ja	Jr	RQD	GSI
Carbonate	1	3	100	89

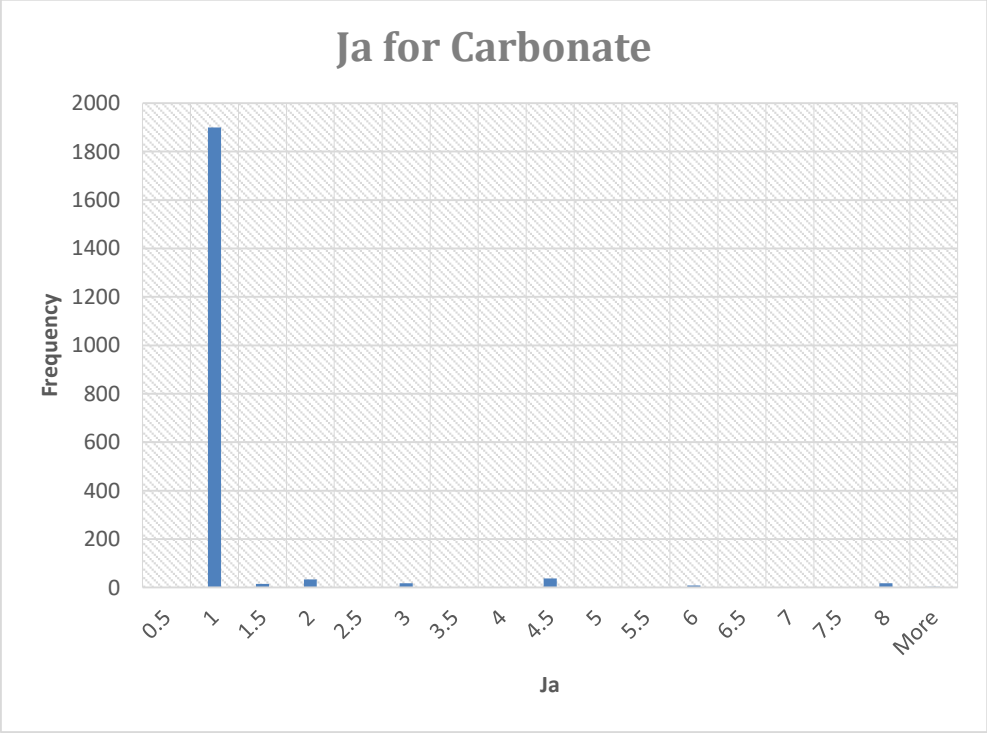


Figure A4. Histogram showing the joint alteration.

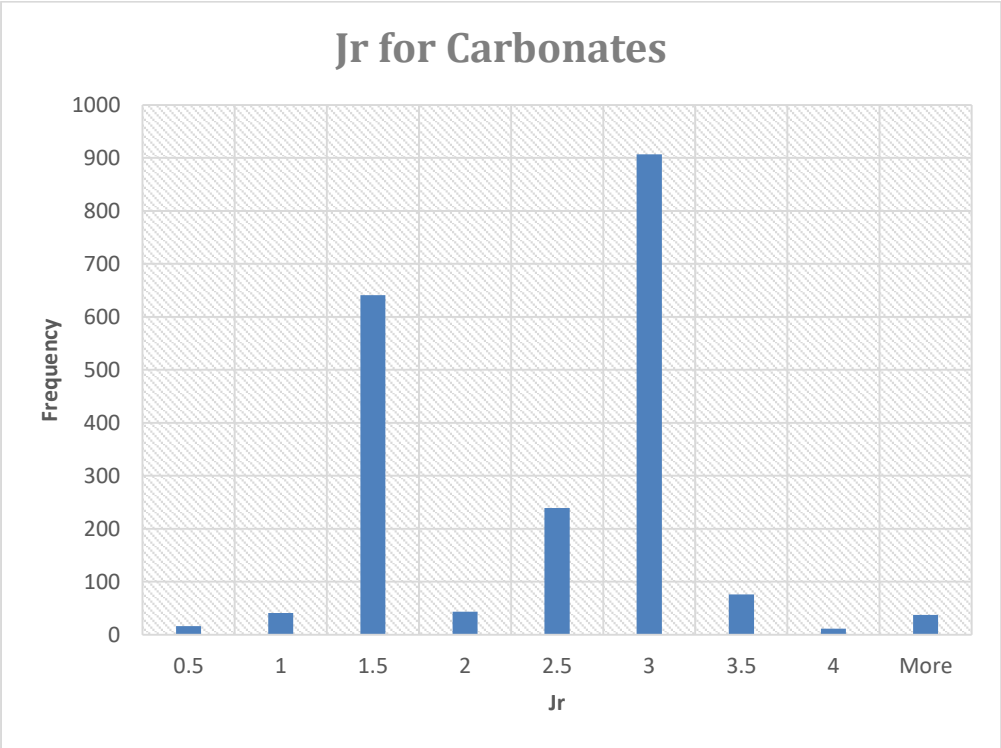


Figure A5. Histogram showing the joint roughness coefficient.

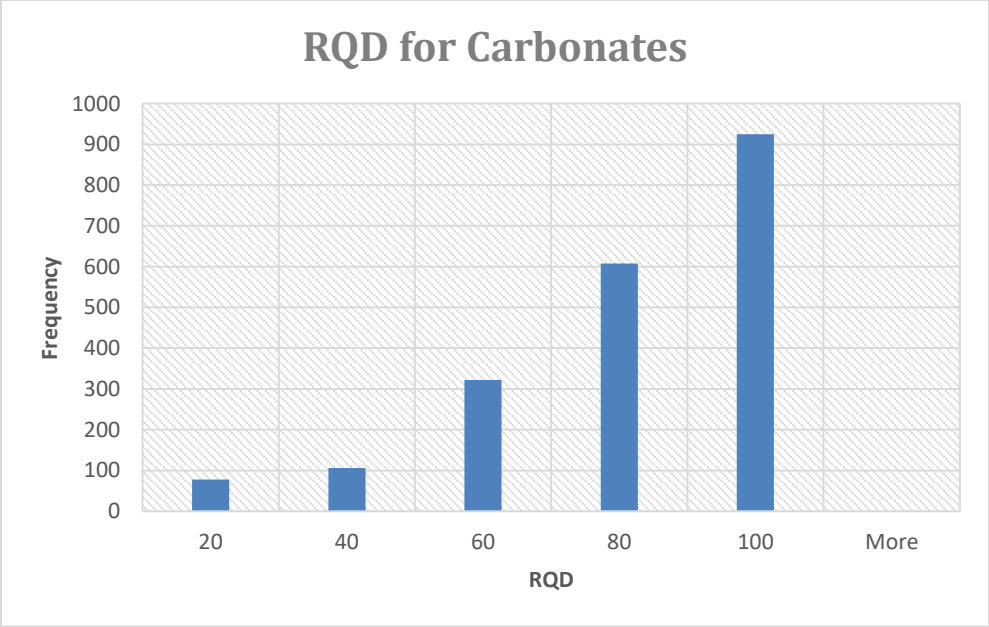


Figure A6. Histogram showing the RQD.

c) Argilite

	Ja	Jr	RQD	GSI
Argilite	1	2	100	84

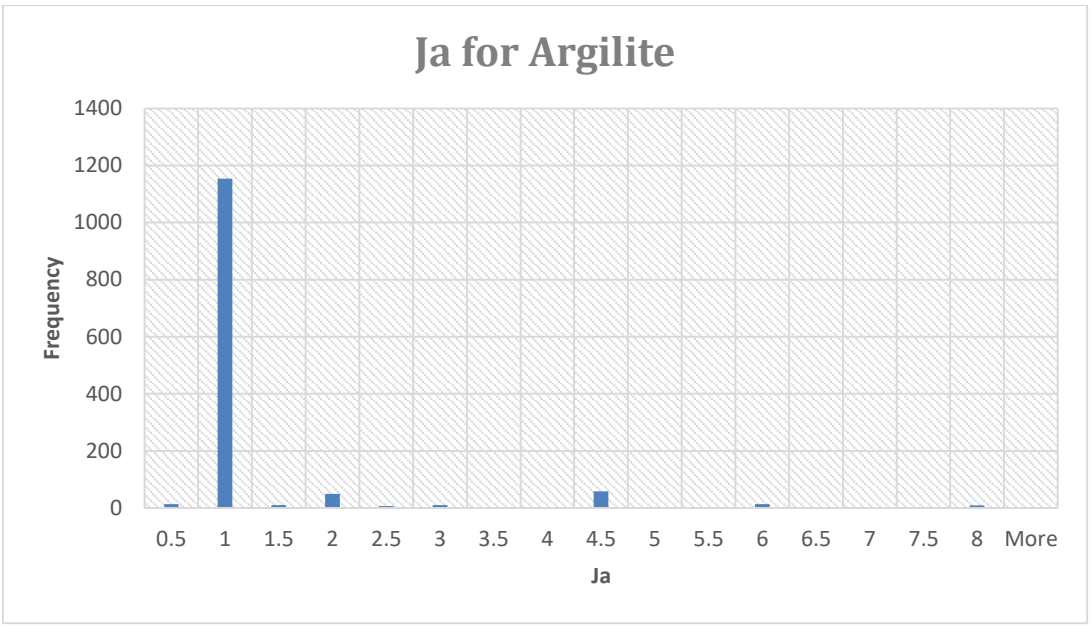


Figure A7. Histogram showing the joint alteration.

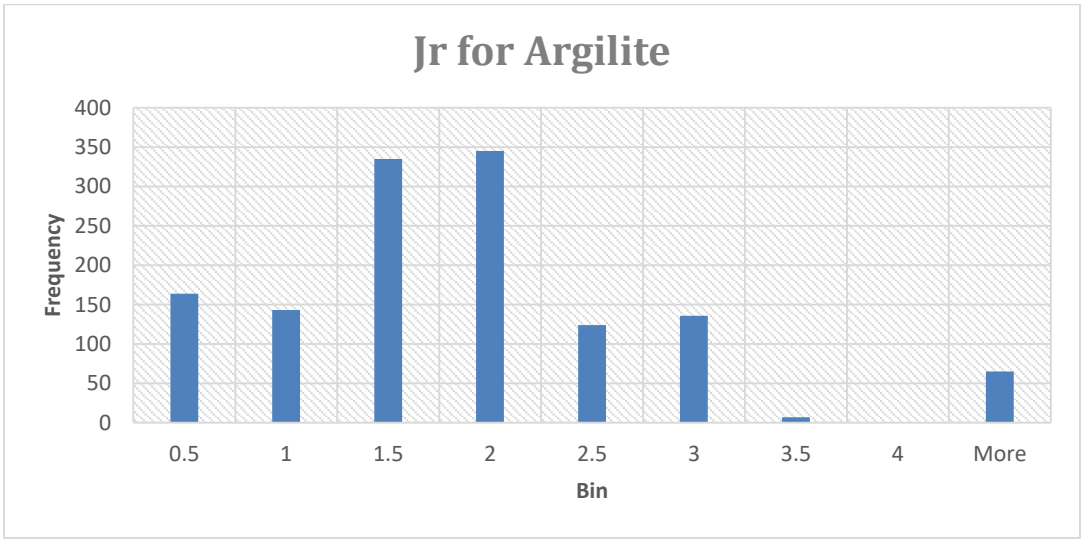


Figure E8. Histogram showing the joint roughness coefficient.

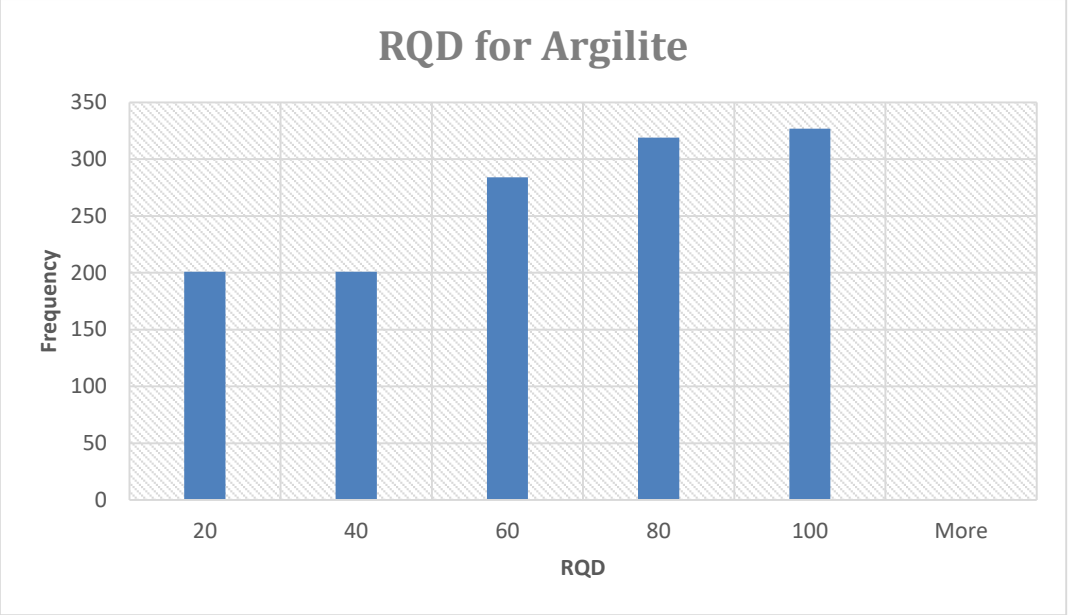


Figure A9. Histogram showing the RQD.

c) Breccia

	Ja	Jr	RQD	GSI
Breccia	1	3	100	89

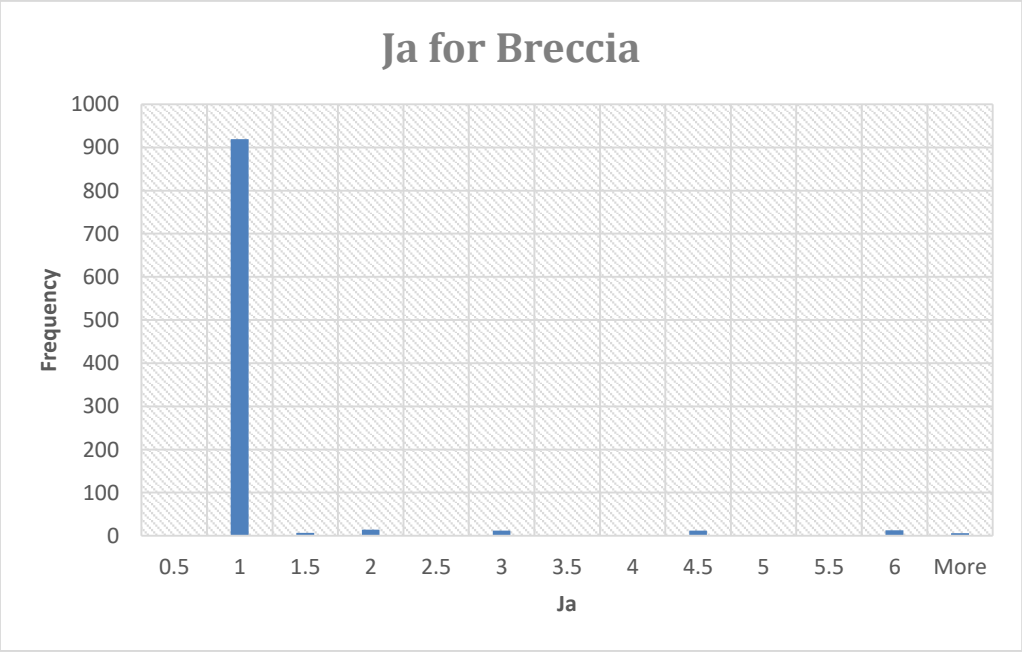


Figure A10. Histogram showing the joint alteration.

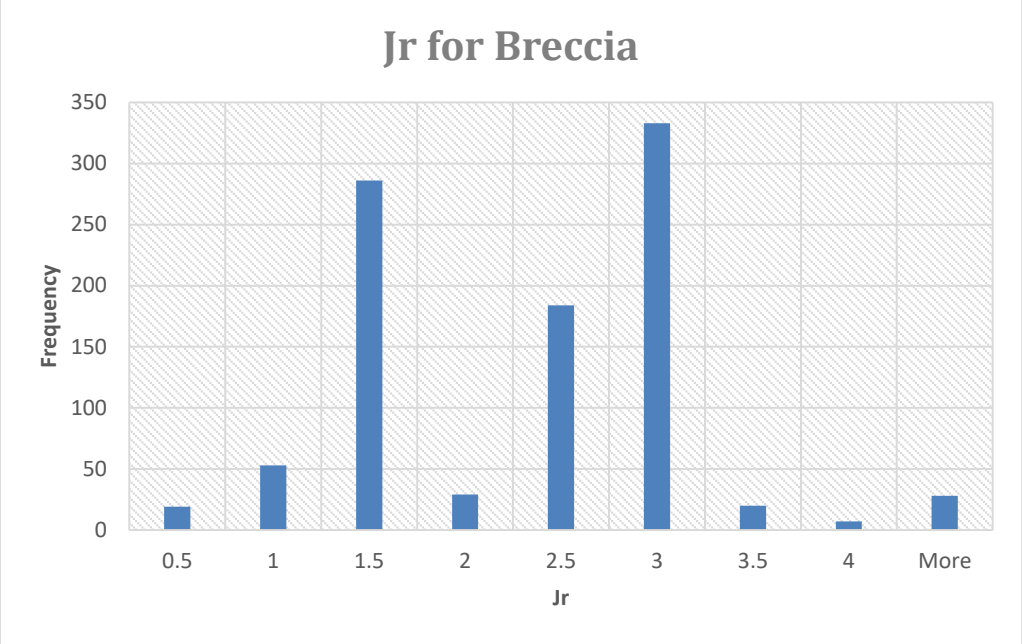


Figure A11. Histogram showing the joint roughness coefficient.

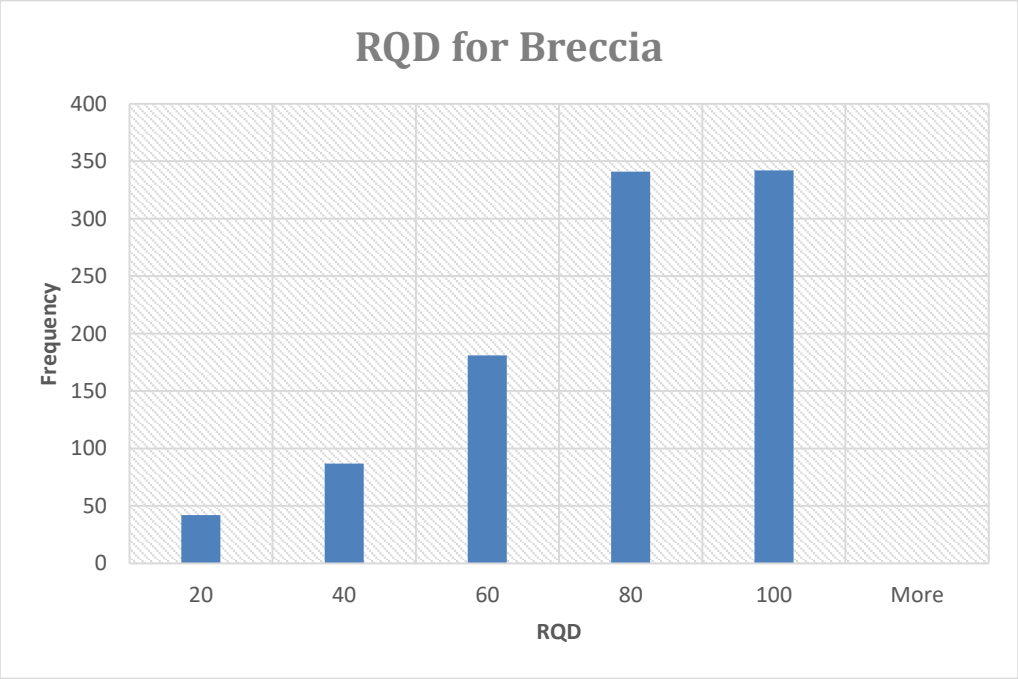


Figure A12. Histogram showing the RQD.